

---

+ + +

UNITARISATION  
OF ANOMALOUS COUPLINGS  
IN VECTOR BOSON SCATTERING

---

Masterarbeit von

Maximilian Löschner

An der Fakultät für Physik  
Institut für Theoretische Physik

Erstgutachter: Prof. Dr. Dieter Zeppenfeld  
Zweitgutachter: Prof. Dr. Margarete Mühlleitner

Bearbeitungszeit: 15. November 2013 – 15. November 2014



Ich versichere, dass ich diese Arbeit selbstständig verfasst und keine anderen als die angegebenen Hilfsmittel benutzt habe.

---

Maximilian Löschner  
Karlsruhe, den 14. November 2014

Als Masterarbeit anerkannt.

---

Prof. Dr. Dieter Zeppenfeld  
Karlsruhe, den 14. November 2014



# Contents

<b>1. Introduction</b>	<b>1</b>
<b>2. Theoretical Provisions</b>	<b>3</b>
2.1. The Standard Model of Particle Physics . . . . .	3
2.2. Interactions in a Quantum Field Theory Framework . . . . .	4
2.3. Glashow-Weinberg-Salam Theory of Weak Interactions . . . . .	6
<b>3. Effective Field Theories</b>	<b>9</b>
3.1. Anomalous Couplings . . . . .	10
3.2. Dimension 8 Operators . . . . .	12
3.3. Redefinition of $\mathcal{L}_{S,0}$ . . . . .	14
<b>4. Unitarisation</b>	<b>17</b>
4.1. Motivation . . . . .	17
4.2. Historic Examples . . . . .	17
4.2.1. Fermi's Interaction . . . . .	17
4.2.2. Scattering of Longitudinally Polarized Massive Vector Bosons . . . . .	19
4.3. Form Factors . . . . .	22
4.3.1. General Remarks . . . . .	22
4.3.2. Energy Scale $\Lambda_{FF}$ . . . . .	23
4.4. Replacement of Mandelstam variables . . . . .	24
4.5. K-Matrix formalism . . . . .	25
4.5.1. Definition of $K$ and Relations . . . . .	25
4.5.2. Unitarisation Procedure . . . . .	27
4.6. Unitarisation of $\mathcal{L}_{S,0}$ and $\mathcal{L}_{S,1}$ . . . . .	30
4.6.1. Amplitudes arising from Effective Operators . . . . .	30
4.6.2. Isospin Eigenamplitudes . . . . .	32
4.6.3. Isospin-Spin Eigenamplitudes . . . . .	34
4.6.4. Unitarized Amplitudes . . . . .	35
4.7. K-Matrix-like Form Factors . . . . .	37
4.8. Unitarisation of $\mathcal{L}_{M,i}$ and $\mathcal{L}_{T,i}$ . . . . .	38
<b>5. Mathematica Framework</b>	<b>41</b>
5.1. From a Lagrangian to Partial Waves . . . . .	41
5.1.1. Feynman Rules . . . . .	41
5.1.2. Amplitudes from FeynArts/FormCalc . . . . .	42
5.1.3. Towards Partial Waves . . . . .	43
5.1.4. Exact Momentum vs. First Order Expansion . . . . .	44
5.1.5. Partial Waves in Helicity Space . . . . .	45
5.2. Contributions by Different Polarization Combinations . . . . .	47
<b>6. Implementation</b>	<b>51</b>
6.1. Introduction into VBFNLO . . . . .	51
6.2. Structure of Anomalous Couplings in VBFNLO . . . . .	52

6.3.	K-Matrix Method for $\mathcal{L}_{S,0}$ and $\mathcal{L}_{S,1}$ . . . . .	53
6.3.1.	General Approach . . . . .	53
6.3.2.	Technical Details . . . . .	54
<b>7.</b>	<b>Analysis</b>	<b>57</b>
7.1.	General Remarks on Vector Boson Scattering . . . . .	57
7.2.	Anomalous couplings at NLO in $\alpha_s$ . . . . .	58
7.3.	Comparison of K-Matrix Approach vs. Form Factors . . . . .	58
7.4.	Comparison of VBFNLO vs. WHIZARD . . . . .	60
7.4.1.	Set Up . . . . .	62
7.4.2.	Low Energy Discrepancies . . . . .	63
7.4.3.	Comparison for $\bar{f}_{S,0} = \bar{f}_{S,1} = 100 \text{ TeV}^{-4}$ . . . . .	63
<b>8.</b>	<b>Conclusion</b>	<b>73</b>
	<b>Appendix</b>	<b>75</b>
A.	Optical Theorem . . . . .	75
B.	Wigner's d-Functions . . . . .	75
C.	Legendre Polynomials . . . . .	76
D.	Polarization vectors . . . . .	76
E.	Clebsch-Gordon Coefficients in the Total Isospin Basis . . . . .	77
F.	Dimension 6 operators . . . . .	77
G.	Some Mathematica Definitions for Partial Wave Analysis . . . . .	78
G.1.	Polarization Vectors . . . . .	79
G.2.	Helicity eigenvectors . . . . .	79
G.3.	Taylor Expansion of Momentum . . . . .	79
G.4.	replaceEpsWWWW . . . . .	80
H.	VBFNLO and WHIZARD Input Files for Comparison of $W^+W^+$ -processes . .	81
H.1.	VBFNLO Input Files . . . . .	81
H.2.	Whizard Input File . . . . .	85
	<b>Bibliography</b>	<b>87</b>

## Introduction

*There is nothing new to be discovered in physics now.  
All that remains is more and more precise measurement.*

*(Lord Kelvin, 1900)*

Finding the fundamental building blocks of nature and the interactions among these has posed a challenge for physicists practically ever since physics existed. In the course of the last century vast progress has been made in describing these constituents at ever growing granularity. Beginning with the discovery of the substructure of atoms via Rutherford scattering in 1911, scattering experiments of higher and higher energies have continued to give insights on the structure of nature's building blocks. This field of research, *particle physics*, still represents a very active field of science. Only the experiments have grown largely from using decay products of radioactive materials and gold-foils to building kilometer long devices for accelerating and colliding particles. The highest energetic and largest collider ever built and still under use is the Large Hadron Collider (LHC) at CERN in Geneva, Switzerland.

The first continuous running period of the LHC has finished about a year ago. With the discovery of a Standard Model-like Higgs boson [1, 2], this run already marked a big step for particle physics in this century. Still, physicists are hoping for more to come in the upcoming runs which are just about to start. The discovery of other new particles has been absent so far. Therefore a lot of interest is drawn by the study of effects that might indirectly yield signs of "New Physics".

One of today's areas of interest is the mechanism of electroweak symmetry breaking (EWSB). This mechanism describes the interactions and masses of vector bosons in terms of a small number of parameters. From the theory side, an elegant and complete description of this part of physics is available, but due to the challenging nature of the associated measurements, there is a lot of room for deviations from the predictions on the experimental side.

This thesis is dedicated to vector boson selfcouplings. With the vector boson 4-vertices not accurately measured so far, this particular subject serves as an appealing playing ground for theorists and experimentalists alike. Already in Run 1 of the LHC, first experimental data on same sign  $W$ -boson scattering has been collected [3], but with the center of mass energy going up to 13 TeV and a luminosity of up to  $100 \text{ fb}^{-1}$  in Run 2 [4], a lot more results are expected to arrive in the near future.

One way of modeling new physics effects in the electroweak sector is the approach of effective field theories, or in this case often called anomalous couplings. These serve as an open-minded way of describing low energy effects of new physics at much higher energy scales  $\Lambda$ . In typical analyses of vector boson scattering at hadron colliders, observables like the invariant mass of a vector boson pair often can not be limited to a narrow energy range [5]. Working in broad energy ranges, one might already include energies so close to the scale  $\Lambda$ , that the effective field theory approximation breaks down and the anomalous couplings start showing unphysically large scattering probabilities. When theoretical predictions are compared to experimental data, this would naively imply that the anomalous couplings need to be zero.

A full theory with new particle resonances should be used to describe these high energy ranges. Without knowing this theory, different methods can be used to get meaningful physical results. A way to treat this problem is the so called *unitarisation* of anomalous couplings. This means suppressing the anomalous couplings at energies larger than a certain energy scale, such that their low energy behavior is kept and the unphysical high energy behavior is suppressed. The choice for this scale depends on the method used. One of these methods is the introduction of *form factors*. These are functions resembling propagators of resonances with two input parameters: an exponent controlling the power of suppression and a mass scale at which the suppression sets in. The structure of the form factor and the choice for the input parameter lack a strong physical motivation, which is why some consider them as rather unattractive.

The approach under consideration in this thesis is called *K-matrix unitarisation* [5, 6, 7]. Based on a partial wave analysis of the scattering amplitudes resulting from anomalous couplings, unitarity bounds are derived and used to control the cut-off of the amplitudes. No input parameters are needed to control the behavior in contrast to form factors.

After a quick introduction into the theoretical framework, a derivation of the K-matrix formalism is given. This is in turn used for an implementation into the parton level Monte Carlo program VBFNLO [8]. In the analysis part a comparison to a similar program also using the K-matrix formalism, WHIZARD [9], is given in order to check the implementation. Not all anomalous couplings can be unitarized in the K-matrix formalism, which is why in the unitarisation section a new K-matrix-like approach is proposed for those.

## Theoretical Provisions

This chapter is a short introduction into the subjects and definitions that represent the foundation of quantum field theoretical frameworks, rather than a complete mathematical description. It is based on the findings in [10, 11].

### 2.1. The Standard Model of Particle Physics

In order to describe the fundamental forces and properties of nature at the smallest scales, the theory that evolved in the last century and so far endured every experimental challenge is the *Standard Model of particle physics* (SM). It is based in the framework of quantum field theories, i.e. the treatment of particles as discrete excitations of an underlying field.

The particle content of the SM consists of six quarks, six leptons, four types of force mediators, i.e. the gauge bosons and, as has been consolidated in the past two years, the Higgs boson. Quarks and leptons are grouped into three families, all carrying an identical structure. The interactions between these particles are described based on the concept of *local gauge invariance*. This means that the theory is invariant under transformations that are elements of certain groups, analogous to the gauge freedom that was already known in classical electrodynamics and with *local* meaning that these transformations are space-time dependent. The combination of groups that describes the symmetries of the SM is

$$\mathcal{G}_{\text{SM}} = SU(3)_C \times SU(2)_L \times U(1)_Y, \quad (2.1)$$

standing for unitary ( $U$ ) respectively special unitary ( $SU$ ) groups, i.e. unitary transformations with determinant  $+1$ . The indices indicate the nature of the interaction.

$C$  stands for “color” referring to the color-charge of strongly interacting particles, the quarks. With  $\dim[SU(3)] = 3$  we know that this group, or rather the corresponding Lie-Algebra is formed by  $3^2 - 1 = 8$  generators. These correspond to the eight gluons that serve as massless force mediators of the strong interaction with Spin = 1.

The index  $L$  refers to the interesting fact that the weak force is maximally parity violating, i.e. only left-chiral fermions and right-chiral antifermions interact weakly.  $Y$  stands for the weak hypercharge of a particle that is defined as

$$Y = 2(Q - T_3), \quad (2.2)$$

where  $Q$  is the electric charge and  $T_3$  the third component of the weak isospin of a particle. The combination of the electric and weak charge into  $Y$  gives a hint at one of the great successes of the SM: the unification of the weak and the electromagnetic force into the electroweak force.

Another ingredient to the SM that is not directly visible from the gauge groups, is the Higgs-mechanism. It cures the inconvenience that adding mass terms to the Lagrangian of

the SM, which describes all interactions among the particles, spoils the gauge invariance that the theory was constructed from in the first place. Including the Higgs-field into the theory dynamically generates mass terms for the massive vector bosons and also fermion masses can be included via the so called *Yukawa couplings* to the Higgs.

Although the SM is extraordinarily successful in the description of experimental results of particle physics it does not describe all fundamental forces of nature, with the gravitational force being the one left out. Due to the non-renormalizability of gravity in a quantum field theoretical framework [12], it so far has not been possible to extend the SM to also contain the last fundamental force that we know of. This and a number of other facts show there is reason to believe that *physics beyond the Standard Model* (BSM) exist.

Note that throughout this thesis we will work in *natural units* as it is typically done in particle physics. Effectively this mean setting

$$\hbar = c = 1. \quad (2.3)$$

The result is that the units of length, time and mass are all just different powers of the unit of energy, i.e.

$$[\text{length}] = [\text{time}] = [\text{mass}]^{-1} = [\text{energy}]^{-1}. \quad (2.4)$$

## 2.2. Interactions in a Quantum Field Theory Framework

The starting point of most quantum field theoretical frameworks is the dimensionless<sup>1</sup> quantity  $S$ , called the action. Classically it is expressed as the time integral over a Lagrangian  $L$ , but with time and spatial dimensions being treated equally in a relativistic framework, we rather want to look at the *Lagrangian density*  $\mathcal{L}$  in terms of one or more fields  $\phi(x)$ , i.e.

$$S = \int dt L(\phi, \partial_\mu \phi) = \int d^4x \mathcal{L}(\phi, \partial_\mu \phi). \quad (2.5)$$

As we know from classical mechanics, with the help of the *Lagrangian formalism* and the *principle of least action*, we can derive classical paths of particles in some configuration space between two points in time  $t_1$  and  $t_2$ . This is done by finding the stationary points (typically the minima) of  $S$  by demanding that the variation  $\delta S$  along the field configurations vanishes.

$$0 = \delta S = \int d^4x \left\{ \frac{\partial \mathcal{L}}{\partial \phi} \delta \phi + \frac{\partial \mathcal{L}}{\partial (\partial_\mu \phi)} \delta (\partial_\mu \phi) \right\} \quad (2.6)$$

From this we can derive the *Euler-Lagrange equation* of motion for a field, i.e.

$$\partial_\mu \left( \frac{\partial \mathcal{L}}{\partial (\partial_\mu \phi)} \right) - \frac{\partial \mathcal{L}}{\partial \phi} = 0, \quad (2.7)$$

which directly corresponds to the equation of motion we know from classical mechanics. Historically the equations of motions for fields like the Dirac-equation for fermions of Spin 1/2 and the Klein-Gordon-equation for massless scalar fields have been known before the introduction of this formalism. They give us the hint of how to construct Lagrangian densities, namely by defining them such that the equations of motions are reproduced by plugging them into 2.7. For the case of a single scalar field  $\phi(x)$  the right choice for  $\mathcal{L}$  is

$$\mathcal{L}_{\text{KG}} = \partial_\mu \phi \partial^\mu \phi - \frac{1}{2} m^2 \phi^2, \quad (2.8)$$

---

<sup>1</sup> $S$  carries the dimension  $[\text{energy}] \times [\text{time}]$ . Therefore we can treat it as dimensionless in natural units.

yielding the aforementioned Klein-Gordon-equation

$$\square\phi(x) + m^2\phi(x) = 0. \quad (2.9)$$

Note that from now on we will call Lagrangian densities  $\mathcal{L}$  just Lagrangians. The equations of motion are exactly soluble if we insert the fields in the form of Fourier-expansions. These do not need to be classical anymore in the sense that we interpret the Fourier-coefficients in the expansion as creation/annihilation operators and impose the right (anti-)commutator relations among these, a step often called *second quantization*.

At this point we are now able to define the so called *Feynman propagator*  $\Delta_F(x - y)$ . For the case of a scalar field we denote it by

$$i\Delta_F(x - y) = \langle 0 | T[\phi(x)\phi^\dagger(y)] | 0 \rangle, \quad (2.10)$$

where  $T[\dots]$  stands for time ordering, which is bringing the products of the fields respectively their operators in the order with the latest to the left. This propagator is a solution to the Klein-Gordon equation and can be interpreted as the probability amplitude of a freely propagating field that is created at some space-time coordinate  $y$  and annihilated at  $x$  (if  $x_0 > y_0$ ).

So far we have only considered free propagation described by quadratic terms of the fields in the Lagrangian. We can now include interactions among the fields by adding terms with three or more fields. It is then convenient to split the Lagrangian in a kinetic part  $\mathcal{L}_K$  and an interaction part  $\mathcal{L}_I$ , i.e.

$$\mathcal{L} = \mathcal{L}_K + \mathcal{L}_I. \quad (2.11)$$

A well known example is the interaction of fermion fields  $\psi(x)$  and the photon field  $A_\mu(x)$  in quantum electrodynamics (QED), i.e.

$$\mathcal{L}_{I,\text{QED}} = -e\bar{\psi}\gamma_\mu\psi A^\mu. \quad (2.12)$$

In general the equations of motions will then not be exactly soluble anymore, which is why we need to rely on perturbation theory. The expansion parameters will then be the coupling constants ( $e$  in the example above) that come with the interaction terms of the Lagrangian<sup>2</sup>. This method becomes clear if we take a look at the time evolution of some initial state  $|i\rangle$  at  $t = -\infty$ . In the interaction picture, the time evolution is determined by the interaction Hamiltonian  $H_I$  by

$$i\partial_t | \phi \rangle = H_I | \phi \rangle. \quad (2.13)$$

We can reformulate this equation in an integral form and iteratively insert it into itself, finally arriving at

$$| \phi(\infty) \rangle = T[\exp\{-i \int_{-\infty}^{\infty} dt H_I(t)\}] | i \rangle. \quad (2.14)$$

This tells us that we can get the transition amplitude of some initial state  $|i\rangle$  at  $t = -\infty$  to some final state  $|f\rangle$  at  $t = \infty$  by

$$\langle f | T[\exp\{-i \int_{-\infty}^{\infty} dt H_I(t)\}] | i \rangle. \quad (2.15)$$

---

<sup>2</sup>We need to assume that the coupling constants are small enough, so that the perturbative expansion converges.

Now we insert the relation between the interaction Hamiltonian and the corresponding interaction Lagrangian and expand this transition amplitude to get

$$\langle f|T[\exp\{-i \int d^4x \mathcal{L}_I(x)\}]|i\rangle \quad (2.16)$$

$$= \langle f|1 + i \int d^4x T[\mathcal{L}_I] + \frac{i^2}{2} \int d^4x \int d^4y T[\mathcal{L}_I(x)\mathcal{L}_I(y)] + \dots|i\rangle. \quad (2.17)$$

Taking the QED interaction Lagrangian as an example, we see that we end up at a perturbative expansion in terms of the coupling constants and the time ordered products of the fields of our interaction Lagrangian. The question is how to evaluate those time ordered products between initial and final state. For this we need Wick's theorem which tells us that all products of fields can be decomposed to sums of products of the Feynman propagators that we have seen before. Luckily Richard Feynman came up with the idea to diagrammatically represent these products of Feynman propagators, which makes the interpretation and computation of those transition amplitudes far more accessible. For every  $\mathcal{L}_I$ , i.e. for every physical theory in that form, we are now able to derive a set of *Feynman rules* which tell us how to translate the diagrammatic representations to mathematical expressions. These rules are just explicit expressions for the Feynman propagators and the vertices appearing in the theory, i.e. the way different propagators can be connected.

The diagrams now merely represent the transition amplitudes from above for some specific field configuration. These amplitudes are also called matrix elements, denoted by  $\mathcal{M}$ . With this notation we are ready to define a measure for the probability of some process, called differential cross section  $d\sigma$ . Let us restrict ourselves to the case of  $|i\rangle$  representing a two-particle state with definite momentum  $|p_A p_B\rangle$ . Then we can define the differential cross section of this state going to any final state  $|f\rangle$  by

$$d\sigma = \frac{1}{2E_A 2E_B |v_A - v_B|} |\mathcal{M}(p_A, p_B \rightarrow \{p_f\})|^2 d\Phi, \quad (2.18)$$

$$d\Phi = \prod_f \frac{d^3 p_f}{2E_f (2\pi)^3} (2\pi)^4 \delta^{(4)}\left(p_a + p_b - \sum p_f\right). \quad (2.19)$$

Here  $|v_A - v_B|$  denotes the relative velocity of the two initial state particles in the laboratory reference frame. We can get a little more insight on the meaning of this definition, by considering a two-particle final state with all in- and outgoing particles having the same mass and by working in the center of mass frame of the incoming particles. The expression above then reduces to

$$d\sigma = \frac{|\mathcal{M}|^2}{64\pi^2 E_{\text{CM}}^2} d\Omega. \quad (2.20)$$

From this we see that all dynamics of the reaction is incorporated in  $\mathcal{M}$ . This is already an experimentally accessible observable, which tells us how probable it is to find the final state particles in some solid angle  $d\Omega$ . By integrating over this solid angle we arrive at the total cross section  $\sigma_{\text{tot}}$  representing the final quantity of the calculations in this framework. It yields the overall probability of finding final state particles of some process described by  $\mathcal{M}$ .

### 2.3. Glashow-Weinberg-Salam Theory of Weak Interactions

The theory of weak interactions within the Standard Model is the so called *Glashow-Weinberg-Salam theory* (GWS). It was developed in 1967 by the three eponyms and experimentally confirmed indirectly with the detection of neutral currents in the Gargamelle

detector at CERN in 1973 and directly in 1983 by the detection of  $W^\pm$ - and  $Z$ - bosons with the UA1 and UA2 detectors in proton-antiproton collisions.

In order to understand the basics of the theory behind this, let us consider a doublet field  $\Psi$  that transforms under a local unitary transformation  $U \in SU(2)$  as

$$\Psi \rightarrow U\Psi, \quad \Psi^\dagger \rightarrow \Psi^\dagger U^\dagger. \quad (2.21)$$

When we treat this field in a QFT framework, we need to include a kinetic term of the field into the Lagrangian, i.e.

$$\mathcal{L}_{\text{kin}} = i\bar{\Psi}\gamma^\mu\partial_\mu\Psi. \quad (2.22)$$

As it turns out, terms of this structure are not invariant under the transformation mentioned before. We can cure this by replacing the partial derivative  $\partial_\mu$  by the corresponding covariant derivative  $D_\mu$  that transforms just like the fields:

$$D_\mu\Psi \rightarrow U(D_\mu\Psi). \quad (2.23)$$

These covariant derivatives have the form

$$D_\mu = \partial_\mu + igA_\mu^a T^a. \quad (2.24)$$

The  $T^a$  represent the generators of the underlying symmetry group,  $A_\mu^a$  are called gauge fields and  $g$  is a coupling constant of these gauge fields to  $\Psi$ . In the case of  $SU(2)$  we have the three Pauli matrices as generators  $T^a = \sigma^a/2$  and the gauge fields are  $W_\mu^a$  with  $a \in \{1, 2, 3\}$ . Moreover we need the *structure constants*  $f_{abc}$  of  $SU(2)$ . These are

$$f_{abc} = i\epsilon_{abc}. \quad (2.25)$$

With the introduction of the gauge fields in our theory, we also need to include kinetic terms for those fields. This can be done in a Lorentz and gauge invariant way by introducing

$$\mathcal{L}_{\text{kin},SU(2)} = -\frac{1}{4}W_{\mu\nu}W^{\mu\nu}, \quad (2.26)$$

where  $W_{\mu\nu}$  is the field strength tensor

$$W_{\mu\nu} = -\frac{i}{g_w}[D_\mu, D_\nu] = ig_w\frac{\sigma^a}{2}(\partial_\mu W_\nu^a - \partial_\nu W_\mu^a + g_w\epsilon_{abc}W_\mu^b W_\nu^c). \quad (2.27)$$

Compared to the field strength tensor we know from electrodynamics, this tensor also contains a so called non-abelian part, the last term in 2.27. This term leads to cubic and quartic terms in the fields when inserted into the Lagrangian 2.26. Therefore, self interactions among the vector bosons arise by including their kinetic terms in a gauge invariant way.

Transferring the systematics from above to the weak interaction, we arrive at the so called Glashow-Weinberg-Salam theory. The field  $\Psi$  now represents fermion doublets and the correct symmetry group for them is  $SU(2)_L \times U(1)_Y$ . As it turns out, only left-chiral fermions interact weakly. Thus the right-chiral fermions have 0 charge under  $SU(2)_L$ . With this knowledge we can define the covariant derivative by

$$D_\mu\Psi_{L/R} = (\partial_\mu + ig_{w,L/R}W_\mu^a\frac{\sigma^a}{2} + ig\frac{1}{2}B_\mu)\Psi_{L/R}, \quad (2.28)$$

with  $g_{w,L} \neq 0$  and  $g_{w,R} = 0$ . The kinetic terms as well as the electroweak interactions among all the fields can now be written as

$$\begin{aligned} \mathcal{L}_{\text{GWS}} &= \mathcal{L}_{\text{gauge}} + \mathcal{L}_{\text{fermions}} \\ &= -\frac{1}{4}W_{\mu\nu}^a W^{a,\mu\nu} - \frac{1}{4}B_{\mu\nu}B^{\mu\nu} + \sum_{\text{fermions}} (i\bar{\Psi}_L\gamma^\mu D_\mu\Psi_L + i\bar{\Psi}_R\gamma^\mu D_\mu\Psi_R). \end{aligned} \quad (2.29)$$

The only thing missing are the mass terms of the fields. Including them into the Lagrangian above by adding quadratic terms in the fields breaks gauge invariance. The solution is to include another doublet under  $SU(2)$ , the scalar Higgs field  $\Phi$  and a potential for this field. This potential reads

$$V(\Phi) = -\mu^2 \Phi^\dagger \Phi + \lambda (\Phi^\dagger \Phi)^2. \quad (2.30)$$

The special feature of the potential is that it leads to a non-vanishing vacuum expectation value if we choose  $\mu^2 > 0$

$$\Phi_0 = \langle 0 | \Phi | 0 \rangle = \frac{1}{\sqrt{2}} \begin{pmatrix} 0 \\ v \end{pmatrix}, \quad v = 246.22 \text{ GeV}. \quad (2.31)$$

After removing the unphysical degrees of freedom, the doublet can be expressed as

$$\Phi = \frac{1}{\sqrt{2}} \begin{pmatrix} 0 \\ v + h \end{pmatrix}. \quad (2.32)$$

Adding the Higgs-Lagrangian

$$\mathcal{L}_{\text{Higgs}} = (D_\mu \Phi)^\dagger D^\mu \Phi + V(\Phi) \quad (2.33)$$

to the theory dynamically generates mass terms for the vector bosons. We see this by inserting the definition of the covariant derivative and  $\Phi$  into the Higgs Lagrangian and by rearranging the interaction eigenstates  $W^1, W^2, W^3$  and  $B$  into the mass eigenstates  $W^+, W^-, Z$  and  $A$ , via

$$W_\mu^\pm = \frac{1}{\sqrt{2}} (W_\mu^1 \mp iW_\mu^2), \quad (2.34a)$$

$$Z_\mu = \frac{1}{\sqrt{g_w^2 + g^2}} (g_w W_\mu^3 - g B_\mu), \quad (2.34b)$$

$$A_\mu = \frac{1}{\sqrt{g_w^2 + g^2}} (g W_\mu^3 + g_w B_\mu). \quad (2.34c)$$

As expected, there is no quadratic term in  $A_\mu$  leaving the photon massless. For the other fields we find their masses in terms of the vacuum expectation value  $v$  and the couplings constants  $g_w$  and  $g$ , i.e.

$$m_W = \frac{g_w v}{2}, \quad m_Z = \frac{\sqrt{g_w^2 + g^2} v}{2}. \quad (2.35)$$

This completes the discussion of the electroweak sector of the SM. Other interactions like the Higgs-selfcouplings exist, but as they do not contribute to vector boson scattering, they will not be discussed any further here. For a more detailed description see [10, 11]

## Effective Field Theories

There are at least two ways of searching for new physics from the theory side. One of them is the prediction of new particles in connection to new symmetries like in Supersymmetry. Another approach is to look for alterations of interactions of SM particles while keeping the SM particle content. Effective field theories (“EFTs”) belong to the latter case. The main idea behind any kind of EFT is to find the simplest possible framework to describe *interesting* physics in a certain physical region (not necessarily an energy scale) while being able to correct the results to arbitrary precision in some expansion (see e.g. [13]). Two main approaches can be distinguished regarding EFTs:

1. “*top-down*”: A high-energy theory is known, but a simpler theory at lower energy is useful by lowering the degrees of freedom and making computations more affordable. The desired precision is kept by going to a certain expansion order (e.g. **S**oft **C**ollinear **E**ffective **T**heory [14])
2. “*bottom-up*”: A fundamental physical theory is unknown, but one tries to get hints towards unknown effects or new physics by using the known symmetries, particles etc. of a theory and extrapolating by constructing operators with negligible effects at small scales and increasing importance at higher scales, thus showing the desired effects.

The SM itself belongs to the group of *bottom-up* EFTs in the sense that it is the most general theory incorporating quark and lepton fields with a single Higgs-doublet field, with operators of mass-dimension 4, solely constructed from products of the fields and their derivatives. Moreover they respect Lorentz invariance and  $SU(3)_C \times SU(2)_L \times U(1)_Y$  gauge symmetries. It is considered by many as an incomplete theory that, despite the tremendous precision in comparisons of predictions vs. measurements achieved so far, will not describe nature up to arbitrary energy scales  $\Lambda$ . Still, it is completely unclear at which scale new effects will appear, but the hope persists that they will be measurable at the Large Hadron Collider (LHC) or future particle colliders.

The EFT studied throughout this thesis also belongs to the *bottom-up* group and concentrates on alterations of the vector boson couplings compared to the SM. The desirable features of such an EFT can be summarized with the following statements [15]:

- The  $S$ -matrix should respect unitarity in the extended model.
- Lorentz invariance and the  $SU(3)_C \times SU(2)_L \times U(1)_Y$  gauge symmetries of the SM need to be respected.
- The theory should be model-independent in order to capture any beyond the SM physics, while still giving some guidance as to where new effects will appear and where they are arising from.
- Radiative corrections need to be calculable at any order in the SM- and the new interactions of the extended theory.

The framework considered in this thesis adds operators constructed from the Higgs-doublet, the covariant derivative and field strength tensors of the vector boson fields to the SM Lagrangian  $\mathcal{L}_{\text{SM}}$ , fulfilling the aforementioned features. These are represented in the form

$$\mathcal{L}_{\text{EFT}} = \mathcal{L}_{\text{SM}} + \sum_{n>2} \sum_i \frac{f_i}{\Lambda^{2n-4}} \mathcal{O}_i. \quad (3.1)$$

Only even dimensions are considered because otherwise baryon and lepton number conservation is not guaranteed [16]. The focus in this work will lie on the dimension 8 operators that affect vector boson couplings, i.e. products of the covariant derivative, the Higgs doublet and the field strength tensors of the vector boson fields. The full list of dimension 8 operators can be found in section 3.2, the dimension 6 operators are listed in appendix F.

### 3.1. Anomalous Couplings

There are two formalisms to describe anomalous couplings: the Lagrangian and the vertex function approach. In the following we will concentrate on the former and show the relations to the EFT approach.

As a first example we take the Lagrangian affecting the three-vector-boson-vertices [15]:

$$\begin{aligned} \mathcal{L}_{WWV}/g_{WWV} = & ig_1^V (W_{\mu\nu}^+ W^{-\mu} - W^{+\mu} W_{\mu\nu}^-) V^\nu + i\kappa_V W_\mu^+ W_\nu^- V^{\mu\nu} \\ & + i \frac{\lambda_V}{m_W^2} W_\mu^{+\nu} W_\nu^{-\rho} V_\rho^\mu + ig_4^V W_\mu^+ W_\nu^- (\partial^\mu V^\nu + \partial^\nu V^\mu) \\ & - ig_5^V \epsilon^{\mu\nu\rho\sigma} (W_\mu^+ \partial_\rho W_\nu^- - \partial_\rho W_\mu^+ W_\nu^-) V_\sigma \\ & + i\tilde{\kappa}_V W_\mu^+ W_\nu^- \tilde{V}^{\mu\nu} + i \frac{\tilde{\lambda}_V}{m_W^2} W_\mu^{+\nu} W_\nu^{-\rho} \tilde{V}_\rho^\mu, \end{aligned} \quad (3.2)$$

where  $V_\mu$  is either the Z-boson field  $Z$  or the photon field  $\gamma$ ,  $W_{\mu\nu}^\pm = \partial_\mu W_\nu^\pm - \partial_\nu W_\mu^\pm$ ,  $\tilde{V}_{\mu\nu} = \frac{1}{2}\epsilon_{\mu\nu\rho\sigma} V^{\rho\sigma}$  and the overall coupling constants  $g_{WWW} = -e$  and  $g_{WWZ} = e \cos \theta_W / \sin \theta_W$ . The Lagrangian is constructed in a way that it contains all possible Lorentz structures, only neglecting the scalar component

$$\partial_\mu V^\mu = 0, \quad \partial_\mu W^{\pm\mu} = 0, \quad (3.3)$$

which is automatically fulfilled in the on-shell case [17]. The last four terms in equation (3.2) violate either C- or P-invariance, while the first three keep both. Furthermore  $U(1)$  gauge invariance implies that  $g_1^\gamma = 1$  and  $g_4^\gamma = g_5^\gamma = 0$  [15]. We are therefore left with five independent CP-conserving parameters:  $g_1^Z, \kappa_\gamma, \kappa_Z, \lambda_\gamma, \lambda_Z$  and six either C- or P-violating ones  $g_4^Z, g_5^Z, \tilde{\kappa}_\gamma, \tilde{\kappa}_Z, \tilde{\lambda}_\gamma, \tilde{\lambda}_Z$ . Within the SM at tree level, we know the values of all these couplings. We have  $g_1^Z = \kappa_Z = \kappa_\gamma = 1$  and all other parameters equal to zero. Deviations from the SM can now in principle be measured in terms of deviations from those parameters.

Even though the Lagrangian approach can describe all trilinear vector boson couplings in a general way, it misses the convenient features of an EFT. First of all with the  $SU(2)_L \times U(1)_Y$  gauge symmetry being consistent with all experimental data, we need to incorporate it in a general approach of modeling BSM physics. It is known that the Lagrangian (3.2) can be interpreted as the unitary gauge expression of an effective Lagrangian respecting the gauge symmetries. Still, direct inspection of (3.2) shows that this feature is not present in an intuitive way [18]. Even more hurting is the fact that one could add an arbitrary number of terms of derivatives  $\partial_\mu$  of the fields to the Lagrangian. In order to keep the dimensions right, every factor of  $\partial_\mu$  would be accompanied by  $m_W^{-1}$ , which is the only mass

scale available in this setting. With  $m_W$  being the only energy scale inherent in the theory, terms of higher order are not suppressed at energies above  $m_W$  and therefore shouldn't be neglected [15]. This comes in contrast to the EFTs where every  $D_\mu$  is accompanied by a factor of  $\Lambda^{-1}$  which is independent of the SM scales and will therefore suppress higher order terms in the energy scales of interest.

With good reasons to stick to the approach of EFTs, we can still make use of the Lagrangian approach from above, because the two need not be complementary. If one is working in a well defined and complete set of operators it is a relatively easy task to express the anomalous couplings from above in terms of the effective couplings accompanying the operators. This is done by choosing a certain gauge and expanding the set of operators in terms of the fields. Then one can bring the result into the form of (3.2) and compare the coefficients multiplied to the fields. Working in the set of dimension 6 operators found in appendix F, the relations read

$$g_1^Z = 1 + \frac{f_W}{\Lambda^2} \frac{m_Z^2}{2}, \quad (3.4)$$

$$\kappa_\gamma = 1 + \left( \frac{f_W}{\Lambda^2} + \frac{f_B}{\Lambda^2} \right) \frac{m_Z^2}{2}, \quad (3.5)$$

$$\kappa_Z = 1 + \left( \frac{f_W}{\Lambda^2} - \frac{f_B}{\Lambda^2} \tan^2 \theta_W \right) \frac{m_Z^2}{2}, \quad (3.6)$$

$$\lambda_\gamma = \lambda_Z = \frac{f_{WWW}}{\Lambda^2} \frac{3g^2 m_W^2}{2}, \quad (3.7)$$

$$g_4^V = g_5^V = 0, \quad (3.8)$$

$$\tilde{\kappa}_\gamma = \frac{f_{\tilde{W}}}{\Lambda^2} \frac{m_W^2}{2}. \quad (3.9)$$

$$\tilde{\kappa}_Z = -\frac{f_{\tilde{W}}}{\Lambda^2} \tan^2 \theta_W \frac{m_W^2}{2}, \quad (3.10)$$

$$\tilde{\lambda}_\gamma = \tilde{\lambda}_Z = \frac{f_{\tilde{W}WW}}{\Lambda^2} \frac{3g^2 m_W^2}{2}. \quad (3.11)$$

In analogous way we are able to define a Lagrangian affecting the 4-vertices of the massive vector bosons.<sup>1</sup> Following the definitions of [19] we define this Lagrangian as

$$\begin{aligned} \mathcal{L}^{VV'V''} &= c_0^{WW} W_\mu^+ W^{-\mu} W_\nu^+ W^{-\nu} + c_1^{WW} W_\mu^+ W^{+\mu} W_\nu^- W^{-\nu} \\ &+ c_0^{WZ} W_\mu^+ Z^\mu W_\nu^- Z^\nu + c_1^{WZ} W_\mu^+ W^{-\mu} Z_\nu Z^\nu \\ &+ c^{ZZ} (Z_\mu Z^\mu)^2. \end{aligned} \quad (3.12)$$

The SM values of the couplings in this Lagrangian are

$$c_{0,\text{SM}}^{WW} = -c_{1,\text{SM}}^{WW} = \frac{2}{\cos^2 \theta_W} c_{0,\text{SM}}^{WZ} = -\frac{2}{\cos^2 \theta_W} c_{0,\text{SM}}^{WZ} = g^2, \quad c_{\text{SM}}^{ZZ} = 0, \quad (3.13)$$

where  $g$  is the electroweak coupling constant. Again we want to study deviations from these values and therefore define alterations  $\Delta c_i^{VV'}$  from these parameters by

$$c_i^{VV'} = c_{i,\text{SM}}^{VV'} + g^2 \Delta c_i^{VV'}. \quad (3.14)$$

We interpret the origin of these deviations as higher dimension operators representing the low energy effects of new physics at a higher scale. There are already dimension 6 operators

<sup>1</sup> the same is of course possible including the photon, but due to the complexity of the operator set affecting also those vertices, we leave them out at this point.

that affect the vector boson 4-vertices (see table F.1), but as we have seen before, these also affect the trilinear couplings. In order to model the 4-vertices in an independent way we need to add other operators. Moreover we can generally find stronger experimental constraints on dimension 6 operators via trilinear couplings, which need not constrain the 4-vertices. With the dimension 8 operators listed in the following section we are able to manage this independent description. Focusing on the effects of the two operators most relevant to this thesis (3.20), we list the relations between their coupling constants and the  $\Delta c_i^{VV'}$  [19]:

$$\begin{aligned}\Delta c_i^{WW} &= \frac{g^2 v^4}{8} \frac{f_{S,i}}{\Lambda^4}, \\ \Delta c_i^{WZ} &= \frac{g^2 v^4}{16 \cos^2 \theta_W} \frac{f_{S,i}}{\Lambda^4}, \\ \Delta c^{ZZ} &= \frac{g^2 v^4}{32 \cos^4 \theta_W} \frac{f_{S,0} + f_{S,1}}{\Lambda^4}.\end{aligned}\tag{3.15}$$

## 3.2. Dimension 8 Operators

The choice of a set of independent dimension 8 operators is not unique. A set that respects the  $SU(2)_L \times U(1)_Y$  gauge symmetry can be realized in different ways depending on the particle content of the effective Lagrangian. Including the Higgs Boson, one can find a *linear realization*, otherwise a *non-linear realization* is needed. The former is referred to as “decoupling physics”, because the scale of new physics can be arbitrarily large in this setting [18].

The set that is being used throughout this thesis is the linear realization and follows the definitions by Eboli et. al. [19]. They are expressed in terms of the Standard Model Higgs doublet  $\Phi$ , the covariant derivative  $D_\mu$  in a given representation of  $SU(2) \times U(1)$  and the field strength tensors  $W_{\mu\nu}$  for the  $SU(2)_L$  and  $B_{\mu\nu}$  for the  $U(1)_Y$  gauge fields. In unitary gauge they are defined as follows

$$\Phi = \frac{1}{\sqrt{2}} \begin{pmatrix} 0 \\ v + h \end{pmatrix},\tag{3.16}$$

$$D_\mu \equiv \partial_\mu + i\frac{g}{2}B_\mu + ig_w W_\mu^i \frac{\sigma^i}{2},\tag{3.17}$$

$$W_{\mu\nu} \equiv ig_w \frac{\sigma^i}{2} (\partial_\mu W_\nu^i - \partial_\nu W_\mu^i + g_w \epsilon_{ijk} W_\mu^i W_\nu^j),\tag{3.18}$$

$$B_{\mu\nu} \equiv i\frac{g}{2}(\partial_\mu B_\nu - \partial_\nu B_\mu),\tag{3.19}$$

where  $\sigma^i/2$  are the generators of the  $SU(2)_L$ .

In this work we will concentrate on the effects of dimension 8 operators, the reason being that these only affect the quartic gauge couplings other than the dimension 6 operators, that also give rise to anomalous triple gauge couplings (ATGC) so the effects on anomalous quartic gauge couplings (AQGC) and ATGCs can not be treated separately (see table F.1). Another reason is that with the latter a full study of every possible gauge boson coupling is not possible, because they do not contain AQGCs among the neutral gauge bosons [16]. Therefore the dimension 8 operators serve as a tool to genuinely model potential deviations of all possible quartic gauge couplings from the SM without having a prejudice on their size

or origin in the first place. For completeness a complete list of the dimension 6 operators can be found in the appendix F. The set of dimension 8 operators can be divided into three classes:

1. Operators built solely from the Higgs doublet and the covariant derivative:

$$\mathcal{O}_{S,0} = [(D_\mu \Phi)^\dagger D_\nu \Phi] \times [(D^\mu \Phi)^\dagger D^\nu \Phi] \quad (3.20a)$$

$$\mathcal{O}_{S,1} = [(D_\mu \Phi)^\dagger D^\mu \Phi] \times [(D_\nu \Phi)^\dagger D^\nu \Phi] \quad (3.20b)$$

This class of operators leads to AQGCs for the massive vector bosons only (the  $WWWW$ ,  $WWZZ$  and  $ZZZZ$  vertices). Moreover the amplitudes arising from  $\mathcal{L}_{S,0}$  and  $\mathcal{L}_{S,1}$  only contain polarization vectors and no momenta. This leads to a great importance of longitudinally polarized particles which will be further discussed in chapter 4.

2. Operators built from field strength tensors, the Higgs doublet and the covariant derivative:

$$\mathcal{O}_{M,0} = \text{Tr}[W_{\mu\nu} W^{\mu\nu}] \times [(D_\beta \Phi)^\dagger D^\beta \Phi] \quad (3.21a)$$

$$\mathcal{O}_{M,1} = \text{Tr}[W_{\mu\nu} W^{\nu\beta}] \times [(D_\beta \Phi)^\dagger D^\mu \Phi] \quad (3.21b)$$

$$\mathcal{O}_{M,2} = [B_{\mu\nu} B^{\mu\nu}] \times [(D_\beta \Phi)^\dagger D^\beta \Phi] \quad (3.21c)$$

$$\mathcal{O}_{M,3} = [B_{\mu\nu} B^{\nu\beta}] \times [(D_\beta \Phi)^\dagger D^\mu \Phi] \quad (3.21d)$$

$$\mathcal{O}_{M,4} = [(D_\mu \Phi)^\dagger W_{\beta\nu} D^\mu \Phi] \times B^{\beta\nu} \quad (3.21e)$$

$$\mathcal{O}_{M,5} = [(D_\mu \Phi)^\dagger W_{\beta\nu} D^\nu \Phi] \times B^{\beta\mu} \quad (3.21f)$$

$$\mathcal{O}_{M,6} = [(D_\mu \Phi)^\dagger W_{\beta\nu} W^{\beta\nu} D^\mu \Phi] \quad (3.21g)$$

$$\mathcal{O}_{M,7} = [(D_\mu \Phi)^\dagger W_{\beta\nu} W^{\beta\mu} D^\nu \Phi] \quad (3.21h)$$

The structure of these operators leads to amplitudes where a mixture of transverse and longitudinal polarizations plays the most important role.

3. Operators containing only field strength tensors:

$$\mathcal{O}_{T,0} = \text{Tr}[W_{\mu\nu} W^{\mu\nu}] \times \text{Tr}[W_{\alpha\beta} W^{\alpha\beta}] \quad (3.22a)$$

$$\mathcal{O}_{T,1} = \text{Tr}[W_{\alpha\nu} W^{\mu\beta}] \times \text{Tr}[W_{\mu\beta} W^{\alpha\nu}] \quad (3.22b)$$

$$\mathcal{O}_{T,2} = \text{Tr}[W_{\alpha\mu} W^{\mu\beta}] \times \text{Tr}[W_{\beta\nu} W^{\nu\alpha}] \quad (3.22c)$$

$$\mathcal{O}_{T,5} = \text{Tr}[W_{\mu\nu} W^{\mu\nu}] \times B_{\alpha\beta} B^{\alpha\beta} \quad (3.22d)$$

$$\mathcal{O}_{T,6} = \text{Tr}[W_{\alpha\nu} W^{\mu\beta}] \times B_{\mu\beta} B^{\alpha\nu} \quad (3.22e)$$

$$\mathcal{O}_{T,7} = \text{Tr}[W_{\alpha\mu} W^{\mu\beta}] \times B_{\beta\nu} B^{\nu\alpha} \quad (3.22f)$$

$$\mathcal{O}_{T,8} = B_{\mu\nu} B^{\mu\nu} B_{\alpha\beta} B^{\alpha\beta} \quad (3.22g)$$

$$\mathcal{O}_{T,9} = B_{\alpha\mu} B^{\mu\beta} B_{\beta\nu} B^{\nu\alpha} \quad (3.22h)$$

In this class only transverse polarizations are of importance. One also can see that the first three operators of this class affect all vector bosons, while the last two only lead to AQGC's for the neutral electroweak gauge bosons [16].

The contributions of the whole set of operators to the various 4-vertices are listed in table 3.1.

All of the operators listed above are fully implemented in VBFNLO, where their effects on processes containing QGC's like  $pp \rightarrow ZZjj \rightarrow e^+ e^- \mu^+ \mu^- jj$  can be studied in the form of distributions or in calculating the total cross section for a specific c.o.m. energy  $\sqrt{s}$  to high accuracy.

	WWWW	WWZZ	ZZZZ	WWAZ	WWAA	ZZZA	ZZAA	ZAAA	AAAA
$\mathcal{O}_{S,0}, \mathcal{O}_{S,1}$	X	X	X						
$\mathcal{O}_{M,0}, \mathcal{O}_{M,1}, \mathcal{O}_{M,6}, \mathcal{O}_{M,7}$	X	X	X	X	X	X	X		
$\mathcal{O}_{M,2}, \mathcal{O}_{M,3}, \mathcal{O}_{M,4}, \mathcal{O}_{M,5}$		X	X	X	X	X	X		
$\mathcal{O}_{T,0}, \mathcal{O}_{T,1}, \mathcal{O}_{T,2}$	X	X	X	X	X	X	X	X	X
$\mathcal{O}_{T,5}, \mathcal{O}_{T,6}, \mathcal{O}_{T,7}$		X	X	X	X	X	X	X	X
$\mathcal{O}_{T,8}, \mathcal{O}_{T,9}$			X			X	X	X	X

Table 3.1.: This table shows which operators affect which QGC for the various vector bosons.

### 3.3. Redefinition of $\mathcal{L}_{S,0}$

Aside from the operator definitions used by Eboli et. al. there is another set of operators commonly used for studying AQC-effects on the massive electroweak gauge bosons. These are part of the non-linear realization, which means that only would-be Goldstone bosons are included in the theory. With no Higgs boson included one can in contrast to the linear realization find a scale at which new physics should appear. This would roughly be around the scale  $\Lambda \lesssim 4\pi v$  [18].

A set of operators of the non-linear realization is implemented in the WHIZARD event generator [9, 6] and reads

$$\mathcal{L}_4 = \alpha_4 [\text{Tr}(\mathbf{V}_\mu \mathbf{V}_\nu)]^2 \quad (3.23)$$

$$\mathcal{L}_5 = \alpha_5 [\text{Tr}(\mathbf{V}_\mu \mathbf{V}^\mu)]^2 \text{ with } \mathbf{V}_\mu = \Sigma D_\mu \Sigma. \quad (3.24)$$

There is no one-to-one correspondence of  $\mathcal{L}_4$  and  $\mathcal{L}_5$  to the operators of Eboli et. al., but a vertex specific conversion of the couplings is possible and reads [16]:

- WWW - Vertex:

$$\alpha_4 = \frac{f_{S,0} v^4}{\Lambda^4 8}; \quad \alpha_4 + 2\alpha_5 = \frac{f_{S,1} v^4}{\Lambda^4 8} \quad (3.25)$$

- WWZZ - Vertex:

$$\alpha_4 = \frac{f_{S,0} v^4}{\Lambda^4 16}; \quad \alpha_5 = \frac{f_{S,1} v^4}{\Lambda^4 16} \quad (3.26)$$

- ZZZZ - Vertex:

$$\alpha_4 + \alpha_5 = \left( \frac{f_{S,0}}{\Lambda^4} + \frac{f_{S,1}}{\Lambda^4} \right) \frac{v^4}{16} \quad (3.27)$$

The difference in the two sets of operators lies in the structure of  $\mathcal{L}_4$  and  $\mathcal{L}_{S,0}$ . The former is symmetric in the Lorentz-indices  $\mu$  and  $\nu$  while the latter is not. Strictly speaking,  $\mathcal{L}_{S,0}$  is not self-adjoint which it should be in order to guarantee the reality of the interaction Lagrangian. This problem can be easily cured by symmetrizing the operator:

$$\mathcal{L}'_{S,0} = \frac{1}{2} [(D_\mu \Phi)^\dagger D_\nu \Phi] \times \left( \frac{f'_{S,0}}{\Lambda^4} [(D^\mu \Phi)^\dagger D^\nu \Phi] + \frac{f'^*_{S,0}}{\Lambda^4} [(D^\nu \Phi)^\dagger D^\mu \Phi] \right) \quad (3.28)$$

By choosing  $f'_{S,0} \in \mathbb{R}$  one gets an operator completely equivalent to  $\mathcal{L}_4$  in terms of the AQC-contributions of the electroweak gauge bosons. Now the conversion of the couplings for all vertices reads:

$$\alpha_4 = \frac{f'_{S,0} v^4}{\Lambda^4 16}; \quad \alpha_5 = \frac{f_{S,1} v^4}{\Lambda^4 16}. \quad (3.29)$$

Throughout this thesis it will be convenient in some places to work with a different set of operators. This other set consists of the well known  $\mathcal{L}_{S,0}$  and  $\mathcal{L}_{S,1}$  plus another operator that facilitates the comparison to  $\mathcal{L}_4$  and  $\mathcal{L}_5$ . The extra operator is

$$\mathcal{L}_{S,2} = \frac{f_{S,2}}{\Lambda^4} [(D_\mu \Phi)^\dagger D_\nu \Phi] \times [(D^\nu \Phi)^\dagger D^\mu \Phi], \quad (3.30)$$

which has the same structure as  $\mathcal{L}_{S,0}$ , only with the last two Lorentz-indices interchanged. Using the new set  $\mathcal{L}_{S,0} + \mathcal{L}_{S,1} + \mathcal{L}_{S,2}$  it is easier to compare to  $\mathcal{L}_4 + \mathcal{L}_5$  and keeping the possibility to recover the original operator list of Eboli et. al. Note that this set is equivalent to  $\mathcal{L}'_{S,0} + \mathcal{L}_{S,1}$  when choosing  $f_{S,0} = 2f'_{S,0}$  and  $f_{S,2} = f'^*_{S,0}$ .

In order to compare the results using this new set to the result one gets from  $\mathcal{L}_4 + \mathcal{L}_5$ , one simply needs to choose

$$f_{S,2} = f_{S,0}, \quad (3.31)$$

where the couplings are treated as real numbers, and use the replacement

$$f_{S,0} = 8\alpha_4 \frac{\Lambda^4}{v^4}; \quad f_{S,1} = 16\alpha_5 \frac{\Lambda^4}{v^4}. \quad (3.32)$$

Note that the relative factor of 2 between the two replacements is resulting from taking the sum of the three operators in this case, instead of introducing a factor 1/2 as in the case of  $\mathcal{L}'_{S,0}$ . If one wants to return to the results from the original set of Eboli et.al. it is sufficient to set  $f_{S,2} = 0$ .

The symmetrized form of  $\mathcal{L}_{S,0}$  could make the two Monte-Carlo event generators VBFNLO and WHIZARD more easily comparable in terms of corrections to the electroweak 4-vertices. Not least is this an important fact for experimentalists in order to have an easy cross-check for bounds on anomalous couplings when comparing data to theoretical predictions. Still, in the implementation to be explained in chapter 6 the original set of operators from Eboli et.al. has been used, as they have already been part of VBFNLO and so that confusion about yet another set of operators can be avoided. The comparison to WHIZARD is still possible, because the conversion (3.25, 3.26, 3.27) has been used.



# Unitarisation

## 4.1. Motivation

The term *unitarisation* describes different procedures that are applied to effective field theories in order to suppress their unphysical behavior at high center of mass energies. All dimension 8 operators, especially the ones considered in this thesis, break tree-level unitarity at different energy scales. This does not necessarily mean that the EFT approach itself is unphysical, but rather that the effective theory is incomplete. Not knowing a self consistent theory of new physics, one can still get relevant hints for new physics from these dimension 8 operators by suppressing their unphysical high energy behavior by hand.

The values for the electroweak 4-vertices are well known within the SM but have not been accurately measured so far, which will change in the upcoming runs of the LHC. This means that there is some room for deviations that could well be modeled by the dimension 8 operators, say if there was an unexpected enhancement in the production of Z-boson pairs. Without unitarisation any fit of AGCs to that kind of data would effectively yield that the anomalous couplings need to be zero, because even for small values of the couplings the high energy tails e.g. in invariant mass distributions would give far too high results. Figure 4.1 makes this point clearer. It exemplarily shows anomalous contributions of different operator types in the process  $W^+W^+ \rightarrow W^+W^+$  in an energy range that is well within the reach e.g. of the Large Hadron Collider. The large contributions in the high energy regime would also force the constraints on the couplings to zero. Therefore this behavior needs to be suppressed while keeping the low energy effects arising from the dimension 8 operators that could describe the aforementioned deviations. Finally this might yield hints at where to look for and how to model new physics phenomena.

## 4.2. Historic Examples

In order to justify the subject of unitarisation from a historic perspective, two examples that show vividly what is meant by this term and moreover give good reason to believe this is a well justified procedure are given below.

### 4.2.1. Fermi's Interaction

The term *Fermi Interaction* stands for an effective theory developed by Enrico Fermi in 1933 describing beta decay. Fermi was able to describe the process  $n \rightarrow p + \bar{\nu}_e + e^-$  to a high level of precision in proposing a 4-point fermion interaction with coupling constant  $G_F$ . Taking a look at the unit of  $[G_F] = \text{GeV}^{-2}$  already reveals the resemblance to other EFTs.

The numerical value for Fermi's coupling constant is [20]

$$\frac{G_F}{\sqrt{2}} = \frac{g^2}{8m_W^2} = 1.166\,378\,7(6) \times 10^{-5} \text{ GeV}^{-2}. \quad (4.1)$$

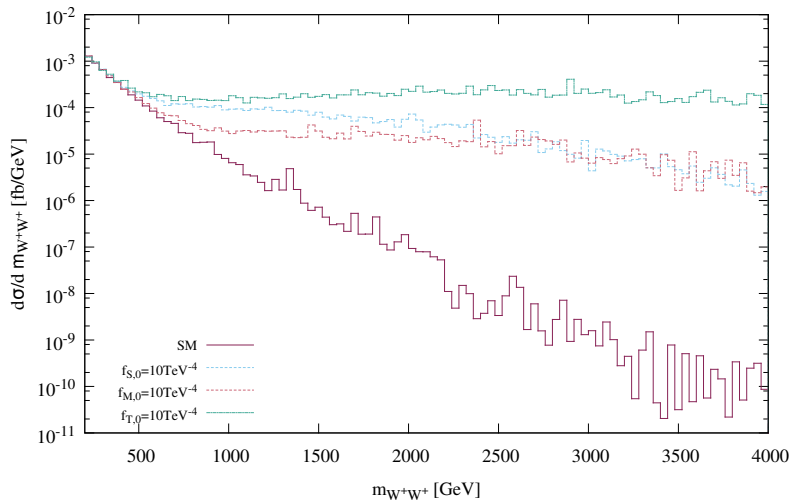


Figure 4.1.: Invariant mass spectrum of the process  $W^+W^+ \rightarrow W^+W^+$ . The solid violet line shows the SM case, the other lines represent different anomalous contributions without unitarisation. (only low statistics have been used in the generation of this plot, because only the qualitative behavior is of interest at this point)

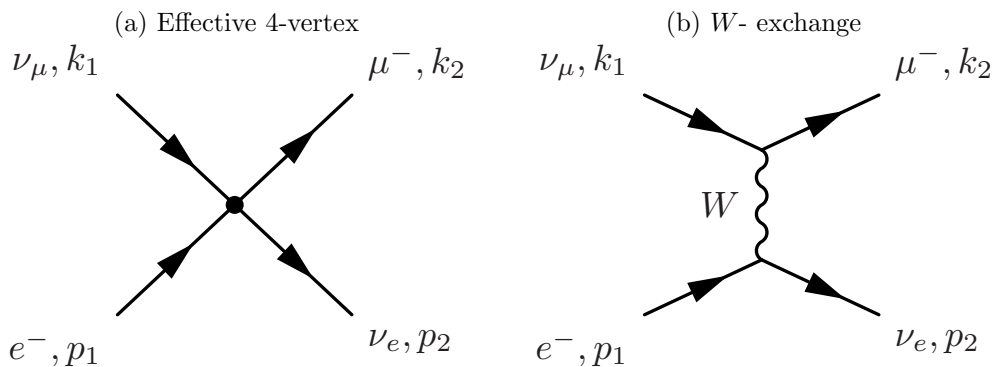


Figure 4.2.:  $\mu^-e^-$  conversion via an effective 4-vertex or the exchange of a massive  $W$  boson.

Instead of the beta decay a similar process will be studied in the following, showing the problems arising from this effective theory and how it was cured later on. The derivation follows the one in [11].

Proposing a 4-point fermion interaction in electron-neutrino scattering ( $e^- + \nu_\mu \rightarrow \mu^- + \nu_e$ ) results in the Feynman diagram 4.2a. It represents the matrix element

$$\mathcal{M} = \frac{G_F}{\sqrt{2}} \bar{u}(k_2) \gamma_\mu (1 - \gamma_5) u(k_1) g^{\mu\nu} \bar{u}(p_2) \gamma_\nu (1 - \gamma_5) u(p_1). \quad (4.2)$$

The generic formula for the unpolarized differential cross section of an elastic  $2 \rightarrow 2$  process is

$$\frac{d\sigma}{dt} = \frac{1}{16\pi s^2} |\overline{\mathcal{M}}|^2, \quad (4.3)$$

where  $s$  and  $t$  are the standard Mandelstam variables and  $|\overline{\mathcal{M}}|^2$  is the spin averaged matrix element squared. In order to calculate the latter one needs to average over polarization states of the incoming electron (factor 1/2) and sum over the polarizations of the outgoing muon. No averaging over the initial state neutrinos is needed, because their only production mechanism is the weak interaction where only left-handed neutrinos take part. The

sum over final state polarizations of the  $\nu_e$  can be included facilitating the calculation by reducing the result to a product of traces. Still it is guaranteed that only the left-handed neutrinos contribute because of the factor  $(1 - \gamma_5)$ . We then have, neglecting the fermion masses

$$|\overline{\mathcal{M}}|^2 = \frac{G_F^2}{2} \text{Tr}[k_2 \gamma_\mu (1 - \gamma_5) k_1 \gamma_\nu (1 - \gamma_5)] \frac{1}{2} \text{Tr}[\not{p}_2 \gamma^\mu (1 - \gamma_5) \not{p}_1 \gamma^\nu (1 - \gamma_5)]. \quad (4.4)$$

After quite some  $\gamma$ -matrix algebra, contracting the resulting products of momenta, inserting Mandelstam variables and using the massless limit, where  $s + t + u = 0$ , one arrives at the simple result

$$\frac{d\sigma}{dt} = \frac{1}{16\pi s^2} \frac{G_F^2}{2} 32s^2 = \frac{G_F^2}{\pi}. \quad (4.5)$$

This in turn leads to a total cross section that rises linearly with the center of mass energy squared  $s$ , i.e.

$$\sigma_{\text{tot}} = \frac{G_F^2}{\pi} s, \quad (4.6)$$

which would lead to the violation of unitarity when  $\sqrt{s}$  is at the order of a few hundred GeV. This shows that despite the well behaved low energy regime, the effective 4-fermion-coupling cannot be used up to arbitrary energies. It turned out that the missing piece of the theory is a heavy particle serving as the mediator of the weak force, the  $W$ -boson. Assuming that the force mediator is a vector boson as in QED, one can insert the corresponding propagator and couplings into the matrix element arriving at

$$\mathcal{M} = \frac{g^2}{2} \bar{u}(k_2) \gamma_\mu \frac{(1 - \gamma_5)}{2} u(k_1) \frac{g^{\mu\nu} - q^\mu q^\nu / m_W^2}{q^2 - m_W^2} \bar{u}(p_2) \gamma_\nu \frac{(1 - \gamma_5)}{2} u(p_1), \quad (4.7)$$

or in the form of a Feynman diagram (figure 4.2b). In the limit  $q^2 \ll m_W^2$  the  $W$ -propagator reduces to

$$-\frac{1}{q^2 - m_W^2} = \frac{1}{m_W^2} + \mathcal{O}\left(\frac{q^2}{m_W^2}\right), \quad (4.8)$$

and the  $q^\mu q^\nu / m_W^2$  part of the numerator can be neglected. Therefore the matrix element 4.7 reduces to 4.2 giving an exact definition of  $G_F$  in terms of a weak coupling constant  $g_w$  and the mass of the  $W$ -boson  $m_W^2$ , i.e.

$$\frac{G_F}{\sqrt{2}} = \frac{g_w^2}{8m_W^2}, \quad (4.9)$$

which also makes clear where the dimension of Fermi's coupling constant is resulting from. Moreover it shows the interesting fact that the weakness in the weak force does not necessarily result from a small coupling, but rather from a heavy force mediator. We now know that the weak coupling constant has a value of  $g_w \simeq 0.6530$  which is of the same order as the electromagnetic coupling constant  $e$ .

We have seen now that the inclusion of the  $W$ -boson leaves the low energy regime as it was, while for energies  $q^2 \gtrsim m_W^2$  the  $W$ -propagator serves as a suppression factor that guarantees unitarity. This is an example of the unitarisation of an effective theory via the well-known ultraviolet completion of the model.

#### 4.2.2. Scattering of Longitudinally Polarized Massive Vector Bosons

Although the inclusion of a massive vector boson saves unitarity in the process above, it generates new divergencies in other processes. Massive vector bosons and their interactions can be included in a QFT formalism via the Glashow-Weinberg-Salam model. This model

includes self-interactions among the vector bosons, which could in principle lead to an unphysical high energy behavior in the scattering of longitudinally polarized massive vector bosons.

Massive vector bosons have an extra degree of freedom compared to the physically allowed polarizations of the photon, which is a longitudinal polarization state. From the equation of motion of a massive vector field  $A_\mu(x)$  we find that the 4-divergence of this field needs to vanish, i.e.

$$\partial^\mu A_\mu = 0. \quad (4.10)$$

Inserting a plane-wave ansatz for the vector field into this equation leads to the constraining equation for the polarization vectors  $\epsilon_\mu^{(\lambda)}$  of the field, sometimes called transversality condition,

$$k^\mu \epsilon_\mu^{(\lambda)} = 0, \quad (4.11)$$

leaving us with three degrees of freedom, i.e. three linearly independent polarization vectors. Another constraint that the polarization vectors need to fulfill is their normalization to

$$\epsilon_\mu^{(\lambda)} (\epsilon^{(\lambda')\mu})^* = -\delta_{\lambda\lambda'}. \quad (4.12)$$

This is seen by going to a frame where  $k^\mu$  is time-like, i.e.  $k^\mu = (m_V, 0, 0, 0)$ , transversality still needs to hold. Therefore the polarization vectors can only be space-like and have a negative norm.

By choosing  $k^\mu$  along the 3-direction as  $k^\mu = (E_k, 0, 0, k)$ , we may set the polarization vectors as

$$\epsilon_1^\mu = \begin{pmatrix} 0 \\ 1 \\ 0 \\ 0 \end{pmatrix}, \quad \epsilon_2^\mu = \begin{pmatrix} 0 \\ 0 \\ 1 \\ 0 \end{pmatrix}, \quad \epsilon_3^\mu = \frac{1}{m_V} \begin{pmatrix} k \\ 0 \\ 0 \\ E \end{pmatrix}, \quad (4.13)$$

where  $k = \sqrt{E^2 - m_V^2}$ . In order to work in a basis of helicity eigenstates we may transform the above set to an equivalent one while ensuring the transversality relation and the normalization condition still hold:

$$\epsilon_\pm^\mu = \frac{1}{\sqrt{2}} (\mp \epsilon_1^\mu - i \epsilon_2^\mu) = \frac{1}{\sqrt{2}} (0, \mp 1, -i, 0) \quad (4.14)$$

$$\epsilon_L^\mu = \epsilon_3^\mu. \quad (4.15)$$

The definitions of polarization vectors for arbitrary momenta  $k^\mu$  that has been used throughout this thesis can be found in the appendix D.

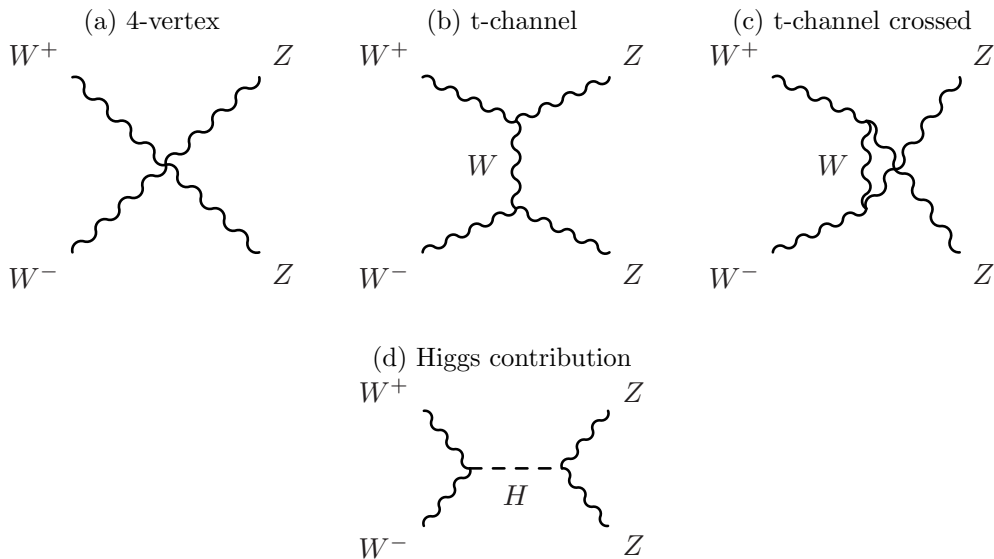
We are now interested in the high energy behavior of processes that include the self-couplings of massive vector bosons. An instructive example is the vector boson fusion process  $W^+W^- \rightarrow ZZ$ . The process consists of the diagrams in fig. 4.3.

The amplitude for process 4.3a reads

$$\mathcal{M}_1 = g_w \cos^2(\theta_W) (\epsilon_1 \cdot \epsilon_4^* \epsilon_2 \cdot \epsilon_3^* + \epsilon_1 \cdot \epsilon_3^* \epsilon_2 \cdot \epsilon_4^* - 2\epsilon_1 \cdot \epsilon_2 \epsilon_3^* \cdot \epsilon_4^*), \quad (4.16)$$

where  $g_w$  is the weak coupling constant and  $\theta_W$  the Weinberg angle. Only polarization vectors appear in this amplitude. By looking at definition (4.13) and (4.14) one sees that only the longitudinal polarization carries an energy dependence that will be translated to the above amplitude. To find out more about the energy dependence of this amplitude in the high energy regime where  $E \gg m_V$ , we now expand  $\epsilon_L^\mu(k)$  in terms of  $\mathcal{O}(m_V/E)$ , i.e.

$$k = \sqrt{E^2 - m_V^2} = E \sqrt{1 - \left(\frac{m_V}{E}\right)^2} = E + \mathcal{O}\left(\frac{m_V^2}{E^2}\right), \quad (4.17)$$

Figure 4.3.: Diagrams contributing to the process  $W^+W^- \rightarrow ZZ$ 

and see that  $\epsilon_L^\mu(k)$  becomes increasingly parallel to  $k^\mu$  componentwise, i.e.

$$\epsilon_L^\mu(k) = \frac{k^\mu}{m} + \mathcal{O}\left(\frac{m}{E}\right). \quad (4.18)$$

Inserting this into amplitude (4.16) and replacing the dot-products of the momenta by the corresponding Mandelstam variables, one finds a quadratic rise of the amplitude in  $s$ . Fortunately this divergence is exactly canceled by the two contributions that result from the vector boson 3-vertices, but the theory is still endangered by a remaining contribution that grows like  $s$ . As it turned out this behavior is nicely cured by the inclusion of the Higgs mechanism, which imposes an extra graph to the  $W^+W^- \rightarrow ZZ$  process (fig. 4.3d).

The accompanying amplitude reads

$$\mathcal{M}_H = \frac{2m_W^2 m_Z^2}{v^2} \frac{(\epsilon_1 \cdot \epsilon_2)(\epsilon_3^* \cdot \epsilon_4^*)}{q^2 - m_H^2}, \quad (4.19)$$

where  $v$  is the vacuum expectation value of the Higgs field and  $q^2 = (p_1 + p_2)^2$ . Like before we insert longitudinal polarization vectors and arrive at

$$\mathcal{M}_H = -\frac{1}{v^2} \frac{s^2}{s - m_H^2} + \mathcal{O}(1). \quad (4.20)$$

In the regime where  $s \gg m_H^2$  the divergence resulting from graphs 4.3b and 4.3c is canceled by the amplitude we just calculated. Therefore with the matrix element altogether being constant in the high energy limit, unitarity is finally restored.

Returning to the subject of unitarisation, one sees from the above examples how the inclusion of new particles can cure an unphysical high energy behavior. The problem about this procedure is that one has to impose a very specific model that should better turn out as being natural in the end. Nowadays we are confident about the existence of the massive vector bosons as well as the Higgs particle, but in order to study deviations from the SM via the EFT approach, we do not want to assume the existence of specific types of new particles in order to cure the unphysical high energy behavior of every part of the theory. Instead we try to cure it in a *model independent* way. The methods of the following sections show how this can be achieved.

To some these methods might seem to be based on a hand-waving arguments, but they are just tools to achieve what we want to see: low energy effects of a theory unknown at some higher energy scale  $\Lambda$ . If this scale was at the order of a few TeV, i.e. within the LHC range, we might be able to describe deviations from the SM below that scale, but not without curing the unphysical behavior by hand.

## 4.3. Form Factors

### 4.3.1. General Remarks

One of the simplest ways to guarantee unitarity in the framework of effective field theories beside simple cut-off functions, is the use of a so called *form factor*  $\mathcal{F}(s)$ .

$$\mathcal{F}(s) = \frac{1}{(1 + s/\Lambda_{FF}^2)^n}. \quad (4.21)$$

This function gets multiplied to the couplings  $f_i$  and suppresses the high energy tail of amplitudes arising from the operators of an EFT. The choice of the form factor structure is pretty much arbitrary. The form shown in here is chosen in order to resemble the propagators one would get by introducing new particles (which have been shown to potentially cancel the unwanted high energy behavior in 4.2.2).

At a certain energy scale  $\Lambda_{FF}$  the suppression sets in and depending on  $n$  either pushes the amplitudes to 0, or lets them saturate at some bounding amplitude value for very high energies. A typical value for a dimension 8 operator is  $n = 2$  which is due to the quadratic rise in  $s$  of the 0th partial wave of the helicity amplitude in at least one of the combinations of polarizations that the in- and outgoing vector bosons can have. In this way the amplitude gets suppressed by  $s^{-2}$  for energies  $\sqrt{s} \gtrsim \Lambda_{FF}$ .

In figure 4.4 the shapes of form factors with different input parameters are shown. Other than a step function  $\Theta(\Lambda^2 - s)$  one sees a very smooth transition from 1 to 0 independent of these parameters. Another property is that the suppression starts already at relatively small values of  $s$  which will be an important point in comparing form factors to other unitarisation methods in section 7.3.

Though form factors can be used as a simple approach for guaranteeing unitarity, it inherits the problem of fine-tuning  $\Lambda_{FF}$  for a chosen  $n$ , depending on the strength of the couplings. One can get adequate values for these parameters in a partial wave expansion of the amplitudes arising from the EFT. By virtue of the unitarity of the  $S$ -matrix (see section 4.5.1) the real parts of these partial waves exhibit an upper bound that represents the bound for the violation of unitarity. This upper bound can be calculated depending on the values of the couplings  $\{f_i\}$  and used to set the energy scale and exponent of the form factor.

The form factor as described above is fully implemented into VBFNLO. For the calculation of  $\Lambda_{FF}$  for a chosen  $n$  there exists an external program `calc_formfactor` [21, 22]. The unitarity bound is determined via a partial wave analysis. The non-unitarized 0th partial waves of all eligible  $VV \rightarrow VV$  processes for different sets of polarization combinations are calculated. Then all contributions are used for the analysis via diagonalizing the resulting  $T$ -matrix. Using the eigenvalues as upper bounds for the partial waves,  $\Lambda_{FF}$  gets determined by trying out one value at a time, multiplying the corresponding form factor to the amplitudes and see whether the suppression is sufficient in order not to cross the upper bound. This procedure is then repeated until a small enough  $\Lambda_{FF}$  is found in order to stay below this bound.

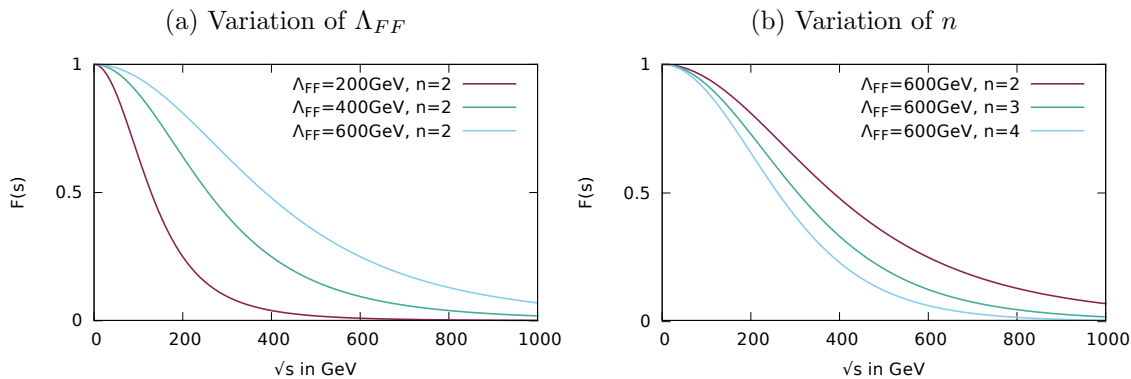


Figure 4.4.: Form factor  $\mathcal{F}(s)$  for different choices of the energy scale and exponent.

### 4.3.2. Energy Scale $\Lambda_{FF}$

As stated above, so far the values for  $\Lambda_{FF}$  need to be calculated in a relatively involved way, i.e. a partial wave analysis in a numerical Fortran routine. To this point this can not be avoided completely, but it can be shown that the calculation for one value of a coupling  $f_i \neq 0$  is sufficient to determine the values for all other sizes of the same coupling.

As will be shown later, the partial waves giving the strongest contributions to the violation of unitarity are all of the same simple form (as long as we only look at one  $f_i \neq 0$  at a time). Neglecting all terms  $s^k$  with  $k < 2$  this general form is

$$A^{J=0}(s) = c_{J=0,i} \frac{f_i}{\Lambda^4} s^2, \quad (4.22)$$

where the  $c_{J,i}$  are some numerical constants that one gets from a partial wave analysis. If we want to determine the center of mass energy  $\sqrt{s_{\max}}$  where unitarity would be broken, we set  $A^{J=0}(s_{\max}) = A_{\text{bound}}^1$ .

In order to get a reasonable value for  $\Lambda_{FF}$ , we now multiply the form factor  $\mathcal{F}$  to the amplitude, i.e.

$$A^{J=0}(s)\mathcal{F}(s) = c_{J=0,i} \frac{f_i}{\Lambda^4} \frac{s^2}{(1 + s/\Lambda_{FF}^2)^n}, \quad (4.23)$$

and look for its absolute maximum. This maximum will be at

$$s_{\max} = \frac{\Lambda_{FF}^2}{n/2 - 1}. \quad (4.24)$$

If we insert this back, we find

$$A^{J=0}(s_{\max})\mathcal{F}(s_{\max}) = c_{J=0,i} \frac{f_i}{\Lambda^4} \left(\frac{n}{2}\right)^{-n} \left(\frac{n}{2} - 1\right)^{n-2} \Lambda_{FF}^4. \quad (4.25)$$

Note that the exponent of  $\Lambda_{FF}$  is independent of  $n$ . In order to find a proper  $\Lambda_{FF}$  that guarantees unitarity one will now set (4.25) equal to some bound  $A_{\text{bound}}$ . This bound is set independent of the coupling, so if we take the ratio of the right side of (4.25) for one value of the coupling over the same thing for another coupling size, we will find by solving for the ratio of the form factor energy scales

$$\frac{\Lambda_{FF,1}}{\Lambda_{FF,2}} = \left(\frac{f_{i,1}}{f_{i,2}}\right)^{-\frac{1}{4}}. \quad (4.26)$$

<sup>1</sup>Typically one chooses  $A_{\text{bound}} = 16\pi$ . See section 4.5.2 for details.

This means if one  $\Lambda_{FF}$  is fixed for one specific value of a coupling  $f_{i,1}$ , then all others can be determined via (4.26). This relation has been checked against the table found in [21], appendix B.4, that shows  $\Lambda_{FF}$  values for all dimension 8 operators,  $n = 2$  and various coupling sizes all determined via the aforementioned Fortran routine. Accordance of  $\lesssim 4\%$  was found when taking the first or last column as input.

#### 4.4. Replacement of Mandelstam variables

Throughout this thesis it will often be necessary to replace Mandelstam variables by some angular dependence and vice versa. A priori the replacements are not as trivial as one might expect, which is why a few thoughts and definitions on this subject are concluded in this section.

Only  $2 \rightarrow 2$  processes have been studied in this thesis in terms of unitarity considerations. Therefore the only definitions of Mandelstam variables for the processes of the form  $V(k_1) + V(k_2) \rightarrow V(k_3) + V(k_4)$  needed are

$$s = (k_1 + k_2)^2 = (k_3 + k_4)^2, \quad (4.27)$$

$$t = (k_1 - k_3)^2 = (k_2 - k_4)^2, \quad (4.28)$$

$$u = (k_1 - k_4)^2 = (k_2 - k_3)^2, \quad (4.29)$$

where the  $k_i$  are the momenta of the four vector bosons in the processes under consideration. One relation that we will particularly often make use of is

$$s + t + u = \sum_{i=1}^4 m_i^2. \quad (4.30)$$

This relation is true in the case of  $2 \rightarrow 2$  scattering processes, obviously in any reference frame and just a consequence of the definition of the Mandelstam variables and 4-momentum conservation. The energy range of interest in this thesis furthermore allows to set the masses to zero, so we arrive at

$$s + t + u = 0. \quad (4.31)$$

In order to justify this, take a look at a typical unitarity bounds from a partial wave analysis. Taking the result 4.90a and using the unitarity bound  $|\Re[A_{IJ}(s)]| \leq 16\pi$ , the energy at which unitarity is broken is

$$\sqrt{s} = \left( \frac{96\pi}{7\frac{f_{S,0}}{\Lambda^4} + 11\frac{f_{S,1}}{\Lambda^4}} \right)^{\frac{1}{4}}. \quad (4.32)$$

Using typical values for the couplings of  $f_{S,i}/\Lambda^4 = 10 \text{ TeV}^{-4}$  results in

$$\sqrt{s} \simeq 1138 \text{ GeV}. \quad (4.33)$$

This means we end up with an error of  $\approx 2\%$  in (4.31) if we compare the sum of the W-boson masses squared to this energy squared which seems like a reasonable approximation.

In order to calculate the on-shell scattering amplitudes for the partial wave analyses, the center of mass frame of the incoming two particles has been chosen as the working-reference frame in this thesis. The 4-momenta are then defined by

$$k_1^\mu = \begin{pmatrix} E_1 \\ 0 \\ 0 \\ p \end{pmatrix}, k_2^\mu = \begin{pmatrix} E_2 \\ 0 \\ 0 \\ -p \end{pmatrix}, k_3^\mu = \begin{pmatrix} E_3 \\ p \sin \theta \cos \phi \\ p \sin \theta \sin \phi \\ p \cos \theta \end{pmatrix}, k_4^\mu = \begin{pmatrix} E_4 \\ -p \sin \theta \cos \phi \\ -p \sin \theta \sin \phi \\ -p \cos \theta \end{pmatrix}. \quad (4.34)$$

Moreover we can neglect the  $\phi$ -dependence in all the processes of interest due to rotational invariance along the z-axis in the systems we are studying. So by choosing  $\phi = 0$ , we arrive at

$$k_1^\mu = \begin{pmatrix} E_1 \\ 0 \\ 0 \\ p \end{pmatrix}, k_2^\mu = \begin{pmatrix} E_2 \\ 0 \\ 0 \\ -p \end{pmatrix}, k_3^\mu = \begin{pmatrix} E_3 \\ p \sin \theta \\ 0 \\ p \cos \theta \end{pmatrix}, k_4^\mu = \begin{pmatrix} E_4 \\ -p \sin \theta \\ 0 \\ -p \cos \theta \end{pmatrix}. \quad (4.35)$$

Inserting these definitions of the 4-momenta into the definitions of the Mandelstam variables (4.28), (4.29) and again neglecting all  $m_i^2$ , we find

$$t = \frac{s}{2}(\cos \theta - 1), \quad u = -\frac{s}{2}(\cos \theta + 1). \quad (4.36)$$

At this point it becomes clear that  $t$  and  $u$  are not independent. Therefore an ambiguity in the inversion of (4.36) appears. In practice the replacement that was used throughout the calculations is

$$\cos \theta = \frac{t - u}{s}. \quad (4.37)$$

Quite often products of Mandelstam variables will subsequently appear. These can all be replaced by using (4.31) and expressing the products in terms of the squares of  $s$ ,  $t$  and  $u$ . This might sound trivial, but in the limit (4.31) quite unobvious relations appear like

$$\frac{t - u}{s} = \frac{st - su}{s^2} = \frac{u^2 - t^2}{s^2}. \quad (4.38)$$

In this way we are able to go back and forth in using either the Mandelstam variables or  $\theta$  in the partial wave analysis and unitarisation procedure, which is an essential feature in keeping analytic calculations simple and in preparing the results for an off-shell implementation in the end.

## 4.5. *K*-Matrix formalism

### 4.5.1. Defintion of *K* and Relations

The *K*-matrix formalism is a comprehensive way in studying unitarity of scattering processes and gives a general prescription on how to treat unitarity violating processes like those arising from anomalous couplings. Therefore a short introduction into the formalism following the description of Chung et. al. [23] is given below.

We will concentrate on 2 to 2 process of the general form  $ab \rightarrow cd$ . The relevant quantities in studying scattering amplitudes of processes like these are the particle helicities  $\{\lambda_i\}$ , the total angular momentum  $J$  and the z-component of the angular momentum  $M$  involved in the process. In these terms initial state  $|i\rangle$  and final state  $|f\rangle$  are denoted by

$$\begin{aligned} |i\rangle &= |ab; JM\lambda_a\lambda_b\rangle, \\ |f\rangle &= |cd; JM\lambda_c\lambda_d\rangle, \end{aligned} \quad (4.39)$$

which are normalized to

$$\langle f|i\rangle = \delta_{if}. \quad (4.40)$$

Due to conservation of angular momentum the states share the same  $J$  and  $M$ . The angular dependence is encoded in  $J$ ,  $M$  and the helicities  $\{\lambda_i\}$  respectively the differences in helicities of in- and outgoing particles  $\lambda = \lambda_a - \lambda_b$  and  $\mu = \lambda_c - \lambda_d$  and can be expressed

in terms of Wigner's d-functions  $d_{\lambda\mu}^J(\theta)$  [24] (see appendix B for the explicit functions that have been used in this thesis).

In order to study scattering of an initial state  $|i\rangle$  into a final state  $|f\rangle$  one defines the scattering operator  $S$  by

$$S_{fi} = \langle f | S | i \rangle. \quad (4.41)$$

Due to conservation of probability one sees that  $S$  must be unitary, i.e.

$$SS^\dagger = S^\dagger S = I \quad (4.42)$$

with  $I$  being the identity operator. In order to separate the effects of free propagation from scattering effects one separates  $S$  into two parts and in this way defines the so called Transition operator  $T^2$ , i.e.

$$S = I + 2iT. \quad (4.43)$$

Unitarity of the scattering operator (4.42) now results in

$$i(T^\dagger - T) = 2TT^\dagger. \quad (4.44)$$

We now assume that the inverse of  $T$  exists on some subspace of the Hilbert space. Via multiplying  $T^{-1}$  from the left and  $(T^\dagger)^{-1}$  from the right one then gets the corresponding equation for the inverse operator:

$$i\left(T^{-1} - (T^\dagger)^{-1}\right) = 2I. \quad (4.45)$$

In order to define the  $K$ -operator we bring this equation into yet another form, i.e.

$$(T^{-1} + iI)^\dagger = T^{-1} + iI \quad (4.46)$$

and define the right hand side of this equation as the inverse of the  $K$ - operator:

$$K^{-1} \equiv T^{-1} + iI \quad (4.47)$$

From (4.46) it is evident the  $K$  is hermitian:

$$K = K^\dagger \quad (4.48)$$

Due to the invariance of the  $S$  and  $T$  operators under time reversal [25] one sees that  $K$  is symmetric and can be chosen as a real operator [23]. By multiplying (4.46) with  $K$  from the left and  $T$  from the right we see that

$$T = K + iTK \quad (4.49)$$

Subtracting the same equation with the opposite direction of multiplication, one further sees that the two operators commute:

$$[K, T] = 0. \quad (4.50)$$

One can now find explicit forms of  $T$  and  $S$  in terms of  $K$  by inverting (4.49) and plugging this into (4.43).

$$T = \frac{K}{I - iK} \quad (4.51)$$

---

<sup>2</sup>A more commonly used definition is  $S = I + iT$ . The factor of 2 is just introduced for convenience [23]. It avoids factors of 1/2 in the following definitions.

$$S = \frac{I + iK}{I - iK}, \quad (4.52)$$

where the denominators are to be understood as the inverses of the corresponding matrices. With  $K \in \mathbb{R}^{n \times n}$  one sees that by (4.51)  $T$  can be split into a real and an imaginary part:

$$\Re(T) = \frac{K}{I + K^2}, \quad \Im(T) = \frac{K^2}{I + K^2}. \quad (4.53)$$

Equation (4.52) can also be interpreted as the Cayley transform of  $S$  [5]. These equations can in turn be inverted to get expressions for  $K$  in terms of either  $T$  or  $S$  as

$$K = i \frac{I - S}{I + S} = \frac{T}{I + iT}. \quad (4.54)$$

By inserting the decomposition of  $T$  in real and imaginary part into (4.47) we furthermore find the interesting result

$$\Im(T^{-1}) = I. \quad (4.55)$$

The relation described in this section build an important foundation for the calculations in the following section, where we will use them to transform arbitrary real scattering amplitudes to fulfill the unitarity conditions imposed in this section.

#### 4.5.2. Unitarisation Procedure

Let us first return to the beginning of the unitarity discussion in section 4.5.1. From the unitarity of the  $S$ -matrix (4.42) and by inserting the relation between  $S$  and the transition matrix  $T$  we find

$$(I + 2iT)(I + 2iT)^\dagger = I. \quad (4.56)$$

Let us assume that we can transform  $T$  into diagonal form via a unitary transformation  $UTU^\dagger$ . Then (4.56) still holds and we find for the complex eigenvalues  $t_j$  of  $T$ , that this is equivalent to

$$|1 + 2it_j| = 1, \quad (4.57)$$

which can be rewritten into the form known in the literature as *Argand circle condition* [5]:

$$\left| t_j - \frac{i}{2} \right| = \frac{1}{2}. \quad (4.58)$$

This equation has a simple geometric interpretation. It states that with the standard unitarity condition (4.42) fulfilled, the complex eigenvalue  $t_j$  of the transition operator  $T$  will lie on a circle with radius  $1/2$  around the center  $i/2$  in the complex plane.

In figure 4.5 one directly sees a relation often used in calculating unitarity bounds for tree-level amplitudes, when looking at the partial waves  $a_{\lambda\mu}^J$  of Spin  $J$  and with helicity differences of in- ( $\lambda$ ) and outgoing particles ( $\mu$ ):

$$|\Re(a_{\lambda\mu}^J)| \leq \frac{1}{2}. \quad (4.59)$$

In order to make analytic calculations in this framework affordable, it is convenient to work in a basis that diagonalizes  $S$ . The task to find such a basis is not possible in all cases nor would it be easy. Still it is the relevant case for this thesis considering the unitarisation of dimension 8 operators that affect vector boson scattering. There is ongoing work on the use of different unitarisation methods like the *Direct T-Matrix unitarisation* [5], where  $S$  does not need to be diagonal, but those will not further be considered in this thesis.

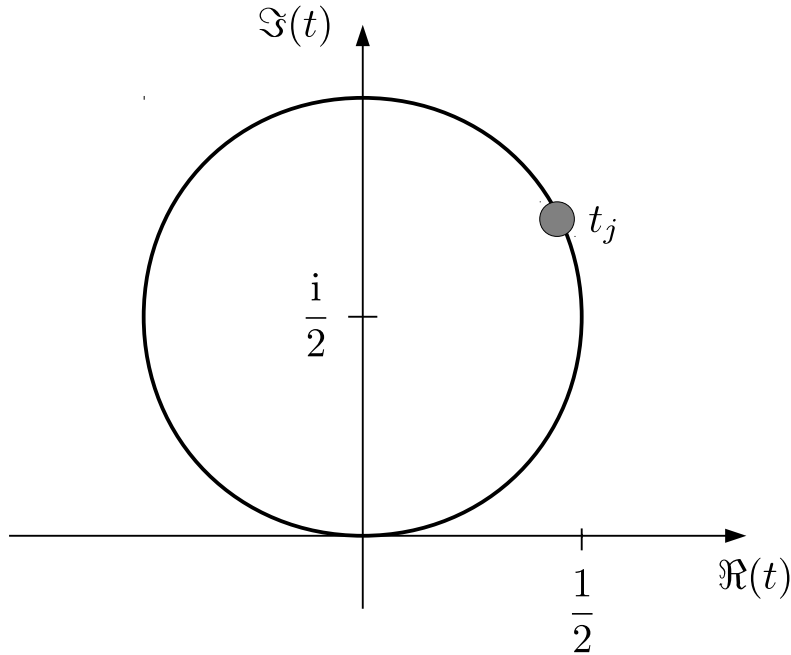


Figure 4.5.: Argand circle in the complex plane showing a  $T$ -eigenvalue  $t_j$ .

Suppose now we can find a diagonal  $S$  then by (4.43) one sees that  $T$  is diagonal too. Further we find that by (4.54) also  $K$  will be diagonal, i.e.

$$\begin{aligned} K_{ij} &= \sum_n T_{in} (I + iT)_{nj}^{-1} = \sum_n t_i (1 + it_j)^{-1} \delta_{in} \delta_{nj} \\ &= \frac{t_j}{1 + it_j} \delta_{ij}, \end{aligned} \quad (4.60)$$

with  $t_j$  being the eigenvalues of  $T$ . In the following part of this section it is assumed that  $S$ ,  $T$  and  $K$  are diagonal.

If there now exists a perturbative expansion of  $T$  to order  $n$  denoted by  $T^{(n)}$ , then the latter formula can be evaluated to get  $K^{(n)}$ , which will be equal to  $T$  in the first order of expansion, when  $T^{(1)}$  is real:

$$\begin{aligned} K^{(1)} &= \frac{T^{(1)}}{I + iT^{(1)}} = \frac{T^{(1)}}{I + (T^{(1)})^2} (I - iT^{(1)}) \\ &= \frac{T^{(1)}}{I + (T^{(1)})^2} - i \frac{(T^{(1)})^2}{I + (T^{(1)})^2} \\ &= T^{(1)} + \mathcal{O}\left((T^{(1)})^2\right). \end{aligned} \quad (4.61)$$

So we found that  $K = T$  in the first order expansion of  $T$ .

As in [5], we will now assume that we have a hermitian  $K$ -matrix from an incomplete approximation to the true amplitude and build a unitary  $S$  or  $T$  matrix as a non-perturbative completion of this approximation. With  $K$  being available in diagonal form, we denote its eigenvalues by  $k_j$ . These will later be calculated from the on-shell elastic scattering amplitudes resulting from tree-level graphs, therefore being real, but not necessarily bounded. In order to get amplitudes respecting the unitarity condition, we now simply put the  $k_j$  into the form implied by the relation between  $K$  and  $T$  (4.51):

$$a_j = \frac{k_j}{1 - ik_j}. \quad (4.62)$$

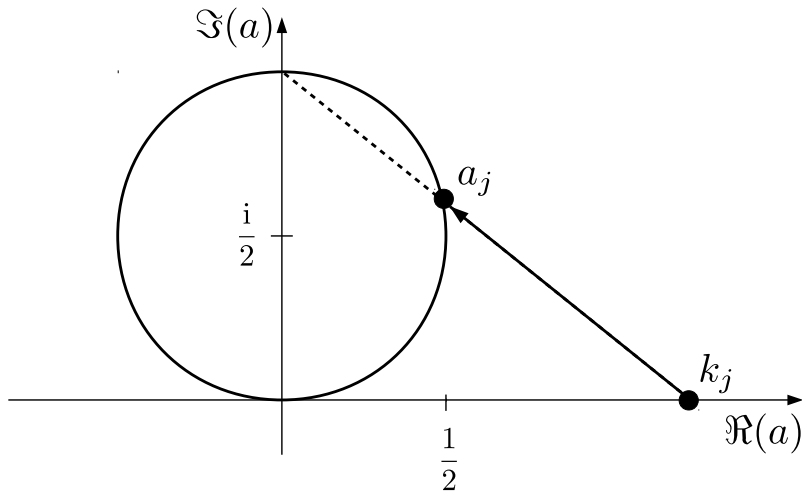


Figure 4.6.: Projection of the real  $k_j$  onto the Argand circle via equation (4.62).

This is just the projection of the real eigenvalues  $k_j$  onto the Argand circle.

In order to guarantee comparability, we will now follow the nomenclature of [6], i.e. use the partial waves  $A_{IJ}$  in the so called isospin(I)- spin(J) basis, that are related to the normalized eigenamplitudes  $a_{IJ}$  by

$$a_{IJ} = \frac{1}{32\pi} A_{IJ}. \quad (4.63)$$

In using  $k_j \rightarrow a_{IJ}$  we can now use (4.62) to get unitarized eigenamplitudes  $\hat{a}_{IJ}$ ,

$$\hat{a}_{IJ} = \frac{a_{IJ}}{1 - ia_{IJ}}, \quad (4.64)$$

and respectively the unitarized partial waves  $\hat{A}_{IJ}$

$$\hat{A}_{IJ} = \frac{A_{IJ}}{1 - iA_{IJ}/(32\pi)}. \quad (4.65)$$

For any  $A_{IJ}(s)$  that grows monotonically with  $s$  we find for the unitarized partial wave

$$\hat{A}_{IJ}(s) \xrightarrow{s \rightarrow \infty} 32\pi i, \quad (4.66)$$

i.e. the real part goes to zero and the imaginary part settles at  $32\pi$ . With the normalized unitary amplitude  $\hat{a}_{IJ}$  saturating at  $i$  for  $s \rightarrow \infty$ , this behavior is often called formally a *resonance at infinity* [6].

Equivalently to (4.65), we may split the unitarized amplitude into the original amplitude and correction terms  $\Delta A_{IJ}$ , by defining

$$\Delta A_{IJ}(s) = \hat{A}_{IJ}(s) - A_{IJ}(s). \quad (4.67)$$

Plugging equation (4.65) into this definition gives us the final prescription of how to unitarize the scattering amplitudes of the following sections,

$$\Delta A_{IJ}(s) = \frac{i}{32\pi} \frac{A_{IJ}(s)^2}{1 - iA_{IJ}(s)/(32\pi)}, \quad (4.68)$$

i.e. do a partial wave analysis in the isospin-spin basis for  $\mathcal{L}_{S,0}$  and  $\mathcal{L}_{S,1}$ , use them to get these correction terms and rebuild the amplitudes from the unitary-guaranteeing partial waves.

## 4.6. Unitarisation of $\mathcal{L}_{S,0}$ and $\mathcal{L}_{S,1}$

The unitarisation procedure of amplitudes altered by the operators  $\mathcal{L}_{S,0}$  and  $\mathcal{L}_{S,1}$  is a bit simpler compared to the unitarisation of the  $\mathcal{L}_{T,i}$  and  $\mathcal{L}_{M,i}$  amplitudes, the reason being the number of processes affected by those types of operators and the simpler amplitude structures. As seen in table 3.1,  $\mathcal{L}_{S,0}$  and  $\mathcal{L}_{S,1}$  only affect processes involving  $W^\pm$  and  $Z$  bosons, whereas for the other operators also various  $\gamma$ -channels need to be included because in principle they can all endanger unitarity. Isospin symmetry can be used to diagonalize the  $S$ -matrix if only the massive vector bosons are of importance, as seen in [26]. This is a necessary feature for the K-matrix unitarisation approach, which cannot be achieved as easily if photons need to be included.

Another facilitating feature of  $\mathcal{L}_{S,0}$  and  $\mathcal{L}_{S,1}$  are the relatively simple amplitudes they generate. For all processes of interest they have a similar structure to (4.16), which means that just as in the SM case (see section (4.2.2)) the strongest contributions result from longitudinally polarized massive vector bosons. In order to make this point obvious we take a look at the amplitude generated by  $\mathcal{L}_{T,0}$  in the process  $W^+W^- \rightarrow ZZ$  which amounts to

$$\begin{aligned} \mathcal{A}_{T,0}(W^+W^- \rightarrow ZZ) = & 8g^4 \frac{f_{T,0}}{\Lambda^4} (k_1 \cdot k_4 k_2 \cdot k_3 \epsilon_1 \cdot \epsilon_4^* \epsilon_2 \cdot \epsilon_3^* \\ & - k_2 \cdot k_3 \epsilon_2 \cdot \epsilon_3^* \epsilon_1 \cdot k_4 \epsilon_4^* \cdot k_1 + k_1 \cdot k_3 k_2 \cdot k_4 \epsilon_1 \cdot \epsilon_3^* \epsilon_2 \cdot \epsilon_4^* \\ & - k_2 \cdot k_4 \epsilon_2 \cdot \epsilon_4^* \epsilon_1 \cdot k_3 \epsilon_3^* \cdot k_1 - k_1 \cdot k_4 \epsilon_1 \cdot \epsilon_4^* \epsilon_2 \cdot k_3 \epsilon_3^* \cdot k_2 \\ & + \epsilon_1 \cdot k_4 \epsilon_2 \cdot k_3 \epsilon_3^* \cdot k_2 \epsilon_4^* \cdot k_1 - k_1 \cdot k_3 \epsilon_1 \cdot \epsilon_3^* \epsilon_2 \cdot k_4 \epsilon_4^* \cdot k_2 \\ & + \epsilon_1 \cdot k_3 \epsilon_2 \cdot k_4 \epsilon_3^* \cdot k_1 \epsilon_4^* \cdot k_2). \end{aligned} \quad (4.69)$$

It carries a much richer structure involving not only polarization vectors, but also the momenta of the in- and outgoing particles. This leads to the fact that transversely polarized bosons contribute strongly to the overall energy dependence. If one takes a look at the  $S$ -matrix in the space of helicities respectively the differences in helicities of in- and outgoing particles  $\lambda$  and  $\mu$ , one will not necessarily find a matrix that only carries one entry with relevant contributions to the overall scattering amplitude as for  $\mathcal{L}_{S,0}$  and  $\mathcal{L}_{S,1}$ . Hence it becomes necessary to think of a way of taking into account all important contributions. We will come back to this subject in 4.8.

For notational simplicity we will drop factors of  $\Lambda$  by denoting

$$\bar{f}_i \equiv \frac{f_i}{\Lambda^4} \quad (4.70)$$

throughout the rest of this thesis.

### 4.6.1. Amplitudes arising from Effective Operators

The amplitudes representing the anomalous part in the various vector boson scattering processes arising from the operator set  $\mathcal{L}_{S,0} + \mathcal{L}_{S,1} + \mathcal{L}_{S,2}$  read

$$\begin{aligned} \mathcal{A}(W^\pm W^\mp \rightarrow ZZ) = & m_W^2 m_Z^2 \\ & \times [(\bar{f}_{S,0} + \bar{f}_{S,2}) (\epsilon_1 \cdot \epsilon_4^* \epsilon_2 \cdot \epsilon_3^* + \epsilon_1 \cdot \epsilon_3^* \epsilon_2 \cdot \epsilon_4^*) + 2\bar{f}_{S,1} (\epsilon_1 \cdot \epsilon_2 \epsilon_3^* \cdot \epsilon_4^*)] \end{aligned} \quad (4.71a)$$

$$\begin{aligned} \mathcal{A}(W^\pm Z \rightarrow W^\pm Z) = & m_W^2 m_Z^2 \\ & \times [(\bar{f}_{S,0} + \bar{f}_{S,2}) (\epsilon_1 \cdot \epsilon_4^* \epsilon_2 \cdot \epsilon_3^* + \epsilon_1 \cdot \epsilon_2 \epsilon_3^* \cdot \epsilon_4^*) + 2\bar{f}_{S,1} (\epsilon_1 \cdot \epsilon_3^* \epsilon_2 \cdot \epsilon_4^*)] \end{aligned} \quad (4.71b)$$

$$\begin{aligned} \mathcal{A}(W^\pm W^\mp \rightarrow W^\pm W^\mp) &= 2m_W^4 \\ &\times [(\bar{f}_{S,1} + \bar{f}_{S,2})(\epsilon_1 \cdot \epsilon_3^* \epsilon_2 \cdot \epsilon_4^* + \epsilon_1 \cdot \epsilon_2 \epsilon_3^* \cdot \epsilon_4^*) + 2\bar{f}_{S,0}(\epsilon_1 \cdot \epsilon_4^* \epsilon_2 \cdot \epsilon_3^*)] \end{aligned} \quad (4.71c)$$

$$\begin{aligned} \mathcal{A}(W^\pm W^\pm \rightarrow W^\pm W^\pm) &= 2m_W^4 \\ &\times [(\bar{f}_{S,1} + \bar{f}_{S,2})(\epsilon_1 \cdot \epsilon_3^* \epsilon_2 \cdot \epsilon_4^* + \epsilon_1 \cdot \epsilon_4^* \epsilon_2 \cdot \epsilon_3^*) + 2\bar{f}_{S,0}(\epsilon_1 \cdot \epsilon_2 \epsilon_3^* \cdot \epsilon_4^*)] \end{aligned} \quad (4.71d)$$

$$\begin{aligned} \mathcal{A}(ZZ \rightarrow ZZ) &= 2m_Z^4 \\ &\times [(\bar{f}_{S,0} + \bar{f}_{S,1} + \bar{f}_{S,2})(\epsilon_1 \cdot \epsilon_2 \epsilon_3^* \cdot \epsilon_4^* + \epsilon_1 \cdot \epsilon_3^* \epsilon_2 \cdot \epsilon_4^* + \epsilon_1 \cdot \epsilon_4^* \epsilon_2 \cdot \epsilon_3^*)] \end{aligned} \quad (4.71e)$$

They have been calculated using the FeynRules package [27] for getting the Feynman rules of the system  $\mathcal{L}_{S,0} + \mathcal{L}_{S,0} + \mathcal{L}_{S,2}$  and the FeynArts/FormCalc package [28] for getting the amplitudes of the specific processes in unitary gauge.

Looking at the structure of these amplitudes one realizes that the longitudinal polarization states will give the strongest contributions due to their energy dependence. As seen in equation (4.18) longitudinal polarization vectors are proportional to the corresponding 4-momentum in the high energy limit. This is why every polarization vector will contribute one power of  $k$ . Taking the transverse polarizations into account it is obvious that with each vector boson transversely polarized, the amplitude will rise with one power of  $k$  less. In the sense of unitarisation it will therefore be sufficient to take into account only the all-longitudinal modes.

In this framework one can easily replace the pairs of polarization vectors in the amplitudes above by the corresponding Mandelstam variables:

$$\epsilon_1 \cdot \epsilon_2 \epsilon_3^* \cdot \epsilon_4^* \underset{s \gg m_i^2}{\simeq} \frac{1}{\prod_i m_i} \frac{s^2}{4}, \quad (4.72a)$$

$$\epsilon_1 \cdot \epsilon_3^* \epsilon_2 \cdot \epsilon_4^* \underset{s \gg m_i^2}{\simeq} \frac{1}{\prod_i m_i} \frac{t^2}{4}, \quad (4.72b)$$

$$\epsilon_1 \cdot \epsilon_4^* \epsilon_2 \cdot \epsilon_3^* \underset{s \gg m_i^2}{\simeq} \frac{1}{\prod_i m_i} \frac{u^2}{4}, \quad (4.72c)$$

to get the results

$$\mathcal{A}(W^\pm W^\mp \rightarrow ZZ) = \frac{1}{4}(\bar{f}_{S,0} + \bar{f}_{S,2})(t^2 + u^2) + \frac{1}{2}\bar{f}_{S,1}s^2, \quad (4.73a)$$

$$\mathcal{A}(W^\pm Z \rightarrow W^\pm Z) = \frac{1}{4}(\bar{f}_{S,0} + \bar{f}_{S,2})(s^2 + u^2) + \frac{1}{2}\bar{f}_{S,1}t^2, \quad (4.73b)$$

$$\mathcal{A}(W^\pm W^\mp \rightarrow W^\pm W^\mp) = \bar{f}_{S,0}u^2 + \frac{1}{2}(\bar{f}_{S,1} + \bar{f}_{S,2})(s^2 + t^2), \quad (4.73c)$$

$$\mathcal{A}(W^\pm W^\pm \rightarrow W^\pm W^\pm) = \bar{f}_{S,0}s^2 + \frac{1}{2}(\bar{f}_{S,1} + \bar{f}_{S,2})(u^2 + t^2), \quad (4.73d)$$

$$\mathcal{A}(ZZ \rightarrow ZZ) = \frac{1}{2}(s^2 + t^2 + u^2)(\bar{f}_{S,0} + \bar{f}_{S,1} + \bar{f}_{S,2}). \quad (4.73e)$$

As already stated in section 3.3, one is able to get the corresponding amplitudes as shown in [6, 7] by setting  $f_{S,2} = f_{S,0}$  and using the replacements (3.32). In order to avoid confusion another set of replacements should be mentioned. Recent developments in the treatment of anomalous couplings by the group of Kilian et. al. show a change in the definitions of the dimension 8 operators. In the paper [5] a set of operators more resembling to the ones of Eboli et.al. is used, but the resulting amplitudes are equivalent to the  $(\mathcal{L}_4 + \mathcal{L}_5)$ - set. The results of this paper can be reproduced by setting

$$\bar{f}_{S,0} = \bar{f}_{S,2} = \frac{1}{2}F_{S,0}; \quad \bar{f}_{S,1} = F_{S,1}. \quad (4.74)$$

Effectively one could go one from here and use the general prescription for unitarising amplitudes in the K-matrix formalism (4.68), ignoring the fact that the  $S$ -matrix is not diagonal:

$$S = \begin{pmatrix} \mathcal{A}(W^\pm W^\pm \rightarrow W^\pm W^\pm) & 0 & 0 & 0 \\ 0 & \mathcal{A}(W^\pm Z \rightarrow W^\pm Z) & 0 & 0 \\ 0 & 0 & \mathcal{A}(W^\pm W^\mp \rightarrow W^\pm W^\mp) & \mathcal{A}(W^\pm W^\mp \rightarrow ZZ) \\ 0 & 0 & \mathcal{A}(ZZ \rightarrow W^\pm W^\mp) & \mathcal{A}(ZZ \rightarrow ZZ) \end{pmatrix} \quad (4.75)$$

The way to do this would be to unitarize the amplitudes from above one by one. A test implementation of this has been implemented in `VBFNLO` for the unitarisation of  $\mathcal{L}_{S,0}$  in  $ZZ$ -scattering. An exemplarily result of this is shown in figure 4.7. One can see that the qualitative behavior is similar between the naive approach and the one to be explained in the following section. The main difference between the two just being a different energy scale  $\Lambda$  where the suppression of the anomalous contribution sets in. As we will see at the end of section 4.6.3, the energy scales of the two cases will differ by  $\sim 40\%$

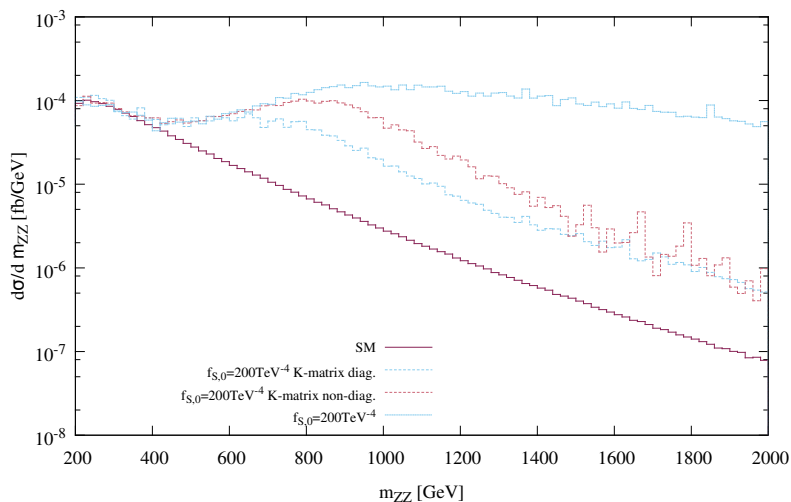


Figure 4.7.: Comparison of K-matrix approach using a diagonalized  $S$ -matrix (see section 4.6.2) in dotted light blue and a more naive approach with with a non-diagonal  $S$ -matrix in dotted dark red for an anomalous coupling  $\tilde{f}_{S,0} = 200 \text{ TeV}^{-4}$ . In solid dark violet the SM contribution and in light blue the anomalous part without unitarisation are shown.

#### 4.6.2. Isospin Eigenamplitudes

The typical K-matrix unitarisation approach is only of use if a diagonal  $S$ -matrix for the processes under consideration is available. In the case of the massive vector boson scattering and only considering the  $\mathcal{L}_{S,i}$  operators, one can find a basis that diagonalizes the  $S$ -matrix [6] by going to the basis of total isospin. The connection between the original basis and the diagonalizing one can be expressed in terms of Clebsch-Gordon coefficients (CGC).

CGCs can be used to express states in an uncoupled tensor basis of a set of spin carrying objects in a basis of total angular momentum states. The same applies to particles represented by different states in an isospin basis, which can be used to build a total isospin basis.

By virtue of the completeness of the set of states, one can express the transition between the two sets by

$$|I, I_z\rangle = \sum_{I_{1z}=-I_1}^{I_1} \sum_{I_{2z}=-I_2}^{I_2} |I_1 I_2; I_{1z} I_{2z}\rangle \underbrace{\langle I_1 I_2; I_{1z} I_{2z} | I, I_z \rangle}_{\text{CGC}}, \quad (4.76)$$

where  $I_i$  represents the Isospin of a single particle and  $I_{iz}$  its 3rd component,  $I$  the total Isospin and  $I_z$  the z-component of it and the product basis

$$|I_1 I_2; I_{1z} I_{2z}\rangle = |I_1, I_{1z}\rangle \otimes |I_2, I_{2z}\rangle. \quad (4.77)$$

We will represent the basis of physical mass eigenstates of the massive vector bosons<sup>3</sup> by

$$|W^\pm\rangle = |1, \pm 1\rangle \quad (4.78)$$

$$|Z\rangle = |1, 0\rangle, \quad (4.79)$$

and respectively the product basis that is relevant for the scattering of two particles by combinations like

$$|W^\pm Z\rangle = |1, \pm 1\rangle \otimes |1, 0\rangle = |11; \pm 10\rangle. \quad (4.80)$$

These can now be related to the total isospin basis

$$\{|I, I_z\rangle\} \quad \text{with } I \in \{0, 1, 2\} \text{ and } I_z \in \{-I, -I+1, \dots, I\} \quad (4.81)$$

The full set of relations between the two representations is listed in appendix E We can now use this to express the original scattering amplitudes of interest, i.e. of physical processes like  $W^+W^- \rightarrow ZZ$ , in terms of only three isospin eigenamplitudes  $\mathcal{A}_I$  as follows [7]:

$$\mathcal{A}(W^\pm W^\mp \rightarrow ZZ) = \frac{1}{3}\mathcal{A}_0 - \frac{1}{3}\mathcal{A}_2, \quad (4.82a)$$

$$\mathcal{A}(W^\pm Z \rightarrow W^\pm Z) = \frac{1}{2}\mathcal{A}_1 + \frac{1}{2}\mathcal{A}_2, \quad (4.82b)$$

$$\mathcal{A}(W^\pm W^\mp \rightarrow W^\pm W^\mp) = \frac{1}{3}\mathcal{A}_0 + \frac{1}{2}\mathcal{A}_1 + \frac{1}{6}\mathcal{A}_2, \quad (4.82c)$$

$$\mathcal{A}(W^\pm W^\pm \rightarrow W^\pm W^\pm) = \mathcal{A}_2, \quad (4.82d)$$

$$\mathcal{A}(ZZ \rightarrow ZZ) = \frac{1}{3}\mathcal{A}_0 + \frac{2}{3}\mathcal{A}_2, \quad (4.82e)$$

where the fact was used, that the operators under consideration are all  $CP$ -conserving and therefore all the amplitudes are invariant under charge conjugation.

In order to get the right Isospin eigenamplitudes we will now use the amplitudes (4.73) and set  $f_{S,2} = f_{S,0} \in \mathbb{R}$ , because otherwise the isospin symmetry would be violated. Then we arrive at a new, even simpler set of amplitudes that can moreover all be expressed in one single master amplitude

$$A(s, t, u) = \mathcal{A}(W^+W^- \rightarrow ZZ) = \frac{1}{2}\bar{f}_{S,0}(t^2 + u^2) + \frac{1}{2}\bar{f}_{S,1}s^2. \quad (4.83)$$

The relation between this master amplitude and the amplitudes of the physical processes reads [6, 7]

$$\mathcal{A}(W^\pm W^\mp \rightarrow ZZ) = A(s, t, u), \quad (4.84a)$$

$$\mathcal{A}(W^\pm Z \rightarrow W^\pm Z) = A(t, s, u), \quad (4.84b)$$

$$\mathcal{A}(W^\pm W^\mp \rightarrow W^\pm W^\mp) = A(s, t, u) + A(t, s, u), \quad (4.84c)$$

$$\mathcal{A}(W^\pm W^\pm \rightarrow W^\pm W^\pm) = A(u, s, t) + A(t, s, u), \quad (4.84d)$$

$$\mathcal{A}(ZZ \rightarrow ZZ) = A(u, s, u) + A(t, s, u) + A(u, s, u). \quad (4.84e)$$

<sup>3</sup>We neglect the photon, because no anomalous couplings for it result from  $\mathcal{L}_{S,i}$ . This means setting  $|Z\rangle \equiv |W^3\rangle$ . We do not need to include any factors of  $\cos\theta_W$  if we use  $\epsilon_\mu(k) = k_\mu/m_Z$  for the Z-bosons. The  $1/m_Z$  factors will then exactly be canceled by the factors  $m_Z$  in the amplitudes resulting from  $\{\mathcal{L}_{S,i}\}$ .

We can finally express the isospin eigenamplitudes in terms of the single master amplitude, by solving the set of equations (4.82) for  $\mathcal{A}_I$  and inserting (4.84). Then we arrive at

$$\mathcal{A}_0(s, t, u) = 3A(s, t, u) + A(t, s, u) + A(u, s, t), \quad (4.85a)$$

$$\mathcal{A}_1(s, t, u) = A(t, s, u) - A(u, s, t), \quad (4.85b)$$

$$\mathcal{A}_2(s, t, u) = A(t, s, u) + A(u, s, t). \quad (4.85c)$$

The conservation of isospin guarantees that no off-diagonal elements will appear in the  $S$ -matrix using the isospin basis.

### 4.6.3. Isospin-Spin Eigenamplitudes

The isospin eigenamplitudes can be further decomposed in terms of a partial wave analysis. In this way we can get rid of the angular dependence, i.e.  $t$  and  $u$  and use the unitarity bounds we found earlier, i.e. the K-matrix prescription (4.68), to unitarize these partial waves one by one. Then we end up with partial waves, that solely depend on  $s$  and respect unitarity. These will finally be used to reconstruct the original on-shell amplitudes and be translated to the off-shell case for an implementation into VBFNLO.

By only looking at the anomalous amplitudes from  $\mathcal{L}_{S,0}$  and  $\mathcal{L}_{S,1}$ , we can restrict ourselves to only include the longitudinal polarization modes and set the differences in helicities of in- and outgoing particles  $\lambda = \mu = 0$ . This means that in the partial wave decomposition the Wigner-d-functions reduce to the Legendre polynomials:

$$d_{\lambda\mu}^J \rightarrow d_{00}^J(\theta) = P_J(\cos(\theta)). \quad (4.86)$$

It is possible to express the Legendre polynomials in terms of the Mandelstam variables (see appendix C), but in order to simplify automatized calculations in a Mathematica framework a little, we will keep the  $\theta$ -dependence and instead replace the Mandelstam variables in the isospin eigenamplitudes.

The decomposition of the isospin eigenamplitudes  $A_I(s, \theta)$  into isospin-spin eigenamplitudes  $A_{IJ}(s)$  is now given by<sup>4</sup>

$$A_I(s, \theta) = \sum_{J=0}^2 (2J+1) A_{IJ}(s) P_J(\cos \theta). \quad (4.87)$$

In taking only the tree-level contributions into account, it suffices to take the sum up to  $J = 2$ . The next step is to calculate the coefficients  $A_{IJ}(s)$  by projecting the various Legendre polynomials onto the isospin eigenamplitudes  $A_I(s, \theta)$  and using the orthogonality relation for the Legendre polynomials

$$\int_{-1}^1 d(\cos \theta) P_k(\cos \theta) P_l(\cos \theta) = \frac{2}{2k+1} \delta_{kl}. \quad (4.88)$$

We then find

$$A_{IJ}(s) = \frac{1}{2} \int_{-1}^1 d(\cos \theta) A_I(s, \theta) P_J(\cos \theta). \quad (4.89)$$

The non-vanishing isospin-spin eigenamplitudes then read

$$A_{00}(s) = \frac{1}{6} (14\bar{f}_{S,0} + 11\bar{f}_{S,1}) s^2, \quad (4.90a)$$

---

<sup>4</sup>This does not contain the SM part.

$$A_{02}(s) = \frac{1}{30}(4\bar{f}_{S,0} + \bar{f}_{S,1})s^2, \quad (4.90b)$$

$$A_{11}(s) = \frac{1}{6}(\bar{f}_{S,0} - \bar{f}_{S,1})s^2, \quad (4.90c)$$

$$A_{20}(s) = \frac{1}{3}(4\bar{f}_{S,0} + \bar{f}_{S,1})s^2, \quad (4.90d)$$

$$A_{22}(s) = \frac{1}{30}(\bar{f}_{S,0} + \bar{f}_{S,1})s^2. \quad (4.90e)$$

At this point one can see the effect of using the isospin basis. It gives slightly stronger bounds than if one would have just used a partial wave analysis of the physical amplitudes like the ones in  $W^+W^- \rightarrow ZZ$ . With  $A_J(W^+W^- \rightarrow ZZ)$  meaning the projections onto the corresponding Legendre polynomials, one finds as non-vanishing contributions

$$A_0(W^+W^- \rightarrow ZZ) = \frac{1}{6}(2\bar{f}_{S,0} + 3\bar{f}_{S,1})s^2, \quad (4.91a)$$

$$A_2(W^+W^- \rightarrow ZZ) = \frac{1}{30}\bar{f}_{S,0}s^2. \quad (4.91b)$$

If we now exemplarily take a look at the case  $f_{S,1} = 0$  and calculate the energy  $\Lambda_b$  at which the unitarity bound  $|\Re[a_{\dots}(s)]| = 1/2$  is reached in both cases, we find for the ratio of  $\Lambda_b$  in the isospin-spin basis over the spin-only basis using the 0th partial waves

$$\frac{(\Lambda_b)_{\text{Isospin}}}{(\Lambda_b)_{\text{Spin}}} = 7^{\frac{1}{4}} \simeq 0.615, \quad (4.92)$$

i.e. the unitarisation procedure in the isospin-spin case already sets in at an energy  $\sim 40\%$  lower than in the spin-only case.

Note that the isospin-spin eigenamplitudes do not give stronger bounds for every process. They exactly coincide with the spin-only eigenamplitudes in the process  $W^\pm W^\pm \rightarrow W^\pm W^\pm$ , because  $\mathcal{A}(W^\pm W^\pm \rightarrow W^\pm W^\pm) \equiv A_{I=2}$ .

#### 4.6.4. Unitarized Amplitudes

We are now in the position to build unitarized on-shell scattering amplitudes using the K-matrix prescription and the partial waves of the last section. First we calculate the  $\Delta A_{IJ}(s)$  from the  $A_{IJ}(s)$  using equation (4.68), that will exactly cancel the high energy behavior of the original amplitudes. These read

$$\Delta A_{00}(s) = -\frac{(14\bar{f}_{S,0} + 11\bar{f}_{S,1})^2 s^4}{6(s^2(14\bar{f}_{S,0} + 11\bar{f}_{S,1}) + 192i\pi)}, \quad (4.93a)$$

$$\Delta A_{02}(s) = -\frac{(4\bar{f}_{S,0} + \bar{f}_{S,1})^2 s^4}{30(s^2(4\bar{f}_{S,0} + \bar{f}_{S,1}) + 960i\pi)}, \quad (4.93b)$$

$$\Delta A_{11}(s) = -\frac{(\bar{f}_{S,0} - \bar{f}_{S,1})^2 s^4}{6(s^2(\bar{f}_{S,0} - \bar{f}_{S,1}) + 192i\pi)}, \quad (4.93c)$$

$$\Delta A_{20}(s) = -\frac{(4\bar{f}_{S,0} + \bar{f}_{S,1})^2 s^4}{3(s^2(4\bar{f}_{S,0} + \bar{f}_{S,1}) + 96i\pi)}, \quad (4.93d)$$

$$\Delta A_{22}(s) = -\frac{(\bar{f}_{S,0} + \bar{f}_{S,1})^2 s^4}{30(s^2(\bar{f}_{S,0} + \bar{f}_{S,1}) + 960i\pi)}. \quad (4.93e)$$

Now we use the partial wave decomposition (4.87) to rebuilt the isospin eigenamplitudes by using the  $\hat{A}_{IJ}$  including the  $\Delta A_{IJ}$  instead of the original partial waves. First we write

the isospin eigenamplitudes in the form

$$\begin{aligned}\hat{\mathcal{A}}_I(s, t, u) &= \sum_{J=0}^2 (2J+1) \hat{A}_{IJ}(s) P_J(s, t, u) \\ &= \mathcal{A}_I(s, t, u) + \underbrace{\sum_{J=0}^2 (2J+1) \Delta A_{IJ}(s) P_J(s, t, u)}_{\equiv \Delta \mathcal{A}_I(s, t, u)},\end{aligned}\quad (4.94)$$

where the  $P_J(s, t, u)$  are of the form found in appendix C. Now we use (4.82) to rebuild the unitarized physical amplitudes. Some rearrangement in terms of the Mandelstam variables is necessary at this point to get the amplitudes into a form, that can be translated into an off-shell implementation. In order to show this we exemplarily calculate the unitarized on-shell amplitude of the process  $W^+W^- \rightarrow ZZ$ .

From (4.82) we have

$$\begin{aligned}\hat{\mathcal{A}}(W^\pm W^\mp \rightarrow ZZ) &= \frac{1}{3} \hat{\mathcal{A}}_0 - \frac{1}{3} \hat{\mathcal{A}}_2 \\ &= \mathcal{A}(W^\pm W^\mp \rightarrow ZZ) + \frac{1}{3} \Delta \mathcal{A}_0 - \frac{1}{3} \Delta \mathcal{A}_2.\end{aligned}\quad (4.95)$$

Now we insert (4.94), evaluate the sums and insert the explicit forms of the Legendre polynomials, i.e.

$$\begin{aligned}\hat{\mathcal{A}}(W^\pm W^\mp \rightarrow ZZ) &= \mathcal{A}(W^\pm W^\mp \rightarrow ZZ) \\ &+ \frac{1}{3} (\Delta A_{00} - \Delta A_{20}) + \frac{5}{3} (\Delta A_{02} - \Delta A_{22}) \frac{3t^2 + 3u^2 - 2s^2}{s^2}\end{aligned}\quad (4.96)$$

Finally, we enhance the second term in (4.96) by an extra factor of  $s^2/s^2$ , insert the explicit non-unitarized amplitude and rearrange the whole in terms of the Mandelstam variables. The resulting unitarized amplitudes for all processes then read

$$\begin{aligned}\hat{\mathcal{A}}(W^\pm W^\mp \rightarrow ZZ) &= \left[ \frac{1}{2} \bar{f}_{S,1} + \frac{1}{3s^2} (\Delta A_{00} - \Delta A_{20}) - \frac{10}{3s^2} (\Delta A_{02} - \Delta A_{22}) \right] s^2 \\ &+ \left[ \frac{1}{2} \bar{f}_{S,0} + \frac{5}{s^2} (\Delta A_{02} - \Delta A_{22}) \right] (t^2 + u^2),\end{aligned}\quad (4.97a)$$

$$\begin{aligned}\hat{\mathcal{A}}(W^\pm Z \rightarrow W^\pm Z) &= \left[ \frac{1}{2} \bar{f}_{S,0} + \frac{1}{2s^2} \Delta A_{20} - \frac{5}{s^2} \Delta A_{22} \right] s^2 \\ &+ \left[ \frac{1}{2} \bar{f}_{S,1} - \frac{3}{2s^2} \Delta A_{11} + \frac{15}{2s^2} \Delta A_{22} \right] t^2 \\ &+ \left[ \frac{1}{2} \bar{f}_{S,0} + \frac{3}{2s^2} \Delta A_{11} + \frac{15}{2s^2} \Delta A_{22} \right] u^2,\end{aligned}\quad (4.97b)$$

$$\begin{aligned}\hat{\mathcal{A}}(W^\pm W^\mp \rightarrow W^\pm W^\mp) &= \left[ \frac{1}{2} \bar{f}_{S,1} + \frac{1}{6s^2} (2\Delta A_{00} + \Delta A_{20}) - \frac{5}{3s^2} (2\Delta A_{02} + \Delta A_{22}) \right] s^2 \\ &+ \left[ \frac{1}{2} \bar{f}_{S,1} + \frac{1}{2s^2} (10\Delta A_{02} - 3\Delta A_{11} + 5\Delta A_{22}) \right] t^2 \\ &+ \left[ 2\bar{f}_{S,0} + \frac{1}{2s^2} (10\Delta A_{02} + 3\Delta A_{11} + 5\Delta A_{22}) \right] u^2,\end{aligned}\quad (4.97c)$$

$$\begin{aligned}\hat{\mathcal{A}}(W^\pm W^\pm \rightarrow W^\pm W^\pm) &= \left[ 2\bar{f}_{S,0} + \frac{1}{s^2} (\Delta A_{20} - 10\Delta A_{22}) \right] s^2 \\ &+ \left[ \frac{1}{2} \bar{f}_{S,1} + \frac{15}{s^2} \Delta A_{22} \right] (t^2 + u^2),\end{aligned}\quad (4.97d)$$

$$\begin{aligned}
\hat{A}(ZZ \rightarrow ZZ) = & \left[ \left( \bar{f}_{S,0} + \frac{1}{2}\bar{f}_{S,1} \right) \right. \\
& + \frac{1}{3s^2}(\Delta A_{00} + 2\Delta A_{20}) - \frac{10}{3s^2}(\Delta A_{02} + 2\Delta A_{22}) \left. \right] s^2 \\
& + \left[ 2\bar{f}_{S,0} + \bar{f}_{S,1} + \frac{5}{s^2}(\Delta A_{02} + 2\Delta A_{22}) \right] (t^2 + u^2). \quad (4.97e)
\end{aligned}$$

At this point it becomes obvious that crossing symmetry is broken. Each of the processes listed above needs its own unitarisation procedure.

The structure of (4.97) is already optimized for the translation to the unitarisation of off-shell amplitudes. In section 6.3 we will show how the transition from to above equations to the actual matrix element calculation inside a Monte Carlo program is done.

## 4.7. K-Matrix-like Form Factors

Having a close look at the way the K-matrix approach is used in a final off-shell implementation shows similarities to the use of form factors. What we have in the very end are complex form-factor like functions that differ for the three scattering channels ( $s/t/u$ ) and every process.

Let us start with the study of a simple case. Take the unitarized amplitude  $\hat{A}(W^\pm W^\pm \rightarrow W^\pm W^\pm)$  (4.97d) with only  $f_{S,1} \neq 0$ , i.e.

$$\begin{aligned}
\hat{A}(W^\pm W^\pm \rightarrow W^\pm W^\pm) &= \left[ \frac{1}{2}\bar{f}_{S,1} + \frac{15}{s^2}\Delta A_{22} \right] (t^2 + u^2) \\
&= \left[ \frac{15}{s^2}\hat{A}_{22} \right] (t^2 + u^2). \quad (4.98)
\end{aligned}$$

The explicit form of  $\hat{A}_{22}(s)$  is

$$\hat{A}_{22}(s) = \frac{A_{22}(s)}{1 - iA_{22}(s)/(32\pi)} = \frac{\bar{f}_{S,1}s^2}{30} \frac{1}{1 - i\frac{\bar{f}_{S,1}s^2}{960\pi}}. \quad (4.99)$$

By inserting this back into (4.98) we find

$$\hat{A}(W^\pm W^\pm \rightarrow W^\pm W^\pm) = \frac{1}{1 - i\frac{\bar{f}_{S,1}s^2}{960\pi}} \frac{\bar{f}_{S,1}}{2} (t^2 + u^2). \quad (4.100)$$

If we compare this now to the original amplitude in terms of Mandelstam variable (4.73d), we see that this is the exact same amplitude multiplied by a function that can be interpreted as a complex form factor, i.e.

$$\mathcal{F}_K(s) = \frac{1}{1 - i\frac{\bar{f}_{S,1}s^2}{960\pi}} = \frac{1}{1 - i\frac{s^2}{\Lambda_K^4}}. \quad (4.101)$$

$\Lambda_K$  represents the energy scale where  $\mathcal{F}_K(s)$  would start the suppression of the anomalous amplitudes. As we have seen in this derivation, it can in principle be determined via a partial wave analysis of the anomalous scattering amplitudes. Furthermore, if only one coupling  $f_i \neq 0$  at a time, the derivation in section 4.3.2 shows that  $\Lambda_K = \Lambda_K(f_i)$  in the sense that

$$\Lambda_K(f_i) \propto f_i^{-\frac{1}{4}}. \quad (4.102)$$

This can be shown in a completely analogous way to the derivation of sec 4.3.2, meaning that equation (4.26) will also hold for the  $\Lambda_K$ .

A plot of the real and imaginary part of this function is shown in figure 4.8. Note that other than implied by this plot, the imaginary part of the amplitudes will not go to zero for very high energies while the real part does. This is because the real part drops like  $s^{-4}$  while the imaginary part only goes down like  $s^{-2}$ . With the amplitudes typically growing like  $s^2$ , multiplying  $\mathcal{F}_K(s)$  to it will result in a finite non-zero imaginary part for very high energies.

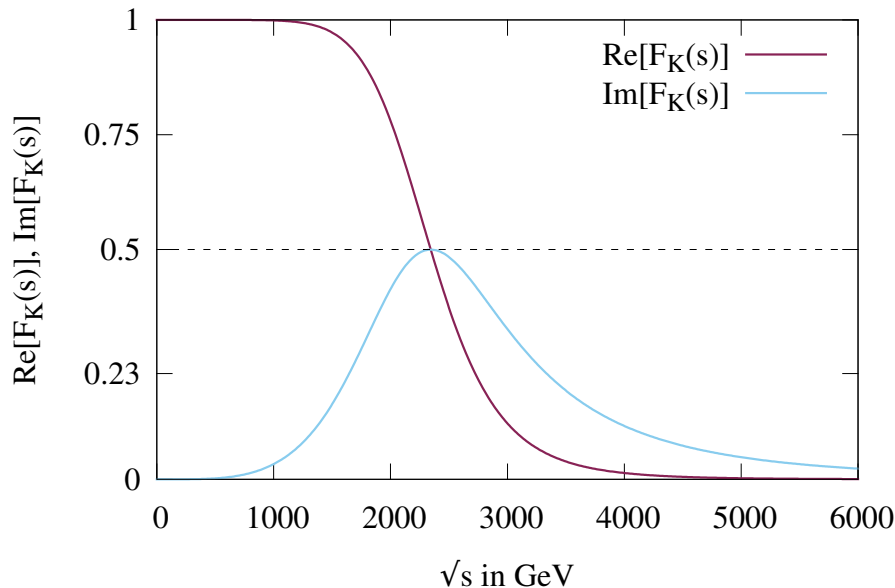


Figure 4.8.: Real and imaginary part of the K-matrix-like form factor  $\mathcal{F}_K(s)$  generated by using prescription (4.103) and the isospin-spin eigenamplitude  $A_{22}(s)$  as input.

The calculation above shows that we can get complex form-factor-like functions from the K-matrix formalism. A simple prescription to build these is taking a unitarized partial wave  $\hat{A}_{IJ}$  and divide by the original one, i.e.

$$\mathcal{F}_K(s) = \frac{\hat{A}_{IJ}(s)}{A_{IJ}(s)} = \frac{1}{1 - iA_{IJ}(s)}. \quad (4.103)$$

Now for  $\mathcal{L}_{S,0}$  and  $\mathcal{L}_{S,1}$ , we already have the complete K-matrix formalism which makes these  $\mathcal{F}_K(s)$  superfluous. The situation is different for all other operators. Here it is difficult to find a diagonal  $S$ -matrix, which is a necessary feature for the K-matrix procedure. Therefore we discuss the use of the K-matrix-like form factors for the operator classes  $\{\mathcal{L}_{T,i}\}$  and  $\{\mathcal{L}_{M,i}\}$  in the following section.

## 4.8. Unitarisation of $\mathcal{L}_{M,i}$ and $\mathcal{L}_{T,i}$

The last section shows that one can get K-matrix like form factors by executing a partial wave analysis of the amplitudes arising from anomalous couplings and using prescription (4.103) to build the form factors. The main problem in transferring this ansatz to the  $\mathcal{L}_{M,i}$  and  $\mathcal{L}_{T,i}$  operators is the final off-shell implementation. In the  $\mathcal{L}_{S,0}$  and  $\mathcal{L}_{S,1}$  case we have three circumstances that significantly simplify the unitarisation procedure:

1. One can find a direct correspondence of the Mandelstam variables to the dot-products of polarization vectors.
2. Only the longitudinal polarizations contribute which reduces the Wigner-d-functions of the partial wave analysis to Legendre polynomials

3. A basis that diagonalizes the  $S$ -matrix is known.

These features are missing for the other operators, but can to some extent be cured. Note that just because an elegant unitarisation method for  $\mathcal{L}_{S,0}$  and  $\mathcal{L}_{S,1}$  is available, their importance in terms of describing anomalous quartic gauge couplings should not be lifted above the importance of the other operators.

The first feature of the list means that the  $s$ -,  $t$ - and  $u$ -channels have separate effective unitarisation factors. By taking a look at a rather simple amplitude generated by the operator  $\mathcal{L}_{T,0}$  in  $W^+W^- \rightarrow ZZ$ , we see that the separation into different Mandelstam channels is not possible that easily:

$$\begin{aligned} \mathcal{A}_{T,0}(W^+W^- \rightarrow ZZ) \\ = \frac{128 \cos^2 \theta_W m_W^4}{v^4} \frac{f_{T,0}}{\Lambda^4} (k_1 \cdot k_2 \epsilon_1 \cdot \epsilon_2 - \epsilon_1 \cdot k_2 \epsilon_2 \cdot k_1) (k_3 \cdot k_4 \epsilon_3^* \cdot \epsilon_4^* - \epsilon_3^* \cdot k_4 \epsilon_4^* \cdot k_3) \end{aligned} \quad (4.104)$$

With dot-products between momenta and polarization vectors appearing, the correspondence between those terms and the Mandelstam variables is not as clear anymore. The strongest rise in energy of this amplitude will occur when all vector bosons are transversely polarized. In this case it might coincidentally happen, that dot-products between momenta and polarization vectors vanish, but this is not guaranteed in all cases. Therefore there is no simple prescription in how to treat those products, compared to the  $\mathcal{L}_{S,0}$  and  $\mathcal{L}_{S,1}$  case.

The simplest circumvention would be to take the  $s$ -channel effective unitarisation factor and use it as an overall form factor. This is more or less equivalent to only taking the  $J = 0$  partial waves into account. Those give the strongest contributions to the partial wave analysis anyway, which means that the resulting unitarisation procedure would lead to a stronger suppression than with taking higher  $J$ 's into account (see figure 7.10 where the bump around 1500GeV would disappear by neglecting the  $J = 2$  partial waves).

When an overall effective form factor is the chosen method, then the second feature can also be cured. Several combinations of helicities for in- and outgoing particles lead to a bad high energy behavior for the  $\mathcal{L}_{M,i}$  and  $\mathcal{L}_{T,i}$  operators. As will be seen in the following chapter, it is possible to set up a general framework for the calculation of all these contributions from different helicity combinations in an analytic way. The final results of the partial wave analysis will feature a  $9 \times 9$  matrix in helicity space that can easily be diagonalized due to the few non-vanishing contributions. We would then be able to take the strongest eigenvalues of these matrices as inputs for equation (4.103). The resulting effective form factors will be a bit weaker than in the  $\mathcal{L}_{S,0}$  and  $\mathcal{L}_{S,1}$  case, meaning they will start the suppression at energies too high, if compared to the values one gets from a numerical analysis like in the `calc_formfactor` routine by Bastian Feigl [21].

The last feature of the list is irrelevant at least for  $W^\pm W^\pm$  scattering, because isospin-spin eigenamplitudes coincide with the spin eigenamplitudes here. As shown in section 4.6.3 the suppression for other processes would probably set in at too high energy scales again, but it would not lead to completely incompatible results.

As we see, a K-matrix-like unitarisation procedure is possible for the  $\mathcal{L}_{M,i}$  and  $\mathcal{L}_{T,i}$  operators and so is an implementation into a Monte Carlo program. In the simplest possible scenario, one could use form factor like functions  $\mathcal{F}_K(s)$  defined in equation (4.101) for an implementation.  $\mathcal{F}_K(s)$  only has one parameter, the energy scale  $\Lambda_K$  that determines when the suppression should set in. The routine `calc_formfactor` could be modified and used together with relation (4.26) in order to determine the values for  $\Lambda_K$ . Another approach would be to use definition (4.103) and an analytic partial wave analysis which will be discussed in the following chapter.



## Mathematica Framework

A bigger part of the thesis was the development and use of a framework making an analytic treatment of partial wave analyses for all kinds of dimension 8 operators affordable. In this section the goal is to showcase some of the findings and functions developed, but more importantly to give a general overview of the procedures involved, so that future studies may use them as a foundation.

### 5.1. From a Lagrangian to Partial Waves

The starting point of the analyses carried out in this thesis is the list of dimension 8 operators with the goal of working the way towards unitarized anomalous amplitudes achieved by using the K-matrix formalism. During the work it became clear, that the original K-matrix approach may not be the optimal solution, or even not applicable at all for the operator groups  $\mathcal{L}_{M,i}$  and  $\mathcal{L}_{T,i}$ . Still, as was shown in the previous section, one can get K-matrix-like form factors for these. Either way a partial wave analysis is necessary in order to find out where the strongest contributions of the anomalous amplitudes arise from and in order to use those partial waves for unitarisation.

#### 5.1.1. Feynman Rules

The first step of the whole analysis is to get Feynman rules from which amplitudes of physical processes can be calculated. For this purpose the Mathematica package FeynRules [27] has been used. FeynRules is a package that can take pretty much any physical theory in the form of a Lagrangian as an input, returning all Feynman rules that the theory inherits. These rules can then be used for further evaluation in other Mathematica packages.

A typical procedure of generating a set of Feynman rules is fairly simple. One starts by loading in the FeynRules package and a model file that contains the necessary Lagrangians by

```
$FeynRulesPath = SetDirectory["FeynRules_dir/feynrules-current"];
<< FeynRules

LoadModel["FeynRules_dir/feynrules-current/Models/myModel.fr"]
```

Afterwards one should choose which gauge to work in. Throughout this thesis, all work is done in unitary gauge, which means setting

```
FeynmanGauge = False;
```

Then we need just one command to generate a file containing all Feynman rules in a specified output:

```
WriteFeynArtsOutput[LS0, FlavorExpand -> True, Output -> "my_FeynRules_Models/LS0"]
```

where `FlavorExpand` means that rules are separately generated for all particles, not only flavor types (e.g. separate rules for d-, s- and b- quarks). This already closes the `FeynRules` procedure. Note that it is possible to insert a sum of operators into the above command by simply writing `WriteFeynArtsOutput[LS0 + LS1 + ..., ...]`.

The more involved part in generating the Feynman rules is defining the Lagrangians in a way understood by `FeynRules`. Fortunately there exists a model file `quartic.fr` by Eboli et. al. [29]. It could directly be used for generating all rules for  $\mathcal{L}_{M,i}$ ,  $\mathcal{L}_{T,i}$  and  $\mathcal{L}_{S,1}$ . The rules for  $\mathcal{L}'_{S,0}$  and  $\mathcal{L}_{S,2}$  have been generated by using adaptations of the original  $\mathcal{L}_{S,0}$ . As an example, consider the definition of  $\mathcal{L}_{S,2}$ :

```
LS2 := Block[{PMVec, WVec, Dc, Dcbar},

  PMVec = Table[PauliSigma[i], {i, 3}];
  Wvec[mu_] := {Wi[mu, 1], Wi[mu, 2], Wi[mu, 3]};

  Dc[f_, mu_] := I del[f, mu] + ee/cw B[mu]/2 f + ee/sw/2 (Wvec[mu].PMVec).f;
  Dcbar[f_, mu_] := -I del[f, mu] + ee/cw B[mu]/2 f + ee/sw/2 f.(Wvec[mu].PMVec);

  FS2 (Dcbar[Phibar, mu]).Dc[Phi, nu] (Dcbar[Phibar, nu]).Dc[Phi, mu ];
```

The functions defined in here are just the fields and covariant derivatives. The Lagrangian itself is the last line of the code. Equivalently one may use the definitions of covariant derivatives provided directly by `FeynRules`. e.g. for  $\mathcal{L}'_{S,0}$ :

```
LpS0 := Block[{ii,jj,mu,nu, feynmangaugerules},
  feynmangaugerules = If[Not[FeynmanGauge], {G0|GP|GPbar ->0}, {}];

  ExpandIndices[FpS0/2*(DC[Phibar[ii],mu] DC[Phi[ii],nu])
    * ( (DC[Phibar[jj],mu] DC[Phi[jj],nu]) + (DC[Phibar[jj],nu] DC[Phi[jj],mu])
    ) , FlavorExpand-> {SU2D,SU2W}]/.feynmangaugerules];
```

It has been checked that both methods lead to equivalent results.

### 5.1.2. Amplitudes from FeynArts/FormCalc

The next step is to generate scattering amplitudes from the Feynman rules created beforehand. For this matter we are using the Mathematica package `FeynArts/FormCalc` [28]. First we make sure to quit the local Mathematica Kernel by using the command `Quit[]`; in order not to mix up `FeynRules` and `FeynArts` definitions. Similar to the `FeynRules` procedure we then start by loading in the packages:

```
<< "FeynArts_dir/FeynArts-3.8/FeynArts.m";
<< "FeynArts_dir/FormCalc-8.2/FormCalc82.m";
```

Next we create the topologies for the process of interest, i.e. tree level  $2 \rightarrow 2$  scattering and only keeping the 4-vertices:

```
topologies = CreateTopologies[0, 2 -> 2, Adjacencies -> {4}];
```

Then we are able to create diagrams by inserting particles into the topologies by specifying the relevant model (i.e. a Lagrangian like  $\mathcal{L}_{M,0}$ ) and particles (i.e. vector bosons with the syntax `V[i]`):

```
diagramWWWLMO := InsertFields[topologies, {V[3],-V[3]}->{V[3],-V[3]},
  InsertionLevel -> {Particles}, Model -> {"LMi/LM0"}, GenericModel -> {"LMi/LM0"}];
```

In our case we will always end up with just one diagram representing the anomalous contribution to the vector boson 4-vertex under consideration. The last step is to use FormCalc to generate the amplitude from the diagram we just created. This is done via:

```
amplitudeWWWLMO = (CalcFeynAmp[CreateFeynAmp[diagramWWWLMO], OnShell->False,
  Invariants->False, Transverse->False, Normalized->False, InvSimplify->False
  ]) //.Subexpr[] //.Abbr[];
```

Here, the options set to `False` prevent FormCalc from performing any simplifications like replacing dot-products of momenta by the corresponding Mandelstam variables and so forth. The meaning of  `//.Subexpr[] //.Abbr[]`; is to expand all abbreviations that FormCalc automatically introduces in order to keep outputs in a compact, readable form. The only thing left to be done, is reading in the couplings that FeynRules generated and save them as a replacement list:

```
<< "FeynArts_dir/FeynArts-3.8/Models/LMi/LMO.mod";
FACouplingsLMO = M$FACouplings;
```

Now we have the complete amplitude resulting from one dimension 8 operator and the information about the couplings, which already ends the use of the packages FeynRules, FeynArts and FormCalc for our analysis.

### 5.1.3. Towards Partial Waves

We are now ready to massage the results from FormCalc into a form that can be used for an analytic partial wave decomposition. Let us first get a little more familiar with some Mathematica syntax.

- `foo[x_,y_] := ...;` is how a function “foo” with two arguments “x” and “y” is defined within Mathematica. The underscores are needed to tell “treat these as input parameters/variables”. The “:=” tells Mathematica not to evaluate the expression immediately, but to wait until the function is called somewhere (other than using just “=”). The semicolon in the end is optional. It just suppresses output that might be generated by defining the function.
- `/.{a -> b, ...}` is called a replacement. The command “/.” tells to use the following list for replacements in the preceding expression, “a->b” tells replace expression “a” by expression “b”.
- `//.{a -> b, ...}` The same as the replacement above, but it is run repeatedly until no appearances of “a” are found anymore.
- `expr//foo` is used as an alternative to evaluate the function “foo” with the preceding expression “expr” as argument. It is completely equivalent to `foo[expr]`.
- `/.{a :> b, ...}` is a delayed replacement rule, meaning that “a” gets replaced by “b”, but “b” is firstly evaluated, when the rule is used.

With this knowledge we are now ready to understand the following lines<sup>1</sup>:

```
resultLSi[pol_, order_] := amplitudeWWWLSi /.{Amp[a_][b_] -> b} /.FACouplingsLSi
  //.replaceEpsDenWWW[pol, order] /.{Pair[aa_, bb_] :> MyPair[aa, bb]} /.
  makeReadable //Expand
```

This is the most gruesome step in the whole calculation, but it is not too difficult to understand. We take the amplitude created beforehand and only keep the amplitude

<sup>1</sup>In order for this command to work, we need to read in the definitions of all functions developed for this analysis, like the ones in appendix G.

itself, i.e. “b”, not the info about particles etc. that is hidden in “a”. Then we replace the couplings by the ones we read in from the model file. The “results” needed for the partial wave decomposition are defined with two arguments “pol” and “order” that are used in the function `replaceEpsDenWWW` in the partial wave definitions file. This file of course needs to be read in before the command above is executed.

The input parameter `pol` represents the helicity states of the vector bosons in the form of a four component vector  $\{\lambda_1, \lambda_2, \lambda_3, \lambda_4\}$  with  $\lambda_i \in \{-1, 0, 1\}$ . The parameter `order` defines to which order in  $\mathcal{O}(m_V^2/E^2)$  the momentum  $p_i = \sqrt{E^2 - m_{V_i}^2}$  is expanded. As it turned out after some time, the expansion to higher orders was not of much use in the calculations and only added unwanted complexity to some definitions. The parameter still is of use though, because one can choose between 0th order, i.e. `order = 0` meaning  $p_i = E = \sqrt{s}/2$  for most processes or setting `order = -1` which means working with the exact momentum. All calculations carried out in this section were computationally still affordable with the exact definition of the momentum modulus, but results are of course a lot simpler when only using the 0th order in  $\mathcal{O}(m_V^2/E^2)$  and moreover more comparable to the results in [6].

The expansion of the momentum and calculation of the helicity eigenvectors is carried out in `replaceEpsDenWWW`. The definitions used for the momenta and helicity eigenvectors can be found in section 4.4 and appendix D. The vectors are introduced in the form of a replacement list, meaning the momenta and polarization vectors of the FormCalc amplitude get replaced by explicit expression in terms of the center of mass energy  $\sqrt{s}$ , the scattering angle  $\theta$  etc.

In the last three steps, first the symbolic definition `Pair[a,b]` gets replaced by the standard Minkowski-space scalar product  $a_\mu b^\mu$ , then we replace some constants like the fine structure constant  $\alpha$  by other constants to get simpler results and finally `Expand` everything which adds another level of simplification and readability. In the end the amplitudes will look like

$$\text{resultLSiWWW}[\{0, 0, 0, 0\}, 0] = \frac{ct^2 f_{S0} S^2}{8\Lambda^4} + \frac{ct^2 f_{S1} S^2}{4\Lambda^4} + \frac{5f_{S0} S^2}{8\Lambda^4} + \frac{f_{S1} S^2}{4\Lambda^4}, \quad (5.1)$$

where  $ct = \cos\theta$ . The sines and cosines have been inserted in this manner, so that unwanted trigonometric simplifications by Mathematica are avoided. This result is the amplitude in  $W^+W^+$  scattering when all vector bosons are longitudinal. Note that by correctly replacing  $\cos\theta$  with the Mandelstam variables, one reproduces equation (4.73d) when  $f_{S,2} = f_{S,0}$ .

#### 5.1.4. Exact Momentum vs. First Order Expansion

We are now in a position to check how good the approximation of neglecting higher order terms in the expansion of  $p_i = \sqrt{E^2 - m_{V_i}^2}$  really is. For that matter we compute the isospin-spin eigenamplitude  $A_{I=2, J=0}(s)$  with the first order expansion mentioned above and with the exact momentum. The results are

$$A_{I=2, J=0}^{\text{1st order}}(s) = \frac{2s^2 f_{S,0}}{3\Lambda^4} + \frac{s^2 f_{S,1}}{3\Lambda^4} \quad (5.2a)$$

$$A_{I=2, J=0}^{\text{exact}}(s) = \frac{f_{S,0}}{3\Lambda^4} (12m_W^4 - 9m_W^2 s + 2s^2) + \frac{f_{S,1}}{3\Lambda^4} (12m_W^4 - 6m_W^2 s + s^2). \quad (5.2b)$$

In setting  $A_{I=2, J=0}(s) = 16\pi$  we are as before able to calculate the energy at which unitarity would be violated. As expected, the difference is rather small, i.e.

$$\sqrt{s_{\text{bound}}^{\text{1st order}}} = 842 \text{ GeV} \quad (5.3a)$$

$$\sqrt{s}_{\text{bound}}^{\text{exact}} = 851 \text{ GeV}, \quad (5.3b)$$

meaning the two only differ by  $\sim 1\%$ .

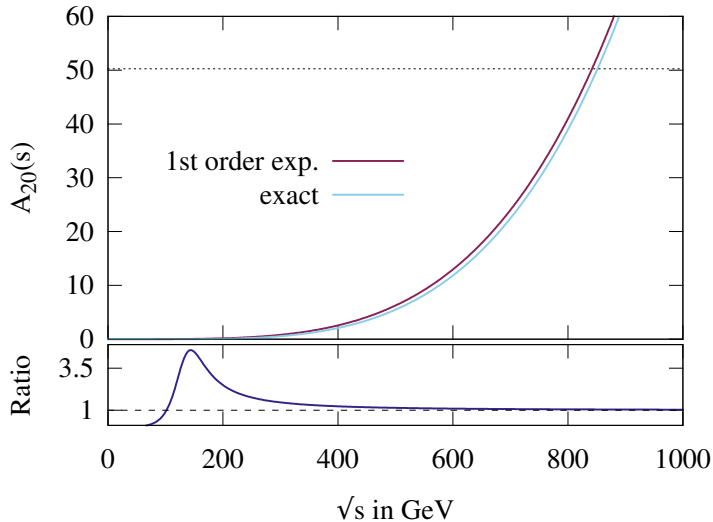


Figure 5.1.: This plot shows the isospin spin Amplitude  $A_{20}(s)$  calculated with exact momentum  $p_i = \sqrt{E^2 - m_{V_i}^2}$  (violet) and the first order expansion  $p_i = \sqrt{s}/2$  (light blue). The ratio of these two versions is shown below. It shows that the differences between the two are negligible in the high energy regime. The dotted line indicates the unitarity bound  $A_{IJ} = 16\pi$ .

### 5.1.5. Partial Waves in Helicity Space

We now almost arrived at the final partial wave decomposition. In the end an overview of all contributions to an amplitude of some operator set is desired. In order to achieve this, we define a helicity basis and collect all amplitudes as matrix elements of the scattering matrix  $S$ , where

$$S_{fi} = \langle \lambda_{3,f}, \lambda_{4,f} | S | \lambda_{1,i}, \lambda_{2,i} \rangle. \quad (5.4)$$

The  $\lambda_i$  can take three different values. Therefore we would normally end up with  $3^2 \times 3^2 = 81$  entries. Fortunately we can make use of several symmetries to relate the amplitudes amongst each other. This will be discussed in detail in section 5.2.

The command to get all amplitudes in matrix form looks like

```
amplitudeMatrixLSi = SparseArray[{6, 4} -> Null] // Normal;
Do[amplitudeMatrixLSi[[aa, bb]] =
  resultLSi[polarisationMatrix[[aa, bb]], 0] // Simplify, {aa, 1, 6}, {bb, 1,
  4}]
```

The first line just creates an empty  $6 \times 4$  matrix which is then filled in a loop with the amplitudes in terms of the entries of the polarization matrix. The output generated in this way will always look quite messy, but close inspection shows that only very few entries are of importance. These are the ones that rise quadratically in  $s$ . When we are only working with  $\mathcal{L}_{S,0}$  and  $\mathcal{L}_{S,1}$ , even only one entry survives, which is the all longitudinal channel.

The matrix created in this way gives a nice overview in terms of the amplitudes, but it still contains some angular dependence that we can get rid of by determining the corresponding partial waves. This does not blow up the outputs too much, because with conserved angular momentum, only  $J \in \{0, 1, 2\}$  partial waves are non-zero. One can get the partial waves in a similar matrix form as before by using

```

WignerDWaveMatrixListLSi = SparseArray[{3, 6, 4} -> Null] // Normal;
Do[
  mm1 = helicityDiffMatrix[[aa, bb, 1]];
  mm2 = helicityDiffMatrix[[aa, bb, 2]];
  WignerDWaveMatrixListLSi[[J + 1, aa, bb]] =
  If[ J >= Abs[mm1] && J >= Abs[mm2],
    AJm1m2theta[ {J, mm1, mm2}, resultLSi[polarisationMatrix[[aa, bb]],0] ]
  ,0]
  ,{J, 0, 2},{aa, 1, 6},{bb, 1, 4}]

```

Here again an empty matrix is created and gets filled with the partial waves  $A_{\lambda\mu}^J(s)$ , where  $\lambda = \text{mm1}$  and  $\mu = \text{mm2}$ . It would now again be nice to see only the  $s^2$  contributions in the output. A safe way to get them is

```

WignerDWaveMatrixListLSiOnlyS2 = {Null, Null, Null};
Do[
  WignerDWaveMatrixListLSiOnlyS2[[J + 1]]
  = (WignerDWaveMatrixListLSi[[J + 1]] -
  Map[# /. {m : Power[S, 2] :> 0} &,
  WignerDWaveMatrixListLSi[[J + 1]]) // Apart, {J, 0, 2}]

```

This means subtracting all entries that do not grow like  $s^2$  from the original entries. The output of the results we get in this way looks like

$$J = 0 : \begin{pmatrix} 0 & 0 & 0 & 0 & 0 & 0 \\ 0 & 0 & \frac{(4f_{S,0}+f_{S,1})s^2}{3\Lambda^4} & 0 & 0 & 0 \\ 0 & 0 & 0 & 0 & 0 & 0 \\ 0 & 0 & 0 & 0 & 0 & 0 \end{pmatrix},$$

$$J = 1 : \begin{pmatrix} 0 & 0 & 0 & 0 & 0 & 0 \\ 0 & 0 & 0 & 0 & 0 & 0 \\ 0 & 0 & 0 & 0 & 0 & 0 \\ 0 & 0 & 0 & 0 & 0 & 0 \end{pmatrix},$$

$$J = 2 : \begin{pmatrix} 0 & 0 & 0 & 0 & 0 & 0 \\ 0 & 0 & \frac{(f_{S,0}+f_{S,1})s^2}{30\Lambda^4} & 0 & 0 & 0 \\ 0 & 0 & 0 & 0 & 0 & 0 \\ 0 & 0 & 0 & 0 & 0 & 0 \end{pmatrix}.$$

These are just the results we already saw in (4.90d) and (4.90e), representing the isospin-spin eigenamplitudes  $A_{I=2,J}(s)$ . They coincide, because  $W^+W^+$  scattering is the only process that contributes to the isospin  $I = 2$  amplitudes.

All what we have seen in this section might look like a huge machinery to get results that we already had, i.e. only all longitudinal modes carry an  $s^2$  proportionality when the operators  $\mathcal{L}_{S,0}$  and  $\mathcal{L}_{S,1}$  are taken into account. The situation looks a lot different for the other operators. The amplitudes can be a lot more complex, which makes an analysis as in section 4.6 unattractive if not impossible. Moreover there can be more than one contribution to the scattering matrix in helicity space that grows like  $s^2$ .

Therefore the use of the procedure introduced in this section only shows up when we take a look at different operator sets. A partial wave analysis for all operators is possible and quite simple.

Another use we can make of this implementation, is checking how good the approximation of only taking a first order in the expansion of the momentum modulus into account. In most cases it will not make too much of a difference for two reasons:

1. The strongest contributions arising from anomalous couplings grow like  $s^2$ . If the suppression supplied by some unitarisation factor falls off with  $s^n$  and  $n \leq -2$ , then all terms appearing in the amplitudes which grow slower than with  $s^2$  will be sufficiently suppressed at high energies
2. The contributions that grow less than  $s^2$  will merely shift the energy bound at which unitarity would be violated by a small amount. These shifts will, generally speaking, be unimportant as we have seen in section 5.1.4.

In conclusion this section shows that getting from an arbitrary operator set to partial waves that can be used in a unitarisation procedure, is possible in an affordable way.

## 5.2. Contributions by Different Polarization Combinations

We have learned already that different combinations of helicity states lead to a bad high energy behavior for the three dimension 8 operator sets. In this section we want to study the different helicity combinations in more detail. For that purpose let us first define a piece of notation. We will denote the helicity states of in- and outgoing vector bosons by

$$(\lambda_1, \lambda_2, \lambda_3, \lambda_4), \quad \lambda_i \in \{-1, 0, 1\}, \quad (5.5)$$

or equivalently in a more symbolic way by

$$\lambda_1 \lambda_2 \lambda_3 \lambda_4, \quad \lambda_i \in \{-, 0, +\}. \quad (5.6)$$

Let us exemplarily have a look at the amplitudes generated by the operators  $\mathcal{L}_{S,1}$ ,  $\mathcal{L}_{M,2}$  and  $\mathcal{L}_{T,0}$  in the process  $W^+W^- \rightarrow ZZ$ . Note that these amplitudes represent relatively simple structures compared to the ones generated by other operators of the same sets.

$$\mathcal{A}_{S,1} = 2m_W^2 m_Z^2 \frac{f_{S,1}}{\Lambda^4} \epsilon_1 \cdot \epsilon_2 \epsilon_3^* \cdot \epsilon_4^*, \quad (5.7a)$$

$$\mathcal{A}_{M,2} = \frac{4m_W^2 m_Z^2 \sin^4 \theta_W}{v^2} \frac{f_{M,2}}{\Lambda^4} \epsilon_1 \cdot \epsilon_2 (k_3 \cdot k_4 \epsilon_3^* \cdot \epsilon_4^* - \epsilon_3^* \cdot k_4 \epsilon_4^* \cdot k_3), \quad (5.7b)$$

$$\mathcal{A}_{T,0} = \frac{128m_W^4 \cos^2 \theta_W}{v^4} \frac{f_{T,0}}{\Lambda^4} (k_1 \cdot k_2 \epsilon_1 \cdot \epsilon_2 - \epsilon_1 \cdot k_2 \epsilon_2 \cdot k_1) (k_3 \cdot k_4 \epsilon_3^* \cdot \epsilon_4^* - \epsilon_3^* \cdot k_4 \epsilon_4^* \cdot k_3) \quad (5.7c)$$

The first equation shows the by now well known  $\mathcal{L}_{S,1}$  amplitude only containing polarization vectors, leading to an  $s^2$  dependence if all vector bosons are longitudinal. The second amplitude has two momenta appearing in every term. These are resulting from the insertion of a field strength tensor in the  $\mathcal{L}_{M,i}$  operator class. Naively one could think that the amplitude might grow like  $s^3$  when all vector bosons are longitudinal, but it turns out that those terms cancel (as for all other operators of this class). The strongest growth will still go like  $s^2$  if we insert longitudinally polarized vector bosons in the initial and transversely polarized ones in the final state, i.e. for the helicity state  $(0, 0, \pm 1, \pm 1)$ . The last amplitude of the set above carries 4 momenta and 4 polarization vectors in every term. We will again find a  $s^2$  growth, but only for the all transverse scattering, i.e. in  $(\pm 1, \pm 1, \pm 1, \pm 1)$  and  $(\pm 1, \pm 1, \mp 1, \mp 1)$ .

In the cases above the high energy behavior can be decoded quite easily. But with this not being very clear in the beginning of the work for this thesis and with the other operators often showing a lot more complicated structure, one task of this work was to get a good overview of where the strongest growths in  $s$  would appear.

The simplest approach to that task was calculating the amplitudes for all possible combinations of helicities, i.e build a  $9 \times 9$  matrix corresponding to all possible states like

$$\begin{pmatrix} ---- & ---0 & ----+ & --0- & --00 & --0+ & ---+- & ---+0 & ---++ \\ -0-- & -0-0 & -0-+ & -00- & -000 & -00+ & -0+- & -0+0 & -0++ \\ -+--- & -+0- & -+--+ & -+0- & -+00 & -+0+ & -+--+ & -+0+ & -+ ++ \\ 0---- & 0--0 & 0--+ & 0-0- & 0-00 & 0-0+ & 0-+- & 0-+0 & 0-++ \\ 00-- & 00-0 & 00-+ & 000- & 0000 & 000+ & 00+- & 00+0 & 00++ \\ 0+--- & 0+-0 & 0+--+ & 0+0- & 0+00 & 0+0+ & 0+--+ & 0+0+ & 0+ ++ \\ +---- & +--0 & +--+ & +0- & +00 & +0+ & +--+ & +0+0 & + ++ \\ +0-- & +0-0 & +0-+ & +00- & +000 & +00+ & +0+- & +0+0 & +0++ \\ +++-- & +++-0 & ++++ & +++- & +++0 & ++++ & +++- & +++0 & ++++$$
(5.8)

A much smaller set of helicity states will be sufficient however, because several symmetries relate the amplitudes amongst each other. For clarity we will focus as above on the case of  $W^+W^- \rightarrow ZZ$  scattering. The symmetries we can use here are

1. Parity  $\mathcal{P}$ , corresponding to a flip of all helicity signs,
2. Charge conjugation  $\mathcal{C}$ , corresponding to the exchange of  $W^+$  and  $W^-$ ,
3. Bose symmetry  $\mathcal{B}$ , meaning the exchange of the Z-bosons.

All dimension 8 operators studied in this thesis were built such that they are  $\mathcal{CP}$  invariant, therefore also the amplitudes will be so. Moreover, the exchange of the final state Z-bosons should not make a difference, because they are identical particles respecting Bose-symmetry. Plugging explicit momenta and helicity eigenvectors as they are defined in appendix D and section 4.4 into the amplitudes, we find the following symmetries corresponding to the list above:

$$\mathcal{A}_{\lambda_1\lambda_2\lambda_3\lambda_4} = (-1)^{\lambda_1+\lambda_2+\lambda_3+\lambda_4} \mathcal{A}_{-\lambda_1-\lambda_2-\lambda_3-\lambda_4}, \quad (5.9a)$$

$$\mathcal{A}_{\lambda_1\lambda_2\lambda_3\lambda_4} = (-1)^{\lambda_1+\lambda_2} \mathcal{A}_{\lambda_1\lambda_2\lambda_4\lambda_3}(\theta \rightarrow \pi - \theta) \quad (5.9b)$$

$$\mathcal{A}_{\lambda_1\lambda_2\lambda_3\lambda_4} = (-1)^{\lambda_1+\lambda_2+\lambda_3+\lambda_4} \mathcal{A}_{\lambda_2\lambda_1\lambda_3\lambda_4}(\theta \rightarrow \pi - \theta) \quad (5.9c)$$

The change in the scattering angle can be understood by looking at figure 5.2. It is just a consequence of inserting explicit momenta into the amplitudes.

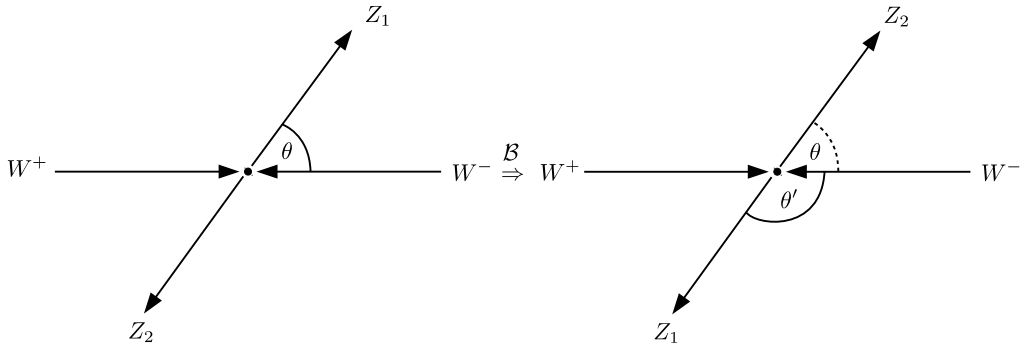


Figure 5.2.: This figure shows the exchange of a Z-bosons in a kinematical representation. Working with explicit momenta and helicity eigenvectors in a center of mass frame, this picture shows that one has to shift  $\theta \rightarrow \theta' = \pi - \theta$  when inserting the vectors into the amplitude in order to get the same result.

These relations have all been explicitly checked on several representative examples of all operator classes. They help reducing the 81 entries of the matrix (5.8) down to 22 independent ones (see figure 5.3).

$$\begin{array}{c}
\mathcal{B} \\
\left( \begin{array}{cccccccc}
--- & --0 & ---+ & \color{blue}{-0-} & --00 & --0+ & \color{blue}{-+--} & \color{blue}{--+0} & --++ \\
-0- & -0-0 & -0-+ & \color{blue}{-00-} & -000 & -00+ & \color{blue}{-0+-} & \color{blue}{-0+0} & -0++ \\
-+- & -+-0 & -+--+ & \color{blue}{-+0-} & -+00 & -+0+ & \color{blue}{-++-} & \color{blue}{-++0} & -++++ \\
\color{green}{0---} & \color{green}{0--0} & \color{green}{0--+} & \color{green}{0-0-} & \color{green}{0-00} & \color{green}{0-0+} & \color{green}{0-+-} & \color{green}{0-+0} & \color{green}{0-++} \\
00- & 00-0 & 00-+ & \color{blue}{000-} & 0000 & 000+ & 00+- & 00+0 & 00++ \\
\color{red}{0+--} & \color{red}{0+-0} & \color{red}{0+--+} & \color{red}{0+0-} & \color{red}{0+00} & \color{red}{0+0+} & \color{red}{0++-} & \color{red}{0++0} & \color{red}{0++++} \\
\color{red}{+-} & \color{red}{+-0} & \color{red}{+-+} & \color{red}{+-0-} & \color{red}{+-00} & \color{red}{+-0+} & \color{red}{+-+-} & \color{red}{+-+0} & \color{red}{+----} \\
\color{red}{+0-} & \color{red}{+0-0} & \color{red}{+0-+} & \color{red}{+00-} & \color{red}{+000} & \color{red}{+00+} & \color{red}{+0+-} & \color{red}{+0+0} & \color{red}{+0+++} \\
\color{red}{++-} & \color{red}{++-0} & \color{red}{++-+} & \color{red}{++0-} & \color{red}{++00} & \color{red}{++0+} & \color{red}{+++-} & \color{red}{+++0} & \color{red}{++++}
\end{array} \right) \mathcal{C} \\
\mathcal{P}
\end{array}$$

Figure 5.3.: This figure shows a pictorial description of how the charge conjugation  $\mathcal{C}$ , parity  $\mathcal{P}$  and Bose-symmetry  $\mathcal{B}$  help reducing the number of independent entries of the matrix down to 22 (the entries without color overlay).

In this way a reduced version of the full matrix (5.8) could be used for analyzing the strongest contributions of all operators. In the end the version that was used looks like

$$\begin{pmatrix}
--- & --00 & ---0 & ---+ \\
++- & ++00 & ++-0 & ++-+ \\
00- & 0000 & 00-0 & 00-+ \\
-0- & -000 & -0-0 & -0-+ \\
0+ & 0+00 & 0+-0 & 0+-+ \\
-+- & -+00 & -+-0 & -+-+
\end{pmatrix}. \quad (5.10)$$

The ordering of the entries is in terms of helicity differences, which are the relevant measure when working with the Wigner-d-functions in a partial wave analysis. By denoting the entries of the above matrix as  $(\lambda, \mu) = (\lambda_1 - \lambda_2, \lambda_3 - \lambda_4)$ , the corresponding matrix in terms of helicity differences reads

$$\begin{pmatrix}
(0,0) & (0,0) & (0,-1) & (0,-2) \\
(0,0) & (0,0) & (0,-1) & (0,-2) \\
(0,0) & (0,0) & (0,-1) & (0,-2) \\
(-1,0) & (-1,0) & (-1,-1) & (-1,-2) \\
(-1,0) & (-1,0) & (-1,-1) & (-1,-2) \\
(-2,0) & (-2,0) & (-2,-1) & (-2,-2)
\end{pmatrix}. \quad (5.11)$$

In this set up it is now possible to have a look at all relevant contributions from any dimension 8 operator. As an example, the amplitudes resulting from  $\mathcal{L}_{M,1}$  that grow like  $s^2$  are

$$J = 0 : \begin{pmatrix}
0 & -\frac{m_W^2}{2v^2} \bar{f}_{M,1} s^2 & 0 & 0 \\
0 & -\frac{m_W^2}{2v^2} \bar{f}_{M,1} s^2 & 0 & 0 \\
\frac{c_w^2 m_W^2}{2v^2} \bar{f}_{M,1} s^2 & 0 & 0 & 0 \\
0 & 0 & 0 & 0 \\
0 & 0 & 0 & 0 \\
0 & 0 & 0 & 0
\end{pmatrix},$$

$$J = 1 : \begin{pmatrix} 0 & 0 & 0 & 0 \\ 0 & 0 & 0 & 0 \\ 0 & 0 & 0 & 0 \\ 0 & 0 & 0 & 0 \\ 0 & 0 & 0 & 0 \\ 0 & 0 & 0 & 0 \end{pmatrix},$$

$$J = 2 : \begin{pmatrix} 0 & 0 & 0 & 0 \\ 0 & 0 & 0 & 0 \\ 0 & 0 & 0 & -\frac{c_w^2 m_W^2}{5\sqrt{6}v^2} \bar{f}_{M,1} s^2 \\ 0 & 0 & 0 & 0 \\ 0 & 0 & 0 & 0 \\ 0 & \frac{m_W^2}{5\sqrt{6}v^2} \bar{f}_{M,1} s^2 & 0 & 0 \end{pmatrix},$$

where  $c_w \equiv \cos \theta_w$ . Results like these could now be used to get partial waves as proper inputs for the definition of the K-matrix-like form factor (4.103).

This concludes the chapter on the partial wave analysis with the help of Mathematica. In the following chapter we will see how the actual implementation of the K-matrix procedure for  $\mathcal{L}_{S,0}$  and  $\mathcal{L}_{S,1}$  into VBFNLO works.

## Implementation

The K-matrix unitarisation procedure for the  $\mathcal{L}_{S,0}$  and  $\mathcal{L}_{S,1}$  operators has been implemented into the Monte Carlo program **VBFNLO**. Therefore a quick general introduction into the software and a quick overview on the implementation of anomalous couplings is given in this chapter. The main part of this chapter is the final implementation of the K-matrix method with the discussion of some technical details.

6.1. Introduction into **VBFNLO**

**VBFNLO** [30] is a parton level Monte Carlo program that simulates hadron collisions for various processes involving electroweak bosons up to next-to-leading order (NLO) in the strong coupling constant  $\alpha_s$ . Its main strength is its speed and reliability. High statistics and accuracy can often be achieved significantly quicker than in comparable Monte Carlo programs. It includes various beyond the Standard Model (BSM) effects like anomalous couplings.

The main focus of **VBFNLO** is to calculate the total cross section of some process  $pp \rightarrow X$  in an efficient way, i.e. solving the integral [31]

$$\sigma = \int dx_1 dx_2 \sum_{\text{subprocesses}} f_{a_1}(x_1) f_{a_2}(x_2) \frac{1}{2\hat{s}} \int d\Phi_n(x_1 p_{a_1} + x_2 p_{a_2}; p_1, \dots, p_n) \Theta(\text{cuts}) \overline{|\mathcal{M}|^2}(a_1 a_2 \rightarrow b_1 b_2). \quad (6.1)$$

The quantities  $f_{a_i}(x_i)$  represent the parton distribution functions (PDFs), i.e. the probability of finding parton  $a_i$  with momentum fraction  $x_i$  inside a (anti-)proton, which are only known numerically. The energy  $\sqrt{\hat{s}}$  represents the center of mass energy of the corresponding partonic subprocess.  $d\Phi_n(P; p_1, \dots, p_n)$  is the Lorentz invariant phase space element and  $\Theta(\text{cuts})$  is called acceptance function, which simply summarizes all the cuts imposed on a specific process. The last quantity  $\mathcal{M}$  represents the Feynman amplitude of the subprocess under consideration where the sum means summing and averaging over the polarizations and colors of the external partons.

With the above (high dimensional) integral not being soluble analytically, one needs educated methods for solving it numerically. In **VBFNLO** this is done via the Monte Carlo method, i.e. replacing the integral by a sum over randomly generated but carefully chosen phase space points. Here, “carefully chosen” means that they are generated in a way such that more points fall into regions that give large contributions to the integral, thus reducing the error in the determination of the integral. This method is called “Importance Sampling”. According to the law of large numbers the integral will be reproduced by going to an infinite number of points. Several iterations are used in order to optimize the importance sampling and therefore the error on the final result. For this matter an adapted version of the **VEGAS** Monte Carlo integrator [32] is used.

An actual run of the VBFNLO program starts with reading in all necessary input parameters that can be manipulated by the user by altering the corresponding input files. Then the calculation itself is set up by starting the two nested main loops, the outer one controlling the iteration steps of the adaptive Monte Carlo algorithm, the inner one just counting the randomly generated phase space points. In every step of the loops, the possible contribution of the corresponding phase space point to the integral is calculated in the following way [21]:

1. The integration routine gives an array of random numbers with the accompanying weight resulting from the importance sampling.
2. The random numbers are converted to particle momenta in the routine `phasespace.F`.
3. The resulting phase space point is only kept if it respects the cuts, otherwise its weight is set to zero.
4. The factorization scale  $\mu_F$  and renormalization scale  $\mu_R$  are calculated for this phase space point.
5. In `amplitude.F` the routines for calculating the amplitude and the corresponding matrix element squared get called for the process under consideration.
6. The result gets multiplied with a phase space factor and together with its weight transferred back to the integration routine.
7. In the las(t) VEGAS iteration the events get transferred not only to the integration, but also to a histogram routine which can easily be modified to include the users own histogram definitions.
8. Finally the resulting total cross section and the accompanying statistical error are written into `xsection.out`

The NLO calculation in principle follows the same steps, but is only started after the full LO calculation and uses the grid, i.e. set of random numbers and weights, of the last iteration step.

A nice feature of the structure of all VBFNLO calculations is the separation of the matrix elements into two parts: the so called leptonic tensor and the quark currents, i.e.

$$\mathcal{M} = J_\mu^1 J_\nu^2 L_{V_1 V_2 \rightarrow X}^{\mu\nu}. \quad (6.2)$$

The leptonic tensor represents the part one can separate from the two quark lines in figure 6.1. Not only does this treatment speed up the running of the code, but it also facilitates the inclusion of NLO corrections to processes involving anomalous couplings. Thanks to this structure, the anomalous couplings need only be included in the leptonic tensor and therefore NLO calculations can be done just as in the SM case.

## 6.2. Structure of Anomalous Couplings in VBFNLO

In this section we will focus on the implementation of anomalous quartic gauge couplings (AQGCs) in the VBFNLO code. All 4-vertex modifying operators, respectively the resulting amplitudes are implemented in the file `anoma14.F`. The subroutines in this file all carry the same structure, similar to

```
subroutine wwzz_anoma14(wm,z1,wp,z2, wwzz)
...      !definitions and decoding of the momenta
```

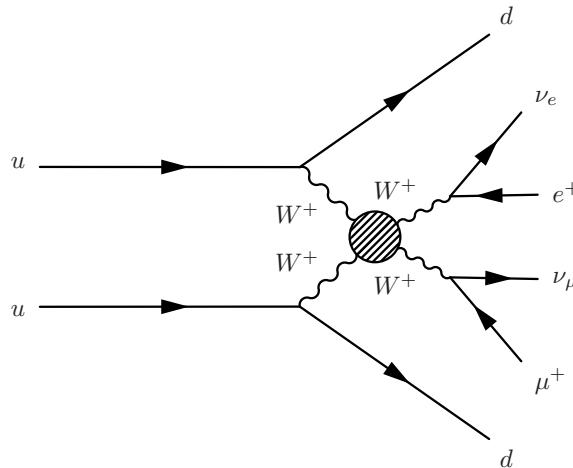


Figure 6.1.: This figure shows the Feynman graph of two  $u$  quarks scattering to two  $d$  quarks and four leptons resulting from  $W^+W^+ \rightarrow W^+W^+$  scattering.

```

if (fS0 .ne. 0) then
  wwzz = wwzz + fS0 * ... !some contribution
endif

if (fS1 .ne. 0) then
  wwzz = wwzz + fS1 * ... !another contribution
endif

...      !and so on

```

They use the four polarization vectors of the vector bosons and the SM amplitude `wwzz` for the process under consideration as an input, add anomalous contributions and return the modified amplitude `wwzz`.

If the use of a form factor has been specified in the input files, then this form factor also gets calculated in `anoma14.F` and multiplied to all dimension 8 couplings like `fS0`. Those modified couplings are in turn used in the subroutines like the one we have seen above. In this way the anomalous contributions are suppressed, depending on the center of mass energy of the electroweak system.

With the work of this thesis, the K-matrix method that has been implemented treats the operators  $\mathcal{L}_{S,0}$  and  $\mathcal{L}_{S,1}$  in a separate way. Furthermore, a method has been proposed to extend the K-matrix method in a simplified way in order to also unitarize the other operators. The main modifications to the `VBFNLO` code have been done in the aforementioned `anoma14.F` and the next section will show those modifications in detail.

### 6.3. K-Matrix Method for $\mathcal{L}_{S,0}$ and $\mathcal{L}_{S,1}$

The question of how to translate the unitarized on-shell scattering amplitudes from section 4.6 to the off-shell case now arises. It is solved by using the expressions found in that section to build up channel-dependent form factors, i.e. in general three different form factor-like functions for the  $s$ -,  $t$ - and  $u$ -channels of an amplitude.

#### 6.3.1. General Approach

In the way we defined the unitarized amplitudes, the implementation of the K-matrix approach into `VBFNLO` is now pretty straightforward. We take (4.97), translate the Mandelstam variables back to the corresponding combinations of polarization vectors and bring

the resulting unitarized amplitude into a form that can directly be mirrored to the original amplitude in the VBFNLO code.

As an example, we take a look at the process  $W^+W^+ \rightarrow W^+W^+$ . We use (4.72) and insert this into the unitarized amplitude to get

$$\begin{aligned} \hat{\mathcal{A}}(W^+W^+ \rightarrow W^+W^+) &= 4m_w^4 \left[ 2\bar{f}_{S,0} + \frac{1}{s^2}(\Delta A_{20} - 10\Delta A_{22}) \right] \epsilon_1 \cdot \epsilon_2 \epsilon_3^* \cdot \epsilon_4^* \\ &\quad + 2m_w^4 \left[ \bar{f}_{S,1} + \frac{30}{s^2}\Delta A_{22} \right] (\epsilon_1 \cdot \epsilon_3^* \epsilon_2 \cdot \epsilon_4^* + \epsilon_1 \cdot \epsilon_4^* \epsilon_2 \cdot \epsilon_3^*), \end{aligned} \quad (6.3)$$

To VBFNLO the relevant part is the final state  $W^+W^+$ , so in the unitarisation procedure one needs to take care that all 4-vertices contributing to the electroweak final state get unitarized accordingly. For  $W^+W^+$  this is a simple task, because the only 4-vertex of importance here is the  $WWWW$ -vertex. So for the unitarisation in VBFNLO we only need to take a look at the anomalous part in the `www`-amplitude. This part reads

$$\begin{aligned} \mathcal{A}(W^+W^+ \rightarrow W^+W^+)_{\text{VBFNLO}} &= 4 * \text{wmass} ** 4 * \text{fS0} * \text{dotcc}(\text{wp1}, \text{wp2}) * \text{dotcc}(\text{wm1}, \text{wm2}) \\ &\quad + 2 * \text{wmass} ** 4 * \text{fS1} * (\text{dotcc}(\text{wp1}, \text{wm2}) * \text{dotcc}(\text{wp2}, \text{wm1}) \\ &\quad + \text{dotcc}(\text{wp1}, \text{wm1}) * \text{dotcc}(\text{wp2}, \text{wm2})), \end{aligned} \quad (6.4)$$

where the `wi` are the polarization vectors associated with the 4 vector bosons and `dotcc(. , .)` is just the dot-product of two complex 4-vectors. We can now match the two amplitudes from above in terms of the dot-products. This again depends on the process we are looking at. Due to crossing symmetry the same  $\mathcal{A}(W^+W^+ \rightarrow W^+W^+)_{\text{VBFNLO}}$  is used e.g. in  $W^+W^- \rightarrow W^+W^-$  with just a permutation of the polarization vectors. In our case the right choice is

$$\epsilon_1 \leftrightarrow \text{wp1}, \quad \epsilon_2 \leftrightarrow \text{wp2}, \quad \epsilon_3^* \leftrightarrow \text{wm1}, \quad \epsilon_4^* \leftrightarrow \text{wm2}. \quad (6.5)$$

The final step is now to replace the couplings `fS0` and `fS1` by the corresponding terms of (6.3) in square brackets.

With the above steps we arrived at a unitarized amplitude that has the exact same behavior as the original amplitude in the low energy regime ( $\Re[\Delta A_{IJ}] \simeq 0$  and  $\Im[\Delta A_{IJ}] \simeq 0$ ) and which approaches zero for high c.o.m. energies. Here the real part of the sum of the  $\Delta A_{IJ}/s^2$  exactly cancels the couplings in front of them.

### 6.3.2. Technical Details

The final implementation into VBFNLO follows the approach of the previous section. All of the following changes are implemented in the file `anomal4.F`. The routines that needed alterations are

- `subroutinewwzz_anomal4(wm, z1, wp, z2, wwzz)`
- `subroutinewww_anomal4(wm1, wp1, wm2, wp2, wwww)`
- `subroutinezzzz_anomal4(z1, z2, z3, z4, zzzz)`.

In the original implementation of anomalous couplings the two operators  $\mathcal{L}_{S,0}$  and  $\mathcal{L}_{S,1}$  have been treated separately, i.e.

```

if (fs0 .ne. 0) then
  www = ...
endif

if (fs1 .ne. 0) then
  www = ...
endif

```

With the K-Matrix unitarisation procedure including relative effects between  $\mathcal{L}_{S,0}$  and  $\mathcal{L}_{S,1}$ , the two anomalous contributions have been merged in each of the subroutines listed above. They are nested inside an `if-else`-structure, that uses a global K-matrix switch. If the switch is set to `true` the merged and unitarized version is used, otherwise the original implementation is chosen. An example of this structure is the code snippet below:

```

if (kmatrix) then
  if (fs0 .ne. 0 .or. fs1 .ne. 0 ) then
    www = www
    & + 4. * wmass**4 * fswp1wp2 * dotcc(wp1,wp2) * dotcc(wm1,wm2)
    & + 2. * wmass**4 * fswp1wm2 * dotcc(wp1,wm2) * dotcc(wp2,wm1)
    & + 2. * wmass**4 * fswp1wm1 * dotcc(wp1,wm1) * dotcc(wp2,wm2)
  endif
else
  ...
endif

```

This snippet also shows the separation between the  $s$ -,  $t$ -, and  $u$ -channels. The aforementioned channel-dependent form factors `fswij` are the ones in front of the dot-products. The reason for not naming the three channels after the Mandelstam variables lies in the fact that the same subroutines get used for different processes that are related by crossing symmetry. This corresponds to a permutation of  $s$ -,  $t$ -, and  $u$ . Therefore the decision of which channel is which needs to be taken elsewhere.

The rest of the unitarisation procedure takes place in the already existent subroutine `anom_formfactor`. Originally this routine is called whenever a vector boson 3- or 4-vertex appears in the calculation of the leptonic tensor. If the global logical variable `formfact` is set to `true` the form factors get calculated according to the settings in the input file `anomV.dat`. The same structure is now used with the logical variable `kmatrix` added. If either of the two is `true`, the center of mass energy squared `ss` of the electroweak system is calculated. This energy corresponds to the Mandelstam variable  $s$  that is later inserted in the form factors and the unitarisation factors of the K-matrix approach.

After the calculation of  $s$  another `if` statement separates the original form factor calculation from the K-matrix procedure. In the latter case a `select case`-statement is used to discriminate between the various VBFNLO processes that support anomalous contributions of the dimension 8 operators in four cases:

1. WPWMjj, WPhadWMjj, WPWMhadjj
2. WPWPjj, WMWMjj, WPhadWPjj, WMhadWMjj
3. WPZjj, WMZjj, WPhadZjj, WPZhadjj, WMhadZjj, WMZhadjj
4. ZZjj\_ll, ZZjj\_lnu, ZZhadjj .

Note that we do not have five cases in here as one would suspect by looking at the processes in section 4.6, which is because we are only selecting final states in VBFNLO. The process not directly seen in here is  $W^\pm W^\mp \rightarrow ZZ$ . Obviously the unitarisation of this process needs to be taken care of in processes that contain either of the two vector boson pairs in the initial state of the electroweak process, i.e. in cases 1. and 4. from the list above.

When the selection is done, the  $\Delta A_{IJ}$  needed for the process are calculated and inserted into the channel-dependent form factors  $f_{svivj}$ , which can be seen in the following code snippet:

```

CASE(ZZjj_l1, ZZjj_lnu, ZZhadjj)

  DA00 = -((7.*fS0 + 11.*fS1)**2*ss**4)/(6.*((0,192)*Pi + (7.*fS0 + 11.*fS1)*ss
    **2))
  DA11 = -((fS0 - 2.*fS1)**2*ss**4)/(12.*((0,384)*Pi + (fS0 - 2.*fS1)*ss**2))
  DA02 = -((2.*fS0 + fS1)**2*ss**4)/(30.*((0,960)*Pi + (2.*fS0 + fS1)*ss**2))
  DA20 = -((2.*fS0 + fS1)**2*ss**4)/(3.*((0,96)*Pi + (2.*fS0 + fS1)*ss**2))
  DA22 = -((fS0 + 2.*fS1)**2*ss**4)/(60.*((0,1920)*Pi + (fS0 + 2.*fS1)*ss**2))

  fswmwp = fs1 + 2./(3.*ss**2) * (DA00 - DA20) - 20./(3.*ss**2) * (DA02 - DA22)
  fswmz1 = fS0 + 20./(ss**2) * (DA02 - DA22)
  fswmz2 = fswmz1

  fsz1z2 = fS0 + fS1 + 2./(3.*ss**2) * (DA00 + 2.*DA20) - 20./(3.*ss**2) * (DA02
    + 2.*DA22)
  fsz1z3 = fS0 + fS1 + 10./ss**2 * (DA02 + 2. * DA22)
  fsz1z4 = fsz1z3

```

These are then finally used in the  $VVVV$ -subroutines that add the corresponding anomalous contribution to the SM amplitude.

Note that in the actual implementation the  $\Delta A_{IJ}$  need to be calculated separately for the  $WWWW$  vertex. This is a result of the isospin-symmetry breaking nature of  $\mathcal{L}_{S,0}$ . In order to get the correction terms, one needs to start from equation (4.73), set  $f_{S,2} = 0$  and redo the partial wave analysis<sup>1</sup>. This is to be considered as rather unphysical, but it guarantees the comparability to the operator  $\mathcal{L}_4$ .

Further changes only include the addition of the logical parameter `KMATRIXX` to the input file `anomV.dat`. This parameter is read in and the global variable `kmatrix` added in `an_couplings.inc` is set to its value. In contrast to the use of form factors no additional parameters need to be set.

---

<sup>1</sup>This is equivalent to taking the results from [6] and using the conversion (3.25).

## Analysis

In this chapter we will see the results of the implementation of the K-matrix unitarisation procedure for the  $\mathcal{L}_{S,0}$  and  $\mathcal{L}_{S,1}$  operators. A qualitative comparison to the approach of using form factors, as well as a quantitative comparison between VBFNLO and WHIZARD is given. We will furthermore see that the results produced are easily transferable to NLO calculations of VBFNLO.

## 7.1. General Remarks on Vector Boson Scattering

Vector Boson Scattering (VBS), i.e. processes of the form  $VV \rightarrow VV$  with  $V \in \{W, Z\}$ , represents an appealing playground for experimentalists and theorists alike in several aspects. With the recent discovery of a Higgs-like particle by the ATLAS and CMS detectors [1, 2], in VBS it is testable whether this particle really unitarizes the longitudinal VBS channels in the way it was discussed in section 4.2.2. Moreover do the VBS processes inherit the trilinear and quartic vector boson vertices. Especially the quartic couplings have not been accurately measured so far.

On the theory side there exist several propositions of how VBS processes could be enhanced, including the dimension 8 operators that we discuss in this thesis. On the experimental side VBS is on the edge of being experimentally accessible. Already with the LHC data collected in 2008 first evidence of VBS in the same sign  $W$ -channel could be shown by the ATLAS collaboration [3]. Figure 7.1 shows some of the findings, including the first limits on the AQGC  $\alpha_4$  and  $\alpha_5$ . A lot more data for this and other processes will follow in the high luminosity/full energy runs of the LHC starting in 2015.

The bounds on the K-matrix unitarized anomalous couplings  $\alpha_4$  and  $\alpha_5$  published in [3] are (only one of the two couplings switched on at a time)

$$-0.14 < \alpha_4 < 0.16; \quad -0.23 < \alpha_5 < 0.24. \quad (7.1)$$

Provided the K-matrix implementation of VBFNLO and WHIZARD give the same results and using the conversion of  $\alpha_i$  to  $f_{S,i}$  (3.25) one can get the limits

$$-304 \text{ TeV}^{-4} < \frac{f_{S,0}}{\Lambda^4} < 348 \text{ TeV}^{-4}, \quad (7.2)$$

$$-805 \text{ TeV}^{-4} < \frac{f_{S,1}}{\Lambda^4} < 870 \text{ TeV}^{-4}. \quad (7.3)$$

These numbers show that there is still a lot of room for the discovery of BSM physics in VBS. If there is new physics hidden in VBS, there are good chances to find it in the course of the next few years. Otherwise the experimentalists will at least be able to push the bounds down by a large factor.

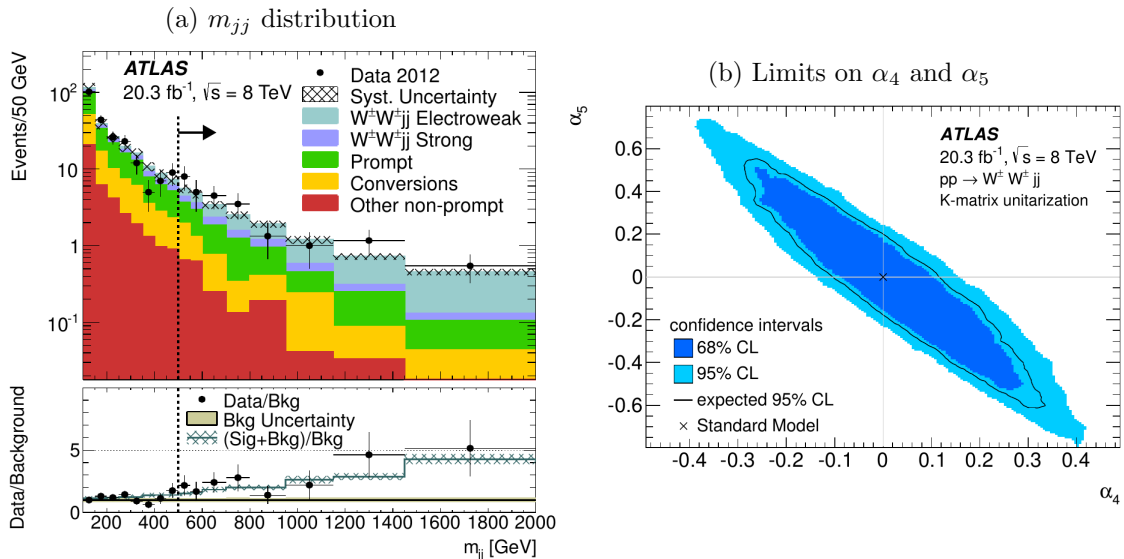


Figure 7.1.: These plots of the ATLAS collaboration [3] show the first experimental evidence of VBS in the form of a  $m_{jj}$  distribution and the first limits on the ACGQs  $\alpha_4$  and  $\alpha_5$  (calculated with WHIZARD, using the K-matrix unitarisation). The light blue area in the  $m_{jj}$  plot represents the electroweak channels of the  $W^\pm W^\pm jj$  production, i.e. weak interactions at Born level including VBS.

## 7.2. Anomalous couplings at NLO in $\alpha_s$

The modular structure of VBFNLO makes possible to go to NLO in the strong coupling constant  $\alpha_s$  without any further modifications. Therefore the anomalous coupling scenarios as well as the K-matrix unitarized versions can easily be used at NLO. An example of this is shown in figure 7.2, where the invariant mass spectrum in the process  $W^+W^+jj$  is plotted in a comparison of the LO to the NLO distributions including the corresponding K-factor. They have been generated by using the same settings as in the previous section and just setting `NLO_SWITCH = true` in the `vbfno.dat` input file. The calculations have been done with 6 iterations and  $2^{26}$  points in both cases. The computation time for one setting, e.g. LO and NLO distributions for the K-matrix unitarized case, was less than half a day on a typical tower PC.

## 7.3. Comparison of K-Matrix Approach vs. Form Factors

Generally speaking a quantitative comparison of the K-matrix versus the form factor approach is relatively difficult due to the very different nature of the two. Qualitatively one can see clear differences by looking at figures 7.3 and 7.5. The first figure shows the two approaches treated in a simple analytic case, i.e. taking a look at the partial wave  $A_{00}(s)$  (4.91a) from section 4.6.3. In order to discuss this figure, let us first have a look at the analytic structure. We can build a unitarized amplitude  $\hat{A}_{IJ}(s)$  following the usual K-matrix prescription, but we can also use this to define a form factor like function  $\mathcal{F}_K(s)$  (see 4.7). With the form factor being a real function, let us take a look at the real part of  $\mathcal{F}_K(s)$ . We can do this by simply dividing  $\hat{A}_{IJ}(s)$  by  $A_{IJ}(s)$  and taking the real part of the result, i.e.

$$\mathcal{F}_K(s) = \Re \left[ \frac{\hat{A}_{IJ}(s)}{A_{IJ}(s)} \right] = \Re \left[ \frac{1}{1 - iA_{IJ}(s)/(32\pi)} \right]$$

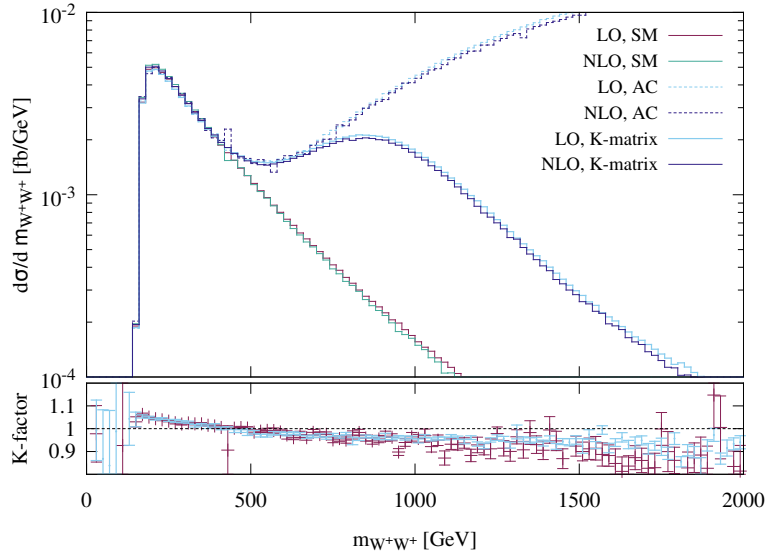


Figure 7.2.: Invariant mass spectrum of the  $W^+W^+$  pair at LO and NLO in  $\alpha_s$  for the SM case and  $\bar{f}_{S,0} = \bar{f}_{S,1} = 100 \text{ TeV}^{-4}$ . The lower plot shows the K-factor, i.e. the NLO/LO-ratio for the SM case in violet and the K-matrix case in light blue.

$$= \frac{1}{1 + [A_{JJ}(s)/(32\pi)]^2} \quad (7.4)$$

We can now insert the explicit form (4.91a) into this and get a version of  $\mathcal{F}_K(s)$  that is comparable to the usual form factor  $\mathcal{F}(s)$ :

$$\mathcal{F}_K(s) = \frac{1}{1 + \left(\frac{f_{S,0}s^2}{96\pi\Lambda^4}\right)^2}; \quad \mathcal{F}(s) = \frac{1}{\left(1 + \frac{s}{\Lambda_{FF}^2}\right)^n}. \quad (7.5)$$

At first sight one might think both give about similar results when choosing

$$n = 4, \quad \Lambda_{FF} = \left(\frac{f_{S,0}}{\Lambda^4} \frac{1}{96\pi}\right)^{-1/4}, \quad (7.6)$$

but figure 7.3a proves differently. The suppression is much stronger for the original form factor  $\mathcal{F}(s)$ , i.e. the unitarity bound we are using in the K-matrix formalism is not reached at all. In figures 7.3b and 7.3c the values for  $\Lambda_{FF}$  are chosen in such a way, that the unitarity bound is just reached. Still the shape of the two unitarized amplitudes strongly differ. The suppression by  $\mathcal{F}(s)$  is somewhat smoother and sets in much earlier. One could pose the question here whether the K-matrix bounds are too weak, or if the form factor energy scale  $\Lambda_{FF}$ , as they are typically calculated<sup>1</sup>, are too low.

The advantage of  $\mathcal{F}_K(s)$  is that the unitarized amplitude follows the original one very closely. This is a desirable feature, because one does not want to spoil the behavior of the original EFT in the low energy regime. When the unitarity bound is reached, the suppression forces the amplitude to zero much quicker than  $\mathcal{F}(s)$  does, which could also be considered as desirable. Moreover,  $\mathcal{F}_K(s)$  automatically guarantees unitarity for very different values of the couplings, because it includes them as input parameters (see figure 7.4).

<sup>1</sup>The routine `calc_formfactor` by Bastian Feigl can be used to calculate the values for  $\Lambda_{FF}$  that are meant here.

The same comparison done in a more realistic environment can be seen in figure 7.5. Here we see the implementation of the K-matrix unitarisation method in VBFNLO compared to the use of form factors in an invariant mass spectrum in  $ZZ$ -scattering. The values for  $\Lambda_{FF}$  are 366 GeV, which is the one listed in [21], appendix B, and 1000 GeV which is just an approximate fit-by-eye value in order to reach the unitarity bound like in the K-matrix unitarisation. The figure shares the exact same features as the ones listed above for the analytic partial waves.

To conclude, it is safe to state that the question of which unitarisation method to use, is more a question of taste than a question of which is 'the right' choice. The K-matrix unitarisation method beats form factors in terms of usability, but at the cost of the introduction of a model dependence that is somewhat hidden in the internals. Form factors serve as a simpler, somewhat less invasive approach at the cost of having to deal with the input parameters  $n$  and  $\Lambda_{FF}$ .

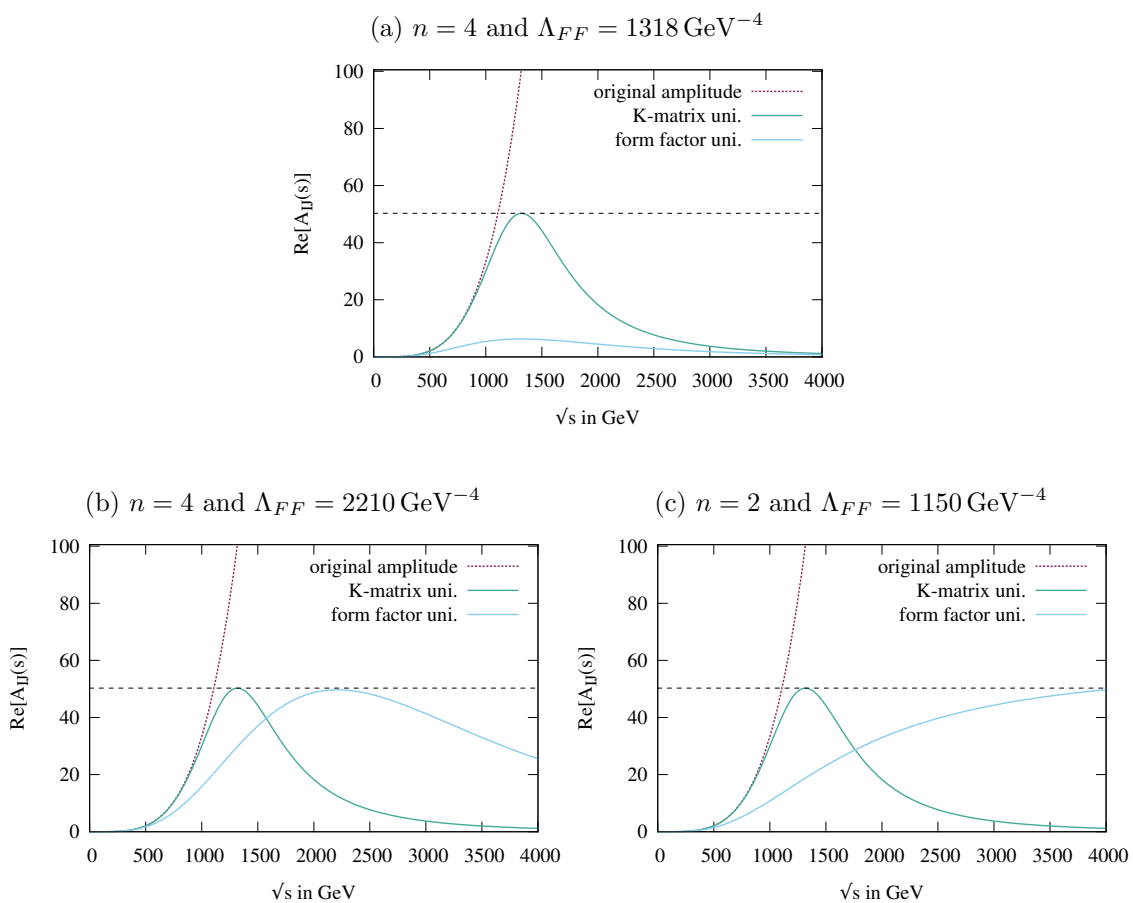


Figure 7.3.: Comparison of the form factor unitarisation versus the K-matrix method for the partial wave  $A_{00}(s) = \bar{f}_{S,0}s^2/3$  and  $\bar{f}_{S,0} = 10 \text{ TeV}^{-4}$ . The plot shows the real part of the (unitarized) partial wave  $A_{IJ}(s)$  over the center of mass energy  $\sqrt{s}$ . The dotted black line represents the unitarity bound  $16\pi$ . The form factors on the two sides feature different exponents  $n$ , where the values  $\Lambda_{FF}$  have been chosen in a 'fit-by-eye' method, such that the unitarity bound is just reached. Note that by taking energies  $\sqrt{s} > 4 \text{ TeV}$  into account, of course a smaller  $\Lambda_{FF}$  would need to be used in figure 7.3c.

## 7.4. Comparison of VBFNLO vs. WHIZARD

A major goal of this thesis is not only to introduce the K-matrix unitarisation method to VBFNLO, but also to make it comparable to another Monte Carlo program that is commonly

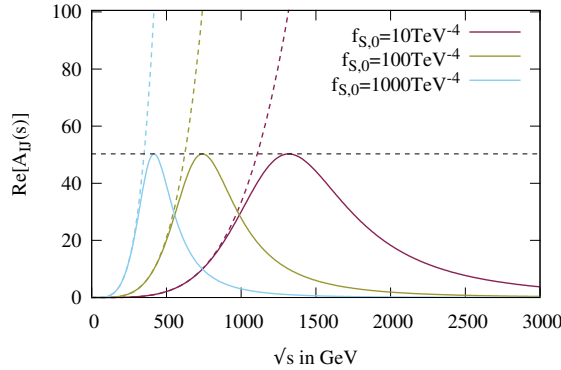


Figure 7.4.: This figure shows a non-unitarized amplitude (dotted) vs. the K-matrix unitarized ones (solid) for three different values of  $f_{S,0}$ . The unitarity bound  $16\pi$  is shown as a black dotted line.

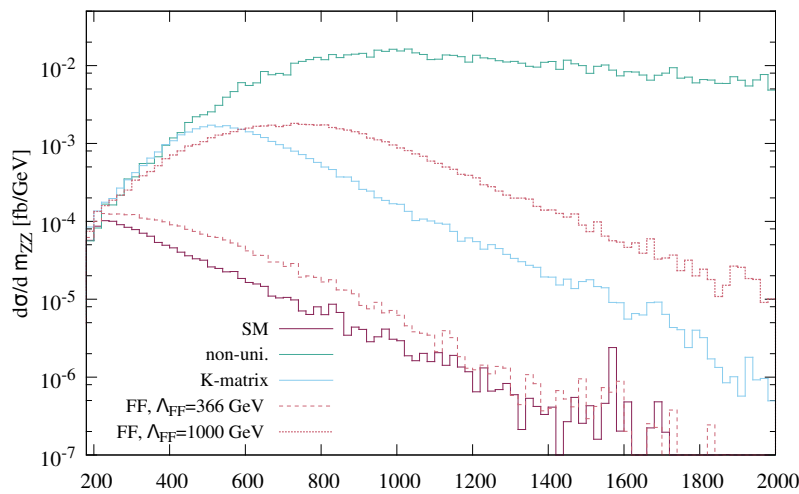


Figure 7.5.: This figure shows the invariant mass spectrum of the  $ZZ$  final state process with  $\bar{f}_{S,1} = 2000 \text{ TeV}^{-4}$  in the K-matrix approach (light blue) and two versions of form factors with  $n = 2$  (light red dotted lines). The violet line on the bottom represents SM contribution, the uppermost turquoise line the anomalous part without unitarisation.

used for studying vector boson processes, WHIZARD [9, 33]. In this way not only the functioning of the implementation can be tested, but also the comparability of the two programs can be checked. The latter is an important fact for experimentalists who are trying to set constraints on the couplings of the dimension 8 operators from measured vector boson scattering data. So far VBFNLO only featured unitarisation via form factors, which is more flexible than the K-matrix unitarisation, but poses the challenge of choosing the 'right' values for  $\Lambda_{FF}$  for a chosen exponent  $n$ . There is a tool that helps finding those values via a partial wave analysis called `calc_formfactor` [21, 22], but still confusion remains on how to properly use form factors among the experimentalists. One cannot say that the K-matrix procedure is the 'better' approach, but it beats form factors in terms of usability, because no adjustment of additional parameters is needed.

With both Monte Carlo programs featuring the same theoretical foundations, but very different ways of implementation, it will be possible to get better estimates on theoretical uncertainties as well as cross-checks considering the constraints on the operators  $\mathcal{L}_{S,0}$  and  $\mathcal{L}_{S,1}$  or  $\mathcal{L}_4$  and  $\mathcal{L}_5$  respectively.

### 7.4.1. Set Up

The set up of the comparison mainly follows the choices of [16], where some cross-checks between VBFNLO and WHIZARD in the process  $pp \rightarrow W^+W^+jj \rightarrow e^+\nu_e\mu^+\nu_\mu jj$  have already been performed. Agreement at the per mill to percent level of the total cross section and invariant mass distributions has been shown for the SM case and two different choices of  $\{f_{S,0}, f_{S,1}\}$ . In this section we will do similar checks for all relevant vector boson scattering processes. Complete input files for the benchmark process  $pp \rightarrow W^+W^+jj \rightarrow e^+\nu_e\mu^+\nu_\mu jj$ , including all relevant cuts can be found in appendix H.

We will focus on leading order calculations in the LHC set up, i.e. proton-proton collisions at a center of mass energy of 14TeV. The PDF set of choice is CETQ6L1 [34] at a fixed factorization scale of  $\mu_F = m_{V_1} + m_{V_2}$  (note that in WHIZARD this is the same as the renormalization scale; both are just called “scale”). External bottom- and top-quarks are neglected and so are the masses of the fermions. The input parameters for masses, particle widths and the Fermi constant read

$$\begin{aligned}
m_W &= 80.398 \text{ GeV}, & \Gamma_W &= 2.097673 \text{ GeV}, \\
m_Z &= 91.1876 \text{ GeV}, & \Gamma_Z &= 2.508420 \text{ GeV}, \\
m_H &= 126 \text{ GeV}, & \Gamma_H &= 4.277 \text{ MeV}, \\
G_F &= 1.16637 \cdot 10^{-5} \text{ GeV}^{-2}.
\end{aligned} \tag{7.7}$$

The cuts on the final state particles are as follows:

$$\begin{aligned}
p_{T,l} &> 20 \text{ GeV}, & |\eta| &< 2.5, \\
p_{T,j} &> 30 \text{ GeV}, & |\eta_j| &< 4.5, \\
|\Delta\eta_{jj}| &> 4, & m_{jj} &> 600 \text{ GeV},
\end{aligned} \tag{7.8}$$

where  $p_T$  is the momentum of a jet or lepton in the plane transverse to the beam axis and  $\eta$  being the rapidity (which coincides with the pseudo rapidity as the final state particles are taken as massless). The values correspond to the ones typically chosen for an experimental analysis at LHC [3].

VBFNLO neglects any s-channel diagrams appearing as well as interference between t- and u-channel, but it has a negligible numerical effect due to the large invariant mass cut on the jets [35]. The vector boson scattering processes of interest, the corresponding final state and VBFNLO process ID are

VBS process	final state	VBFNLO ID
$W^+W^+$	$e^+\nu_e\mu^+\nu_\mu$	250
$W^+W^-$	$e^+\nu_e\mu^-\bar{\nu}_\mu$	200
$W^+Z$	$e^+\nu_e\mu^+\mu^-$	220
$ZZ$	$e^+e^-\mu^+\mu^-$	210

For the comparison to WHIZARD, we set  $\bar{f}_{S,0} = \bar{f}_{S,1} = 100 \text{ TeV}^{-42}$  for all the processes. This choice seems rather large, but it serves as simple visual check of the right qualitative behavior of the unitarisation method. We will concentrate on the invariant mass spectra of the final state leptons, i.e.  $d\sigma/dm_{V_1V_2}$  in the range of [0 GeV, 2000 GeV]. Choosing more realistic values for the couplings does not show the qualitative behavior in such an obvious way in the aforementioned mass range and choosing an even larger mass range would computationally be relatively inefficient.

<sup>2</sup>Note that with  $\mathcal{L}_{S,2}$  not being implemented in VBFNLO so far, we do not need to set some value for  $\bar{f}_{S,2}$ . In the framework of this thesis, e.g. in section 3.3 this we can just set  $\bar{f}_{S,2} = 0$ .

### 7.4.2. Low Energy Discrepancies

A common feature among the processes is the somewhat unstable behavior of WHIZARD in the low energy regime when choosing relatively strong couplings of  $\mathcal{O}(100 \text{ TeV}^{-4})$ . Up to a few hundred GeV one would expect only minor deviations from the SM, but in most cases the anomalous distributions over- or undershoot the SM case by about  $\sim 40\%$  in the WHIZARD case, while the VBFNLO distributions pretty much coincide with the SM case up to  $\sim 400 \text{ GeV}$ . This behavior is exemplarily shown in figure 7.6. In the WHIZARD case the events have been generated up to  $m_{ll} = 1000 \text{ GeV}$  which seems to push the discrepancy down a bit compared to the generation of events without this cut. This argument is enforced by the results seen in figure 7.6c. This plot shows the same distributions, but with a  $m_{ll} \leq 600 \text{ GeV}$  cut. Here we find very good agreement between the SM and the anomalous coupling distributions. In this case the internal WHIZARD routines have been used to produce the distributions, but it has also been checked that the distributions generated with LHA-files give the same results.

The discrepancy might be explainable by differences in the phase space generation of the two Monte-Carlos or the use of weighted events in the generation of the distributions with WHIZARD (which was done in order to decrease computation time and still get reasonable results in terms of statistics). However, the use of unweighted events did neither not resolve the problem. Typically more phase space points and events are generated in regions with high differential cross sections leading to higher fluctuations or even systematic errors in regions with lower values, i.e. the low invariant mass regime.

In figure 7.7 the effect of a coupling strength of  $\bar{f}_{S,0} = \bar{f}_{S,1} = 50 \text{ TeV}^{-4}$  in VBFNLO is shown together with the ratio of (non-) unitarized anomalous coupling distribution over the SM part. As expected we find perfect agreement up to a few hundred GeV. This makes clear, that the effect we see in WHIZARD is most probably not of a physical nature. Due to this so far unexplained behavior in WHIZARD, we will concentrate on the comparison of the two Monte Carlo in the high energy regime. Here we will see that they give a far better agreement.

### 7.4.3. Comparison for $\bar{f}_{S,0} = \bar{f}_{S,1} = 100 \text{ TeV}^{-4}$

The use of this section is to show the qualitative agreement between the K-matrix unitarisation in VBFNLO and in WHIZARD, by comparing distributions and total cross sections in the four affected vector boson scattering processes. As we have seen in the last section, relatively large discrepancies in the distributions can already arise independently of the K-matrix implementation. Unfortunately these discrepancies could not be resolved. Therefore when comparing the two K-matrix implementations, one needs to keep in mind that already in the non-unitarized distributions discrepancies of  $\sim 40\%$  are 'normal'.

The plots of this section show invariant mass distributions of the vector boson system under consideration. These distributions are strongly affected by anomalous couplings and therefore serve as a nice tool for studying their effects and the effects of the unitarisation. The energy range chosen is  $[0, 2000 \text{ GeV}]$ , which represents a regime that is expected to be in the range of the upcoming LHC runs.

The distributions of WHIZARD have been created by generating 500000 up to one million weighted events for each case (SM, non-unitarized, unitarized), which are collected in a `*.lhe` file, i.e. the Les Houches event format [36]. Afterwards some external code is used to read in the file, calculate the invariant mass of the four final state leptons (neutrinos are taken into account) in every event and put them into a histogram. The distributions from VBFNLO are generated internally with the standard utility `histograms.F`, that has been extended to generate an invariant mass histogram (of course also taking neutrinos

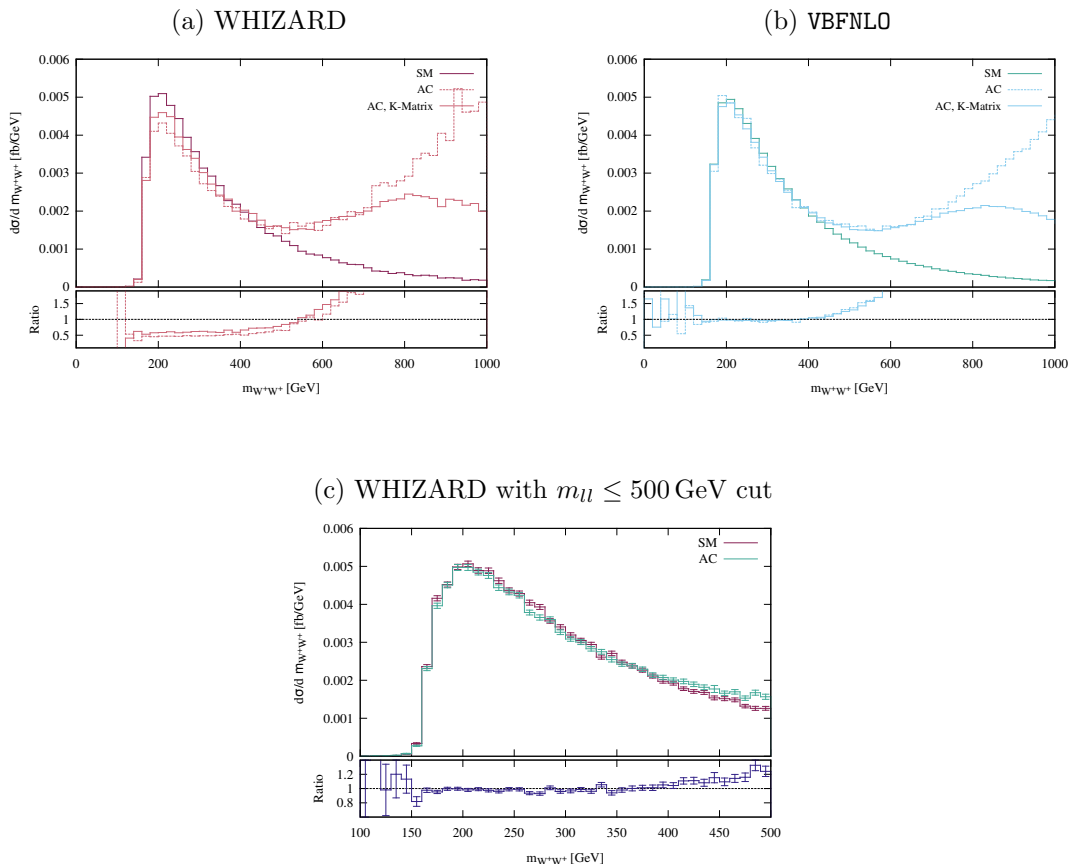


Figure 7.6.: Invariant mass spectra in  $W^+W^+$  scattering. Each of the upper two plots shows three lines: SM contribution, anomalous couplings contribution with  $\bar{f}_{S,0} = \bar{f}_{S,1} = 100 \text{ TeV}^{-4}$  without unitarisation (dotted) and the same couplings with K-matrix unitarisation (same color, solid). Beneath the ratio of the anomalous contributions over the SM only contribution is shown with the same color coding. One sees that the ratio deviates from one by  $\sim 40\%$  in the WHIZARD case while in the VBFNLO case it statistically fluctuates around one in the low energy regime. The third figure shows a similar WHIZARD run, but with an upper cut on the lepton pair masses (including neutrinos) of  $m_{ll} \leq 500 \text{ GeV}$ . Discrepancies are a lot smaller in this case.

into account). The VBFNLO output is in terms of fb/GeV, which is why the WHIZARD distributions have to be scaled accordingly, i.e. divide every bin by the total sum of event weights (which is the sum of XWGTUP from the .lhe file), divide by the bin width (20GeV) and multiply by the total cross section  $\sigma_{tot}$  to be found in the WHIZARD log file.

There are some common features among all of the distributions shown in this section. All of them show a relatively sharp cut off at low invariant masses which is because neutrinos have been included in the calculation of the masses. Neutrinos can of course not be taken into account experimentally, but for the comparison of the programs this serves as a more accurate set up. Each plot features two times three pairs (VBFNLO and WHIZARD) of lines with the lowest two representing the SM case, the top two anomalous couplings with no unitarisation and the two in the middle showing the same anomalous couplings with K-matrix unitarisation switched on.

The distributions begin with a peak close to the sum of the vector boson rest masses and all fall like  $1/s$  in the low energy regime. For the SM case this decrease continues throughout the whole energy range and therefore one sees a linearly decreasing differential cross section in the plots showing logarithmic scale. At some point deviations from the SM induced by

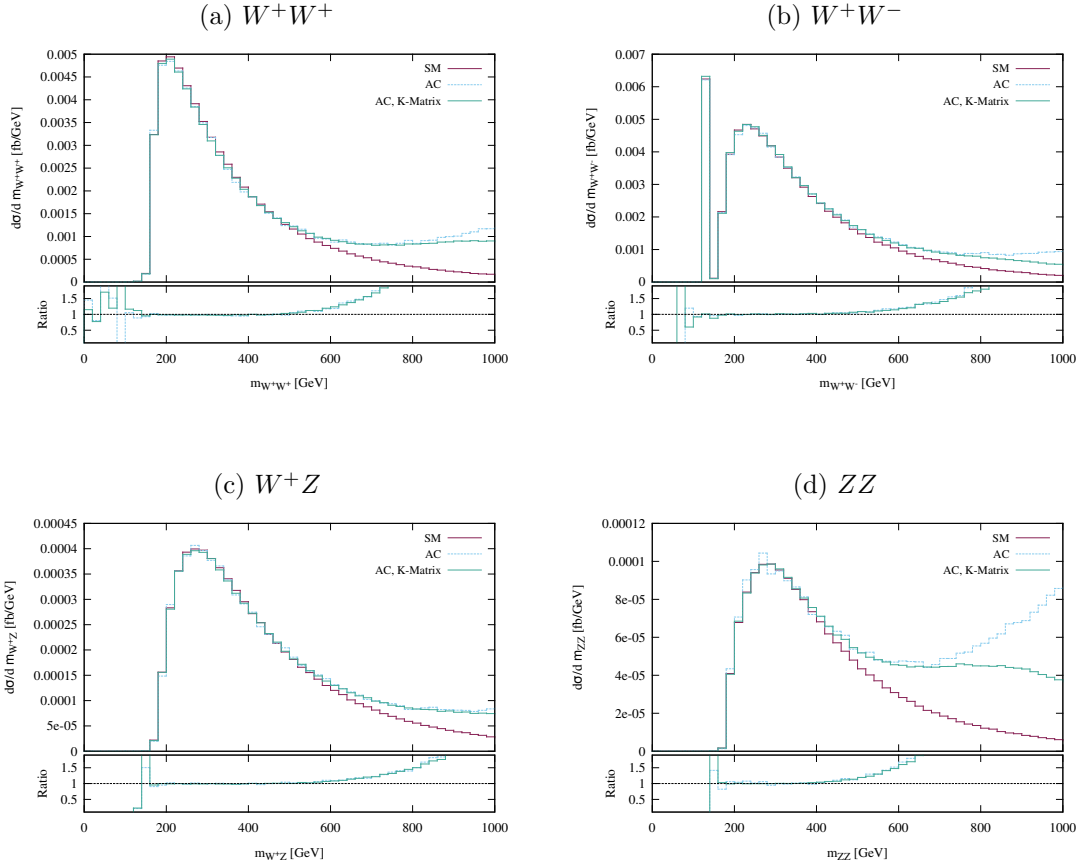


Figure 7.7.: Invariant Mass spectra in  $VV$  scattering generated with VBFNLO. Each plot shows three lines: SM contribution in violet, anomalous couplings contribution with  $\bar{f}_{S,0} = \bar{f}_{S,1} = 50 \text{ TeV}^{-4}$  without unitarisation (dotted, light blue) and the same couplings with K-matrix unitarisation (solid, green). Beneath the ratio of the anomalous contributions over the SM only contribution is shown with the same color coding. For all processes good agreement is found in the low energy regime.

the anomalous couplings become strongly visible. With no unitarisation the differential cross section increases monotonically, because the anomalous amplitude contributing here grows like  $s^2$ . Only the influence of the parton distribution functions (PDFs) cancels some of the growth in the high energy regime, because with growing fraction of the proton momentum, partons are more unlikely to find. In this way by looking at the plots one can suspect a saturation at very high energies. Still it is clear that the behavior is unphysical, with the differential cross sections even exceeding the SM peaks throughout a large energy range. The effects look even more dramatic in linear scale.

This unphysical behavior is under control in the K-matrix scheme. For low energies and with anomalous contributions being small here, the distributions are almost identical to the SM ones. As energy grows, the unitarized contributions begin to deviate, closely following the non-unitarized ones, but quickly drop off again, when the unitarity bound calculated from the on-shell partial wave analysis is reached. After the unitarisation sets in, the distributions become parallel to the SM contribution again, because the real part of all anomalous couplings go to zero and the imaginary parts saturate at a finite value. By comparing the unitarized distributions with the SM ones, keep in mind the logarithmic scale. Even though the deviations seem drastic in the high energy range here, it becomes obvious in linear scale, that the deviations become more and more negligible with growing center of mass energy (see figure 7.8b), at least in terms of the total cross sections.

process	SM		no K-Matrix		K-Matrix	
	VBFNLO	WHIZ	VBFNLO	WHIZ	VBFNLO	WHIZ
$W^+W^+$	1.3102(4)	1.311(1)	51.49(2)	51.54(4)	2.452(1)	2.466(2)
$W^+W^-$	0.9019(7)	0.902(2)	24.594(6)	21.52(4)	1.530(1)	1.455(4)
$W^+Z$	0.1473(1)	0.1480(3)	2.633(1)	2.637(3)	0.2413(2)	0.2426(5)
$ZZ$	0.02840(3)	0.0284(1)	3.141(2)	3.142(6)	0.08301(6)	0.0829(2)

Table 7.1.: This table shows the total cross sections  $\sigma_{tot}$  in [fb] for the four vector boson scattering processes affected by  $\mathcal{L}_{S,0}$  and  $\mathcal{L}_{S,1}$ , calculated with VBFNLO and WHIZARD. The columns “no K-matrix” and “K-matrix” show  $\sigma_{tot}$  [fb] for the couplings  $\bar{f}_{S,0} = \bar{f}_{S,1} = 100 \text{ TeV}^{-4}$  with the K-matrix unitarisation switched off/on.

Apart from the plots showing the qualitative behavior, one can see the corresponding total cross sections  $\sigma_{tot}$  in table 7.1. The values are discussed in the corresponding paragraphs of the various processes, but generally speaking we find agreement at the per mill level in all cases except in  $W^+W^-$  for reasons to be explained later in the corresponding paragraph.

### $W^+W^+$

Figure 7.8 shows the unitarisation behavior for the final state  $W^+W^+jj$ . Considering the unitarisation procedure, this process is rather simple. The only 4-vertex to appear in the calculation is the 4- $W$ -vertex. Therefore only the corresponding  $www$  amplitude in VBFNLO has to be unitarized, which only includes three partial waves vs. up to five in other processes. This makes a comparison to WHIZARD relatively simple in terms of the implementation.

The main feature to notice in figure 7.8 are the unitarized distributions exhibiting the same structure, but the WHIZARD one overshooting the VBFNLO result in the high energy tail. Taking a look at the ratio shows that there seems to be some energy dependence involved. By closely inspecting it, we see that the ratios in the non-unitarized and the unitarized cases agree up to invariant masses of  $\sim 1000 \text{ GeV}$ , which makes this energy dependence irrelevant for checking the K-matrix implementation in VBFNLO. After that point the ratio of the non-unitarized amplitudes settles at 1 with only small statistical fluctuations, but the ratio for the unitarized case shows deviations between the two programs of about  $\sim 30\%$ .

To this point these deviations lack a thorough explanation. The calculations in [6] include one-loop corrections to the anomalous amplitudes and scale dependent couplings  $\alpha_i$ , which have then been implemented in WHIZARD. These corrections have not been implemented in VBFNLO due to their negligible influence on the unitarisation procedure, but the difference in the two codes might still show up in the aforementioned discrepancy. What weakens this argument is the fact that the discrepancies are not as strong in the other processes, even though some of them feature the same  $\Delta A_{JJ}$ .

In terms of the total cross sections, we find agreement among the codes at the per mill level, despite the deviations in the distributions.

### $W^+W^-$

The  $W^+W^-$  comparison is shown in figure 7.9. The general behavior of the K-matrix implementation of both programs looks comparable. Investigating the ratio plot, we find agreement at the percent level up to energies of  $1500 \text{ GeV}$ . Still, the comparison of the total cross sections revealed relatively large discrepancies:

$\sigma_{\text{tot}}[\text{fb}]$	SM	no K-Matrix	K-Matrix
VBFNLO	1.609(2)	25.83(2)	2.261(2)
WHIZARD	1.485(3)	22.55(4)	2.055(5)

The reason for this was found to be the Higgs peak, which is completely missing in the WHIZARD distributions, while it gives a large contribution in all three VBFNLO distributions (see figure 7.9a). This might be due to some unlucky phase space generation in the WHIZARD runs, but it could not be cured by choosing different statistics in an affordable time.

In order to solve this, an invariant mass cut on all leptons including neutrinos has been set to a value of  $m_{ll} \geq 60 \text{ GeV}$ , so that the Higgs peak is not included anymore. The standard VBFNLO cut routine `cutf.F` had to be changed for this, because neutrinos are not included in any lepton cuts otherwise. The result is shown in figure 7.9b.

With this set up the following total cross sections were found:

$\sigma_{\text{tot}}[\text{fb}]$	SM	no K-Matrix	K-Matrix
VBFNLO	0.9019(7)	24.594(6)	1.530(1)
WHIZARD	0.902(2)	21.52(4)	1.455(4)

Strangely enough, we have perfect agreement for the SM model values, while for the anomalous coupling scenario the values disagree even more than before. As it turns out, the reason for this most probably is the conversion between the  $f_{S,i}$  and  $\alpha_i$ . The same conversion as in the  $W^+W^+$  case has been used, which is correct for the process  $W^+W^- \rightarrow W^+W^-$ , but with only choosing the final state  $W^+W^-$  in the two programs, also  $ZZ \rightarrow W^+W^-$  gives a contribution. For the latter process a different conversion is needed, which leads to large deviations in the comparison of the of the anomalous couplings distributions. The same thing might be the reason for the discrepancies in the high energy tails of the K-matrix unitarized distributions.

A noticeable feature in figure 7.9a are the strong deviations in the high energy tail of the unitarized distributions. Fortunately, they have only a minor effect on the total cross section, because the differential cross section is very low in this regime. Still this is an obvious difference in the implementation.

It has been checked that the deviation does not grow when going to even higher energies. Rather we find a small bump around 1500GeV, that is completely absent in the WHIZARD case. This means that the deviation does not arise from numerical instabilities in VBFNLO, because they would typically grow when working with smaller numerical values. Thorough investigation shows that the bump seems to arise from the s-channel unitarisation factor in the  $W^+W^- \rightarrow ZZ$  amplitude (see equation (4.97a)). The sum of the imaginary parts of  $\Delta A_{I,J=2}$  show a bump at the same energy, as seen in figure 7.10. This gives a mayor contribution to the absolute value of the effective s-channel coupling which then shows up in the differential cross section.

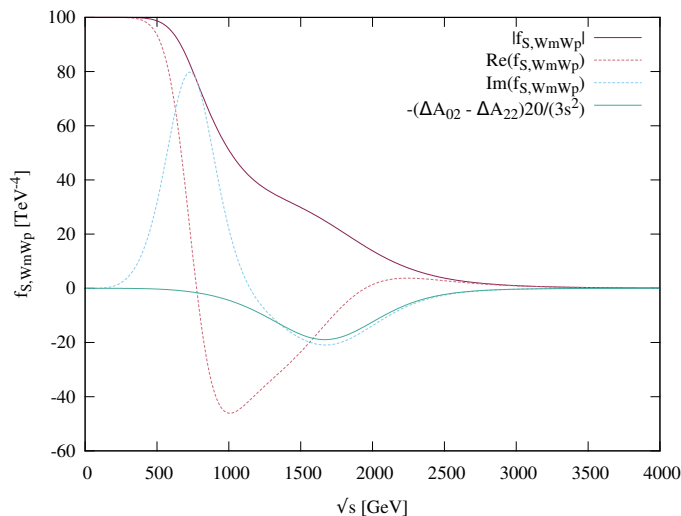


Figure 7.10.: s-channel unitarisation factor from equation (4.97a) for  $\bar{f}_{S,0} = \bar{f}_{S,1} = 100 \text{ TeV}^{-4}$ . The absolute value in violet shows a bump around 1500GeV, which results from the sum of the imaginary parts of  $\Delta A_{I,J=2}$  in turquoise.

It remains unclear whether this is a bug in VBFNLO, if for some reason it is missing in WHIZARD or if this is just another effect of the missing one-to-one correspondence between the two sets of couplings.

### $W^+Z$

An additional cut in order to avoid collinear divergencies by the inclusion of  $\gamma^*$  in the final state has been imposed in this process, i.e.

$$m_{ll} \geq 60 \text{ GeV} \quad (7.9)$$

The way this was implemented in WHIZARD is by defining an alias for the charged leptons and saying that the mass of each pair of those leptons should respect the cut:

```
alias lepton = e1:E1:e2:E2
cuts = ...
  and all M >= 60 GeV [lepton,lepton]
```

In VBFNLO one simply sets the value of `MLL_MIN = 60.0d0` in the cut input file `cuts.dat` and moreover sets the flag `MLL_OSONLY = false`. This means taking all pairs of charged leptons into account, not only the ones with opposite charge.

Using this setup we find relatively strong deviations of the K-matrix implementations in the low energy regime. Looking at the ratio plot in 7.11a we find a similar shape for the non-unitarized and the unitarized distributions oscillating around one in the ratio plot, while for energies above 1TeV we find good accordance with one in both cases. This again might give a hint that the reason for the deviations is not to find in the K-matrix implementation, but is rather due to some differences in phase space generation of the two Monte Carlos, or due to the use of weighted events in the WHIZARD case.

In terms of the total cross section, we find accordance at the per mill level in all cases (see table 7.1).

*ZZ*

As in the  $W^+Z$  case, a minimum invariant mass cut on the lepton pairs of 60GeV was used in this analysis. Figure 7.11b shows again the ratio of the values produced by VBFNLO and WHIZARD. We find very good agreement for the unitarized distributions with a slight tendency of a stronger suppression in VBFNLO like in the  $W^+W^+$  case. The statistical fluctuations are rather strong in the distributions due to the very small total cross section compared to the other processes making an exact comparison more difficult.

Again, the total cross sections agree at the per mill level.

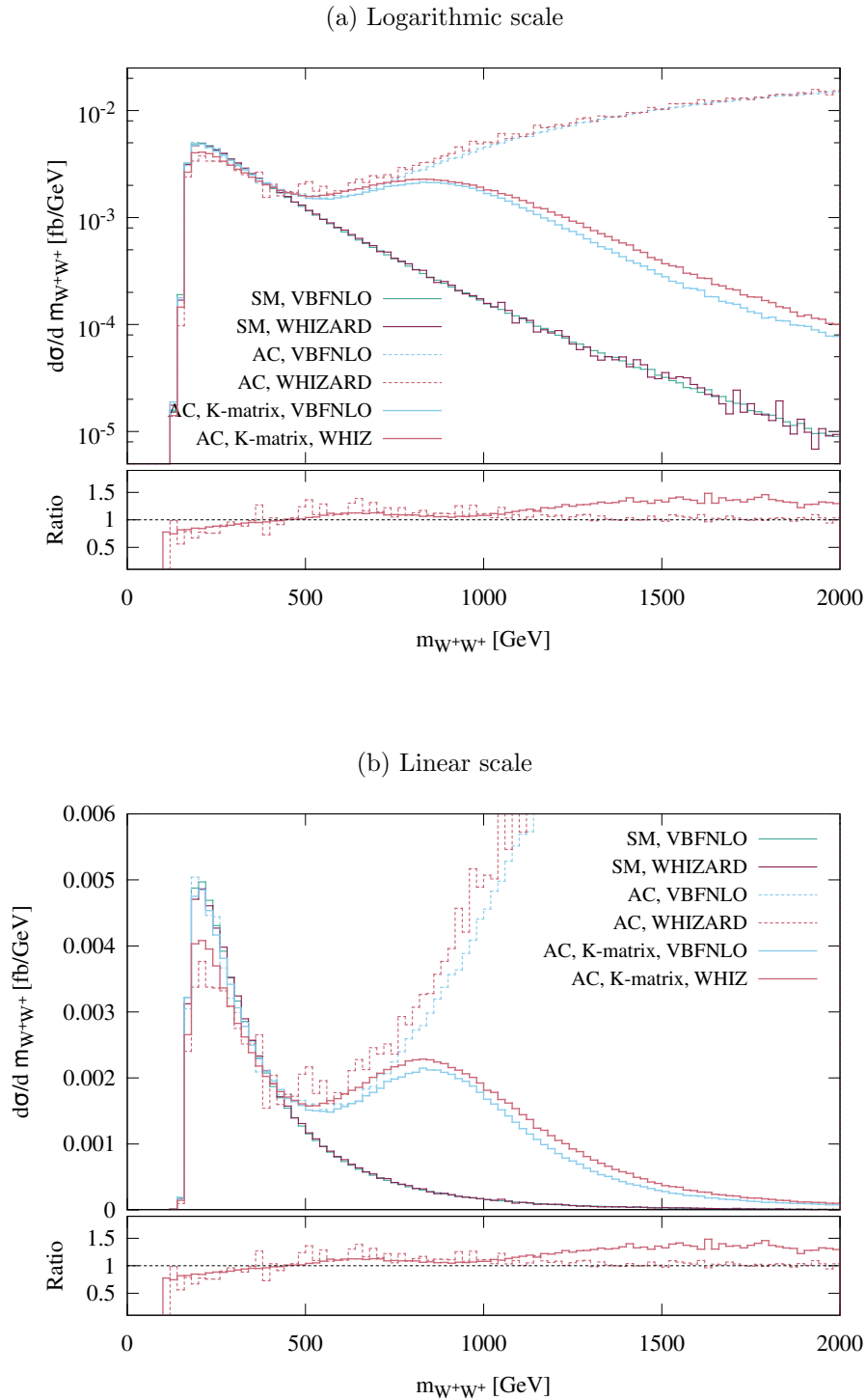


Figure 7.8.: Comparison of VBFNLO vs. WHIZARD in  $W^+W^+ \rightarrow W^+W^+$  scattering for three different cases: the standard model (SM), anomalous couplings (AC) switched on without unitarisation ( $\bar{f}_{S,0} = \bar{f}_{S,1} = 100 \text{ TeV}^{-4}$ ) and the same for K-matrix unitarisation switched on. The lower plot shows the ratio of WHIZARD vs. VBFNLO with (solid line) and without unitarisation (dashed).

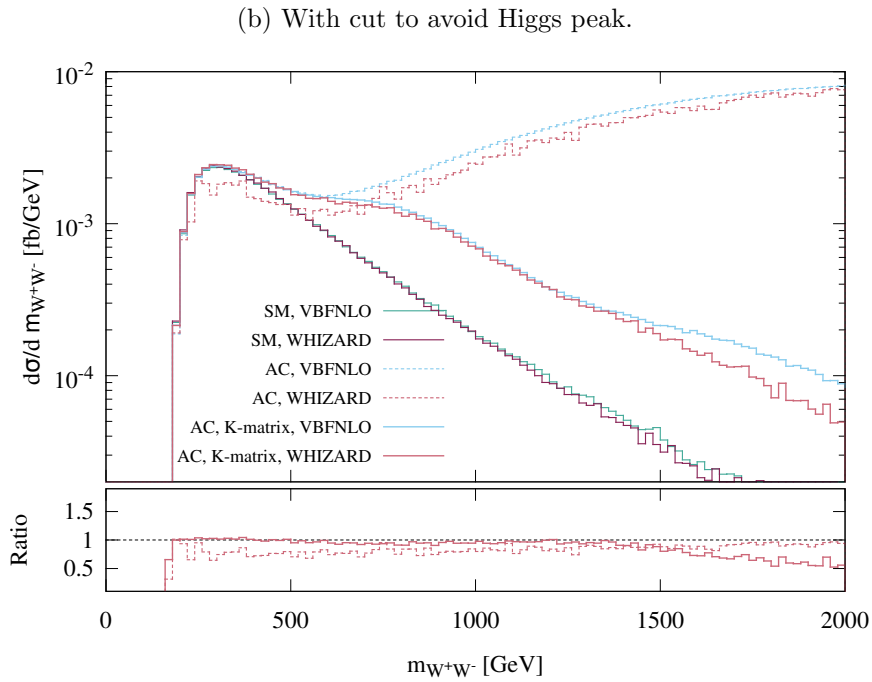
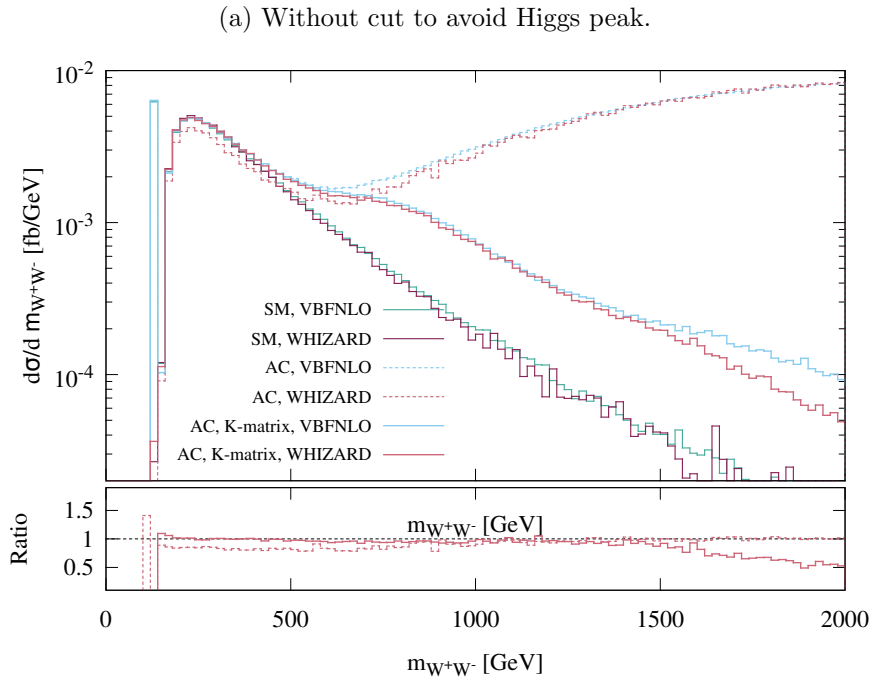


Figure 7.9.: Comparison of VBFNLO vs. WHIZARD in  $W^+W^-$  for three different cases: the standard model (SM), anomalous couplings (AC) switched on without unitarisation ( $f_{S,0} = f_{S,1} = 100 \text{ TeV}^{-4}$ ) and the same for K-matrix unitarisation switched on. The lower plots show the ratio of WHIZARD vs. VBFNLO with (solid line) and without unitarisation (dashed). Two versions featuring different cuts on the leptons are shown: one including only the charged leptons into the cuts (Higgs peak) and the second one including neutrinos into the lepton invariant mass cuts avoiding the Higgs peak.

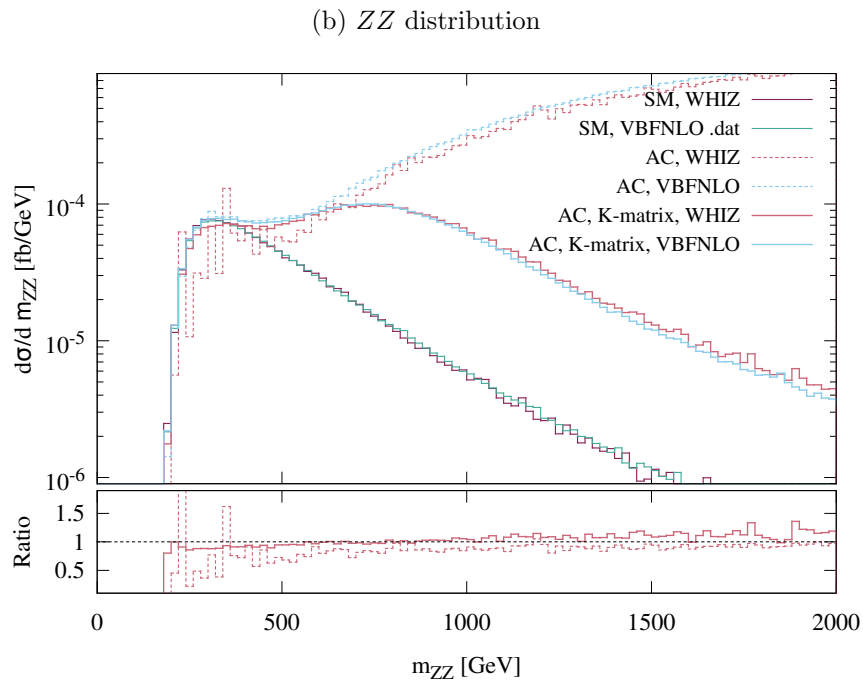
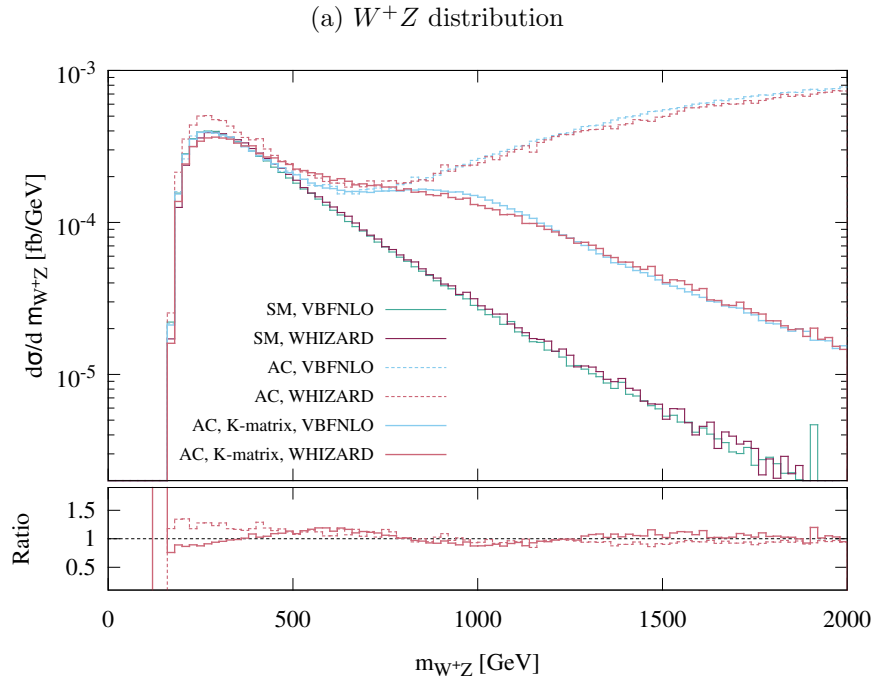


Figure 7.11.: Comparison of VBFNLO vs. WHIZARD in  $W^+Z$  and  $ZZ$  for three different cases: the standard model (SM), anomalous couplings (AC) switched on without unitarisation ( $\bar{f}_{S,0} = \bar{f}_{S,1} = 100 \text{ TeV}^{-4}$ ) and the same for K-matrix unitarisation switched on. The lower plot shows the ratio of WHIZARD vs. VBFNLO with (solid line) and without unitarisation (dashed).

## Conclusion

This thesis took a close look on the subject of unitarisation of dimension 8 operators in the framework of effective field theories. These operators represent a genuine way to model effects of physics beyond the SM on the vector boson 4-vertices. It was argued that unitarisation is a necessary procedure when working with these operators. Otherwise a description of deviations from the SM with those is not be possible when comparing experimental data to theoretical predictions. They would violate unitarity at energies well in the range of experimental analyses already for small coupling constants. An example is  $W^+W^+$ -scattering, where for coupling strengths of  $f_{S,0}/\Lambda^4 = f_{S,1}/\Lambda^4 = 100 \text{ TeV}^{-4}$ , unitarity would be violated around a center of mass energy of  $\sim 800 \text{ GeV}$ .

The unitarisation procedure of interest for this thesis is the K-matrix approach. It uses the unitarity of the scattering operator  $S$  to define unitarity bounds for partial waves of scattering amplitudes. A detailed study of this approach and the resulting unitarisation procedure for the operators  $\mathcal{L}_{S,0}$  and  $\mathcal{L}_{S,1}$  was given. In order to achieve a better comparability to another dimension 8 operator set in the non-linear realization, the introduction of a symmetrized version of  $\mathcal{L}_{S,0}$  has been proposed. This redefinition would also cure the problem of  $\mathcal{L}_{S,0}$  not being a self-adjoint operator and could be translated to other operators of the sets  $\{\mathcal{L}_{T,i}\}$  and  $\{\mathcal{L}_{M,i}\}$ .

With the K-matrix approach not being fully applicable to  $\{\mathcal{L}_{T,i}\}$  and  $\{\mathcal{L}_{M,i}\}$ , K-matrix-like form factors  $\mathcal{F}_K(s)$  have been defined and proposed for the use in the parton-level Monte Carlo program **VBFNLO**. Anomalous scattering amplitudes unitarized with  $\mathcal{F}_K(s)$  would share the same features as in the original K-matrix approach, i.e. keeping the original low energy behavior of the anomalous amplitudes, then cut them off when the unitarity bound is reached. The real part will go to zero for large center of mass energies, while the imaginary part will saturate at a finite value, interpretable formally as a resonance at infinity.

$\mathcal{F}_K(s)$  only has one input parameter, an energy scale  $\Lambda_K$ . The determination of this scale could be done via a modification of the existing routine `calc_formfac` [21], or in an analytic partial wave analysis. A way to do the latter in an affordable manner has been proposed in chapter 5.

The K-matrix approach has been fully implemented into **VBFNLO** for  $\mathcal{L}_{S,0}$  and  $\mathcal{L}_{S,1}$ . In order to check the results, a comparison to another Monte Carlo program, **WHIZARD**, featuring the same unitarisation method was given. Here we found good agreement in terms of the total cross sections for most processes and the same qualitative behavior in invariant mass distributions generated by the two programs. However, in some cases relatively large discrepancies already showed up without the use of the K-matrix unitarisation. Distributions with and without anomalous couplings generated with **WHIZARD** did not agree in the low energy regime, even though the anomalous couplings should have no effect there. This showed that differences in the generation of events between the two programs

exist which could not be completely resolved in the course of this thesis. Moreover are the two codes not completely comparable in terms of the dimension 8 operators, because there is no one-to-one correspondence between the sets both programs have been using at the time this thesis was written. A more thorough comparison will be possible when a symmetrized version of  $\mathcal{L}_{S,0}$ , like the one proposed in this thesis, has been implemented in VBFNLO.

# Appendix

## A. Optical Theorem

The *optical theorem* relates the imaginary part of a forward scattering amplitude to the total cross section of a process. The derivation in this thesis follows the one in [10].

Starting from equation (4.44), which simply restates the unitarity of the  $S$ -matrix, we take the corresponding matrix element of this equation in a two-particle process with initial state  $|\mathbf{p}_1\mathbf{p}_2\rangle$  and final state  $|\mathbf{k}_1\mathbf{k}_2\rangle$ . In order to evaluate the right hand side of the equation, one has to insert a complete set of intermediate states  $|\{\mathbf{q}_i\}\rangle$ , i.e.

$$\langle \mathbf{p}_1\mathbf{p}_2 | TT^\dagger | \mathbf{k}_1\mathbf{k}_2 \rangle = \sum_n \left( \prod_{i=1}^n \int \frac{d^3q_i}{2\pi^3} \frac{1}{2E_i} \right) \langle \mathbf{p}_1\mathbf{p}_2 | T | \{\mathbf{q}_i\} \rangle \langle \{\mathbf{q}_i\} | T^\dagger | \mathbf{k}_1\mathbf{k}_2 \rangle \quad (\text{A.1})$$

The relation of the  $T$ -matrix to the corresponding *invariant matrix element*  $\mathcal{M}$  reads

$$\langle \mathbf{p}_1\mathbf{p}_2 \dots | iT | \mathbf{k}_1\mathbf{k}_2 \rangle = (2\pi)^4 \delta^{(4)} \left( k_1 + k_2 - \sum p_f \right) \cdot i\mathcal{M}(k_1, k_2 \rightarrow p_f). \quad (\text{A.2})$$

It is merely a separation of the kinematic part of a scattering amplitude from the dynamic part resulting from the interaction Hamiltonian. Using this definition the unitarity condition now becomes

$$\begin{aligned} & -i [\mathcal{M}(k_1k_2 \rightarrow p_1p_2) - \mathcal{M}^*(p_1p_2 \rightarrow k_1k_2)] \\ &= \sum_n \left( \prod_{i=1}^n \int \frac{d^3q_i}{2\pi^3} \frac{1}{2E_i} \right) \mathcal{M}^*(p_1p_2 \rightarrow \{q_i\}) \mathcal{M}(k_1k_2 \rightarrow \{q_i\}) \end{aligned} \quad (\text{A.3})$$

$$\times (2\pi)^4 \delta^{(4)} \left( k_1 + k_2 - \sum q_i \right) \quad (\text{A.4})$$

where the overall delta function  $(2\pi)^4 \delta^{(4)}(k_1 + k_2 - p_1 - p_2)$  has been omitted for simplicity. Concentrating on the case of forward scattering, we set  $p_i = k_i$ . Then, by inserting the proper kinematical factors to obtain a cross section, we get the standard form of the *optical theorem*

$$\Im[\mathcal{M}(k_1, k_2 \rightarrow k_1, k_2)] = 2E_{\text{cm}} p_{\text{cm}} \sigma_{\text{tot}}(k_1, k_2 \rightarrow \text{anything}), \quad (\text{A.5})$$

where  $E_{\text{cm}}$  is the total center of mass energy and  $p_{\text{cm}}$  the center of mass momentum of either of the particles.

## B. Wigner's d-Functions

Explicit forms of the Wigner d-functions can be derived using relations to the spherical harmonics, Legendre polynomials and several recursion relations among the  $d_{\lambda\mu}^{(J)}$  themselves (see [24]). The ones most relevant to this thesis read:

$$d_{00}^{(0)} = 1,$$

$$\begin{aligned}
d_{00}^{(1)} &= \cos \theta, \\
d_{11}^{(1)} &= \frac{1}{2}(1 + \cos \theta), & d_{10}^{(1)} &= -\frac{1}{\sqrt{2}} \sin \theta, & d_{1-1}^{(1)} &= \frac{1}{2}(1 - \cos \theta), \\
d_{00}^{(2)} &= \frac{3}{2} \cos^2 \theta - \frac{1}{2}, \\
d_{11}^{(2)} &= \frac{1 + \cos \theta}{2}(2 \cos \theta - 1), & d_{10}^{(2)} &= -\sqrt{\frac{3}{2}} \sin \theta \cos \theta, & d_{1-1}^{(2)} &= \frac{1 - \cos \theta}{2}(2 \cos \theta + 1), \\
d_{22}^{(2)} &= \frac{1}{4}(1 + \cos \theta)^2, & d_{21}^{(2)} &= -\frac{1}{2}(1 + \cos \theta) \sin \theta, & d_{20}^{(2)} &= \frac{1}{2}\sqrt{\frac{3}{2}} \sin^2 \theta, \\
d_{2-1}^{(2)} &= -\frac{1}{2}(1 - \cos \theta) \sin \theta, & d_{2-2}^{(2)} &= \frac{1}{4}(1 - \cos \theta)^2.
\end{aligned}$$

Two helpful relations give the rest of the functions with opposite helicities to the ones above [24]:

$$d_{\lambda\mu}^{(J)}(\theta) = d_{-\mu-\lambda}^{(J)}(\theta) = (-1)^{\lambda-\mu} d_{\mu\lambda}^{(J)}(\theta) \quad (\text{B.6})$$

and

$$d_{\lambda\mu}^{(J)}(\theta) = (-1)^{J+\lambda} d_{\lambda-\mu}^{(J)}(\pi - \theta) \quad (\text{B.7})$$

## C. Legendre Polynomials

In the unitarisation procedure of the operators  $\mathcal{L}_{S,0}$  and  $\mathcal{L}_{S,1}$  the Legendre polynomials  $P_J(\cos \theta)$  are of great importance. For helicity differences of in- and outgoing particles  $\lambda = \mu = 0$  in a  $2 \rightarrow 2$  scattering process, they coincide with the Wigner-D functions. Nevertheless, due to some ambiguities in going from a  $\theta$ -dependence to Mandelstam variables, we list the versions used throughout this thesis for clarity:

$$P_0(\cos \theta) = 1 \quad \rightarrow P_0(s, t, u) = 1, \quad (\text{C.8})$$

$$P_1(\cos \theta) = \cos \theta \quad \rightarrow P_1(s, t, u) = \frac{u^2 - t^2}{s^2}, \quad (\text{C.9})$$

$$P_2(\cos \theta) = \frac{3}{2} \cos^2 \theta - \frac{1}{2} \quad \rightarrow P_2(s, t, u) = \frac{3t^2 + 3u^2 - 2s^2}{s^2}. \quad (\text{C.10})$$

## D. Polarization vectors

The definitions used throughout this thesis, especially in the Mathematica functions, follow closely the ones in [37].

When we write the input-momentum  $k$  as

$$k^\mu = (E, k_x, k_y, k_z), \quad (\text{D.11})$$

then we can define three linearly independent polarization vectors satisfying the transversality relation  $k^\mu \epsilon_\mu^{(\lambda)}$  by

$$\epsilon_1^\mu(k) = \frac{1}{|\vec{k}|k_T} \begin{pmatrix} 0 \\ k_x k_z \\ k_y k_z \\ -k_T^2 \end{pmatrix}, \quad \epsilon_2^\mu(k) = \frac{1}{k_T} \begin{pmatrix} 0 \\ -k_y \\ k_x \\ 0 \end{pmatrix}, \quad \epsilon_3^\mu(k) = \frac{E}{m|\vec{k}|} \begin{pmatrix} |\vec{k}|^2/E \\ k_x \\ k_y \\ k_z \end{pmatrix}, \quad (\text{D.12})$$

with

$$m = \sqrt{E^2 - |\vec{k}|^2} \quad (\text{D.13})$$

$$k_T = \sqrt{k_x^2 + k_y^2} \quad (\text{D.14})$$

For  $\epsilon_1$  and  $\epsilon_2$  an ambiguity is appearing when  $k_T \rightarrow 0$ . It is fixed by taking  $k_y = 0$  in this case and letting

$$\begin{cases} k_x \rightarrow +0 & \text{if } k_z > 0 \\ k_x \rightarrow -0 & \text{if } k_z < 0. \end{cases} \quad (\text{D.15})$$

From combinations of the above polarization vectors, we can build helicity eigenvectors for  $\lambda = \pm 1, 0$  for massive vector bosons and  $\lambda = \pm 1$  in the massless case:

$$\epsilon_{\pm}^{\mu}(k) = \frac{1}{\sqrt{2}} (\mp \epsilon_1^{\mu}(k) - i \epsilon_2^{\mu}(k)) \quad (\text{D.16})$$

$$\epsilon_L^{\mu}(k) = \epsilon_3^{\mu}(k). \quad (\text{D.17})$$

## E. Clebsch-Gordon Coefficients in the Total Isospin Basis

Following the definitions of section 4.6.2, the CGCs for the translation of a mass eigenstate basis to a total isospin basis using the Condon-Shortley convention reads

$$|2, \pm 2\rangle = |W^{\pm}W^{\pm}\rangle, \quad (\text{E.18a})$$

$$|2, \pm 1\rangle = \frac{1}{\sqrt{2}} (|ZW^{\pm}\rangle + |W^{\pm}Z\rangle), \quad (\text{E.18b})$$

$$|2, 0\rangle = \frac{1}{\sqrt{6}} (|W^-W^+\rangle + 2|ZZ\rangle + |W^+W^-\rangle), \quad (\text{E.18c})$$

$$(\text{E.18d})$$

$$|1, \pm 1\rangle = \frac{1}{\sqrt{2}} (|W^{\pm}Z\rangle - |ZW^{\pm}\rangle), \quad (\text{E.18e})$$

$$|1, 0\rangle = \frac{1}{\sqrt{2}} (|W^+W^-\rangle - |W^-W^+\rangle), \quad (\text{E.18f})$$

$$(\text{E.18g})$$

$$|0, 0\rangle = \frac{1}{\sqrt{3}} (|W^+W^-\rangle - |ZZ\rangle + |W^-W^+\rangle). \quad (\text{E.18h})$$

The inversion of this basis reads

$$|W^{\pm}W^{\pm}\rangle = |2, \pm 2\rangle, \quad (\text{E.19a})$$

$$|W^{\mp}W^{\pm}\rangle = \frac{1}{\sqrt{6}} |2, 0\rangle \mp \frac{1}{\sqrt{2}} |1, 0\rangle + \frac{1}{\sqrt{3}} |0, 0\rangle, \quad (\text{E.19b})$$

$$|W^{\pm}Z\rangle = \frac{1}{\sqrt{2}} (|2, 1\rangle \pm |1, \pm 1\rangle), \quad (\text{E.19c})$$

$$|ZW^{\pm}\rangle = \frac{1}{\sqrt{2}} (|2, 1\rangle \mp |1, \pm 1\rangle), \quad (\text{E.19d})$$

$$|ZZ\rangle = \frac{2}{\sqrt{6}} |2, 0\rangle - \frac{1}{\sqrt{3}} |0, 0\rangle. \quad (\text{E.19e})$$

## F. Dimension 6 operators

For completeness a full list of the dimension 6 operators is given below. The effects they have on TGCs and QGCs are summarized in table F.1.

	ZWW	AWW	HWW	HZZ	HZA	HAA	WWWW	ZZWW	ZAWW	AAWW
$\mathcal{O}_{WWW}$	X	X					X	X	X	X
$\mathcal{O}_W$	X	X	X	X	X		X	X	X	
$\mathcal{O}_B$	X	X		X	X					
$\mathcal{O}_{\Phi d}$			X	X						
$\mathcal{O}_{\Phi W}$			X	X	X	X				
$\mathcal{O}_{\Phi B}$				X	X	X				
$\mathcal{O}_{\tilde{W}WW}$	X	X					X	X	X	X
$\mathcal{O}_{\tilde{W}}$	X	X	X	X	X					
$\mathcal{O}_{\tilde{W}W}$			X	X	X	X				
$\mathcal{O}_{\tilde{B}B}$				X	X	X				

Table F.1.: This table shows which operators affect which TGC for the various vector bosons [16].

There are three CP-conserving dimension six operators affecting the TGCs and QGCs of the vector boson only:

$$\mathcal{O}_{WWW} = \text{Tr}[W_{\mu\nu}W^{\nu\rho}W_{\rho}{}^{\mu}], \quad (\text{F.20})$$

$$\mathcal{O}_W = (D_{\mu}\Phi)^{\dagger}W^{\mu\nu}(D_{\nu}\Phi), \quad (\text{F.21})$$

$$\mathcal{O}_B = (D_{\mu}\Phi)^{\dagger}B^{\mu\nu}(D_{\nu}\Phi) \quad (\text{F.22})$$

and two of similar type, but CP- violating

$$\mathcal{O}_{\tilde{W}WW} = \text{Tr}[\tilde{W}_{\mu\nu}W^{\nu\rho}W_{\rho}{}^{\mu}], \quad (\text{F.23})$$

$$\mathcal{O}_{\tilde{W}} = (D_{\mu}\Phi)^{\dagger}\tilde{W}^{\mu\nu}(D_{\nu}\Phi). \quad (\text{F.24})$$

Another set of operators models also couplings to the Higgs. There are again three CP-conserving ones

$$\mathcal{O}_{\Phi d} = \partial_{\mu}(\Phi^{\dagger}\Phi)\partial^{\mu}(\Phi^{\dagger}\Phi), \quad (\text{F.25})$$

$$\mathcal{O}_{\Phi W} = (\Phi^{\dagger}\Phi)\text{Tr}[W^{\mu\nu}W_{\mu\nu}], \quad (\text{F.26})$$

$$\mathcal{O}_{\Phi B} = (\Phi^{\dagger}\Phi)B^{\mu\nu}B_{\mu\nu}, \quad (\text{F.27})$$

and two CP-violating ones

$$\mathcal{O}_{\tilde{W}W} = \Phi^{\dagger}\tilde{W}_{\mu\nu}W^{\mu\nu}\Phi, \quad (\text{F.28})$$

$$\mathcal{O}_{\tilde{B}B} = \Phi^{\dagger}\tilde{B}_{\mu\nu}B^{\mu\nu}\Phi. \quad (\text{F.29})$$

The tilde in the CP- violating operators stand for the use of dual field strength tensors, which are just contractions of the usual field strength tensors with the epsilon-tensor  $\epsilon_{\mu\nu\rho\sigma}$ :

$$\tilde{W}_{\mu\nu} = \frac{1}{2}\epsilon_{\mu\nu\rho\sigma}W^{\rho\sigma}. \quad (\text{F.30})$$

With the epsilon tensor being odd under parity, all operators that involve one of this kind become CP- violating.

## G. Some Mathematica Definitions for Partial Wave Analysis

The main functions for calculating and inserting the helicity eigenvectors in the partial wave analysis in the Mathematica framework are shown here. The definitions of polarization vectors and helicity eigenvectors directly follow the ones in [37].

## G.1. Polarization Vectors

```

kT[k_] := Sqrt[k[[2]]^2 + k[[3]]^2];
kk[k_] := Sqrt[k[[2]]^2 + k[[3]]^2 + k[[4]]^2];

chiP[k_] := 1/Sqrt[2 kk[k] (kk[k] + k[[4]])]*{kk[k] + k[[4]], k[[2]] + I*k[[3]]};
chiM[k_] := 1/Sqrt[2 kk[k] (kk[k] + k[[4]])]*{-k[[2]] + I*k[[3]], kk[k] + k
  [[4]]};

omega[\[Lambda]_, k_] := Sqrt[k[[1]]^2 + \[Lambda]*kk[k]];

uuP[k_] := {omega[-1, k]*chiP[k][[1]], omega[-1, k]*chiP[k][[2]], omega[1, k]*
  chiP[k][[1]], omega[1, k]*chiP[k][[2]]};
uuM[k_] := {omega[1, k]*chiM[k][[1]], omega[1, k]*chiM[k][[2]], omega[-1, k]*chiM
  [k][[1]], omega[-1, k]*chiM[k][[2]]};
vvP[k_] := {-1*omega[1, k] chiM[k][[1]], -1*omega[1, k] chiM[k][[2]], +1*omega
  [-1, k]*chiM[k][[1]], +1*omega[-1, k]*chiM[k][[2]]};
vvM[k_] := {1*omega[-1, k] chiP[k][[1]], 1*omega[-1, k] chiP[k][[2]], -1*omega[1,
  k]*chiP[k][[1]], -1*omega[1, k]*chiP[k][[2]]};

eps1[k_] := (
  If[kT[k] != 0,
    Simplify[1/(kk[k]*kT[k])*{0, k[[2]]*k[[4]], k[[3]]*k[[4]], -kT[k]^2}],
    If[k[[4]] != 0,
      {0, Simplify[Sign[k[[4]]], {S > 0, S > 4 MZ2, S > 4 MW2}], 0, 0},
      Print["Polarization vector not defined for this momentum"]
    ]
);

eps2[k_] := (
  If[kT[k] != 0,
    Simplify[1/kT[k]*{0, -k[[3]], k[[2]], 0}],
    If[k[[4]] != 0,
      {0, 0, 1, 0},
      Print["Polarization vector not defined for this momentum"]
    ]
);

eps3[k_, m_] :=
  If[m != 0,
    If[kk[k] != 0,
      Simplify[k[[1]]/(m*kk[k])*{kk[k]^2/k[[1]], k[[2]], k[[3]], k[[4]]},
      Limit[k[[1]]/(m*kkk)*{kkk^2/k[[1]], k[[2]], k[[3]], k[[4]]}, kkk -> 0]],
    {0, 0, 0, 0}
  Print["Massless Gauge Boson doesn't exist in longitudinal polarization."];

```

## G.2. Helicity eigenvectors

```

epsP[k_] := Simplify[1/Sqrt[2]*(-eps1[k] - I*eps2[k]) /. {ct^2 + st^2 -> 1}, {S
  > 4 MZ2, st > 0}];
epsPc[k_] := Simplify[1/Sqrt[2]*(-eps1[k] + I*eps2[k]) /. {ct^2 + st^2 -> 1}, {S
  > 4 MZ2, st > 0}];

epsM[k_] := Simplify[1/Sqrt[2]*(+eps1[k] - I*eps2[k]) /. {ct^2 + st^2 -> 1}, {S >
  4 MZ2, st > 0}];
epsMc[k_] := Simplify[1/Sqrt[2]*(+eps1[k] + I*eps2[k]) /. {ct^2 + st^2 -> 1}, {S
  > 4 MZ2, st > 0}];

epsL[k_, m_] := Simplify[eps3[k, m] /. {ct^2 + st^2 -> 1}, {S > 4 MZ2, st > 0}];
epsLc[k_, m_] := Simplify[eps3[k, m] /. {ct^2 + st^2 -> 1}, {S > 4 MZ2, st > 0}];

```

## G.3. Taylor Expansion of Momentum

```
pTaylor[ECM_, M_, order_] := Block[{seriesEpsilon},
  seriesEpsilon = Normal[Series[Sqrt[1 - \[Epsilon]], {\[Epsilon], 0, order}]];
  Simplify[
    ECM*seriesEpsilon /. {\[Epsilon] -> M^2/ECM^2}, {Element[S, Reals], S > 0}
  ]
];
```

#### G.4. replaceEpsWWWW

```
replaceEpsWWWW[pol_, order_] := Block[

  {E1, E2, E3, E4,
   p1, p2, p3, p4,
   kk1, kk2, kk3, kk4,
   m1, m2, m3, m4,
   massList,
   printOption = 0},

  m1 = MW;
  m2 = MW;
  m3 = MW;
  m4 = MW;

  E1 = ECM[m1, m2];
  E2 = ECM[m2, m1];
  E3 = ECM[m3, m4];
  E4 = ECM[m4, m3];

  If[order == -1,
    p1 = Simplify[Sqrt[E1^2 - m1^2]];
    p2 = Simplify[Sqrt[E2^2 - m2^2]];
    p3 = Simplify[Sqrt[E3^2 - m3^2]];
    p4 = Simplify[Sqrt[E4^2 - m4^2]];
    ,
    p1 = pTaylor[E1, m1, order];
    p2 = pTaylor[E2, m2, order];
    p3 = pTaylor[E3, m3, order];
    p4 = pTaylor[E4, m4, order];];

  kk1 = {E1, 0, 0, p1};
  kk2 = {E2, 0, 0, -p2};
  kk3 = {E3, p3*st, 0, p3*ct};
  kk4 = {E4, -p4*st, 0, -p4*ct};

  {e[1] -> Switch[pol[[1]], -1, epsM[kk1], 0, epsL[kk1, m1], 1, epsP[kk1]],
   e[2] -> Switch[pol[[2]], -1, epsM[kk2], 0, epsL[kk2, m2], 1, epsP[kk2]],
   e[3] -> Switch[pol[[3]], -1, epsM[kk3], 0, epsL[kk3, m3], 1, epsP[kk3]],
   e[4] -> Switch[pol[[4]], -1, epsM[kk4], 0, epsL[kk4, m4], 1, epsP[kk4]],
   ec[1] -> Switch[pol[[1]], -1, epsMc[kk1], 0, epsLc[kk1, m1], 1, epsPc[kk1]],
   ec[2] -> Switch[pol[[2]], -1, epsMc[kk2], 0, epsLc[kk2, m2], 1, epsPc[kk2]],
   ec[3] -> Switch[pol[[3]], -1, epsMc[kk3], 0, epsLc[kk3, m3], 1, epsPc[kk3]],
   ec[4] -> Switch[pol[[4]], -1, epsMc[kk4], 0, epsLc[kk4, m4], 1, epsPc[kk4]],

   k[1] -> kk1,
   k[2] -> kk2,
   k[3] -> kk3,
   k[4] -> kk4,

  (*replaces denominator abbreviation sometimes introduced by FormCalc*)
  Den[x_, y_] -> 1/(x - y)}];
```

## H. VBFNLO and WHIZARD Input Files for Comparison of $W^+W^-$ -processes

In order to make the comparison of the two Monte Carlo programs VBFNLO and WHIZARD as transparent as possible, the complete input files used in the benchmark process  $W^+W^-$  are shown below. Note that all comments and descriptions have been left out for better readability. The standard input files of VBFNLO feature detailed commentation.

### H.1. VBFNLO Input Files

- vbfno.dat

In this file one sets the main input parameters for VBFNLO, i.e. the process ID, number of iterations and points in the calculation, masses and widths of the particles etc.

```

PROCESS                = 250
LOPROCESS_PLUS_JET    = false
LEPTONS                = -11 12 -13 14
DECAY_QUARKS          = 93

LO_ITERATIONS          = 6
NLO_ITERATIONS        = 6
LO_POINTS              = 24
NLO_POINTS            = 22
LO_GRID                = "grid2_1" "grid2_2" "grid2_3" "grid2_4" "grid2_5"
NLO_GRID              = "grid3_1" "grid3_2" "grid3_3" "grid3_4" "grid3_5"
PHTN_GRID             = "grid4_1" "grid4_2" "grid4_3" "grid4_4" "grid4_5"
FLOOP_GRID            = "grid5_1" "grid5_2" "grid5_3" "grid5_4" "grid5_5"

NLO_SWITCH            = false
EWCOR_SWITCH          = false
FERMIONLOOP           = 3

NLO_SEMILEP_DECAY    = 0

ECM                   = 14000d0
BEAM1                 = 1
BEAM2                 = 1

ID_MUF                = 0
ID_MUR                = 0
MUF_USER              = 160.796d0
MUR_USER              = 160.796d0
XIF                   = 1d0
XIR                   = 1d0

HMASS                 = 126.0d0
HATYPE                = 0

MODEL                 = 1
EWScheme              = 3
DEL_ALFA              = 0.059047686d0
ANOM_CPL              = true
KK_MOD                = false
SPIN2                 = false
EW_APPROX             = 5

H2MASS                = 600d0
H2WIDTH               = -999d0

```

```

SIN2BA      = 1d0
COS2BA      = -999d0

HWIDTH      = -999d0
TOPMASS     = 172.4d0
BOTTOMMASS  = 4.855d0
CHARMMASS   = 1.65d0
TAU_MASS    = 1.77684D0
FERMI_CONST = 1.16637d-5
INVALFA     = 128.944341122D0
SIN2W       = 0.222646d0
WMASS       = 80.398d0
ZMASS       = 91.1876d0

LHA_SWITCH      = true
LHA_FILE        = event.lhe
HEPMC_SWITCH    = false
HEPMC_FILE      = event.hePMC
UNWEIGHTING_SWITCH = true
DESIRED_EVENT_COUNT = 100000

PARTIAL_UNWEIGHTING = true

TAUMASS        = false

PDF_SWITCH     = 1

LO_PDFNAME     = cteq6ll.LHpdf
NLO_PDFNAME    = CT10.LHgrid
LO_PDFMEMBER   = 0
NLO_PDFMEMBER  = 0

XSECFILE       = xsection
ROOT           = false
TOP            = false
GNU           = false
DATA          = true
REPLACE       = false
ROOTFILE      = histograms
TOPFILE       = histograms
GNUFILE       = histograms
DATAFILE      = histograms

```

- cuts.dat

As the name suggests it already, this file contains all cuts that VBFNLO applies in the generation of events and its calculation of the total cross section.

```

RJJ_MIN      = 0.4d0
Y_P_MAX      = 5.0d0
PGENKTJET    = -1.0d0
PT_JET_MIN   = 30.0d0
Y_JET_MAX    = 4.5d0

Y_L_MAX      = 2.5d0
PT_L_MIN     = 20.0d0
MLL_MIN      = 0.0d0
MLL_MAX      = 1d20
MLL_OSONLY   = true
RLL_MIN      = 0.0d0

```

```

RLL_MAX    = 50.0d0

Y_G_MAX    = 2.37d0
PT_G_MIN   = 20d0
RGG_MIN    = 0.7d0
RGG_MAX    = 50.0d0
PHISOLCUT = 0.7d0
EFISOLCUT = 1d0

RJL_MIN    = 0.0d0
RJG_MIN    = 0.7d0
RLG_MIN    = 0.7d0

MLG_MIN    = 0.0d0
MLG_MAX    = 1.d20

PTMISS_MIN = 0.0d0

ETAJJ_MIN  = 4d0
YSIGN      = false
LRAPIDGAP = false
DELY_JL    = 0.0d0
GRAPIDGAP = false
DELY_JG    = 0.0d0

MDIJ_MIN   = 600.0d0
MDIJ_MAX   = 1d20

JVETO      = false
DELY_JVETO = 0.0d0
YMAX_VETO  = 4.5d0
PTMIN_VETO = 50.0d0

DEF_TAGJET = 1

ETA_CENTRAL = 2.0d0

PTMIN_TAG_1 = 20d0
PTMIN_TAG_2 = 20d0
HARD_CENTRAL = false
PTMIN_CENTRAL = 20d0
VBF CUTS_ALWAYS = false

RECONST_HAD_V = 0

V_MASS_RANGE = 20d0

SINGLE_DECAYJET = 0

QSQAMIN_ZDEC = 0d0

```

- anomV.dat

In this file all the settings for the anomalous couplings are chosen. In the example only FS0, FS1 and the switch KMATRIX have been modified, compared to the standard input files.

```

TRIANOM    = 1

FWWW       = 0D-6

```

```

FW          = OD-6
FB          = OD-6

LAMBDAO     = ODO
ZDELTAKAPPAO = ODO
ZDELTA G1   = ODO
ADELTAKAPPAO = ODO

FWW = ODO
FBB = ODO
FWWt = ODO
FBWt = ODO
FBBt = ODO
FWt = ODO
FBt = ODO
FWWt = ODO
FDWt = ODO

FS0          = 100D-12
FS1          = 100D-12

FM0          = OD-12
FM1          = OD-12
FM2          = OD-12
FM3          = OD-12
FM4          = OD-12
FM5          = OD-12
FM6          = OD-12
FM7          = OD-12

FT0          = OD-12
FT1          = OD-12
FT2          = OD-12
FT5          = OD-12
FT6          = OD-12
FT7          = OD-12
FT8          = OD-12
FT9          = OD-12

FORMFAC      = .false.
KMATRIX      = .true.
FFMASSSCALE  = 2000DO
FFEXP        = 2

FORMFAC_IND  = .false.

MASS_SCALE_FWWW = 2000DO
FFEXP_FWWW      = 2
MASS_SCALE_FW   = 2000DO
FFEXP_FW        = 2
MASS_SCALE_FB   = 2000DO
FFEXP_FB        = 2

MASS_SCALE_AKAPPA = 2000DO
FFEXP_AKAPPA     = 2
MASS_SCALE_ZKAPPA = 2000DO
FFEXP_ZKAPPA     = 2
MASS_SCALE_LAMBDA = 2000DO
FFEXP_LAMBDA     = 2

```

```
MASS_SCALE_G      = 2000D0
FFEXP_G          = 2
```

## H.2. Whizard Input File

Below the input file for WHIZARD is shown. Other than in VBFNLO, WHIZARD does not provide input files containing lists of all necessary parameters, but needs to create his own file to be written in the WHIZARD-internal programming language Sindarin.

```
model = SM_rx

alias pr = u:d:s:c:gl:U:D:S:C
alias lepton = e1:E1:e2:E2
process wppj = pr,pr => E1,n1,E2,n2,pr,pr

# Define model parameters
# f_S0 = 10 10^-12GeV^-4
# f_S1 = 10 10^-12 GeV^-4
a4 = 0.0045941
a5 = 0.

me = 0. GeV
mmu = 0. GeV
mtau = 0. GeV
ms = 0. GeV
mc = 0. GeV
mH = 126. GeV
wH = 0.004277 GeV
mW = 80.398 GeV
mZ = 91.1876 GeV
wW = 2.097673 GeV
wZ = 2.508420 GeV
alphas = 0.          # alpha_s set to suppress QCD background

# Define reasonable cuts and integrate the cross section(s)
# in order to initialize the phase space grids for simulation
cuts = all Pt >= 20 GeV [lepton]
      and all -2.5 <= Eta <= 2.5 [lepton]
      and all Pt >= 30 GeV [pr]
      and all -4.5 <= Eta <= 4.5 [pr]
      and all abs(Eta) >= 4 [pr,pr]
      and all M >= 600 GeV [pr,pr]

# Define the process scale
scale = 160.796 GeV

# Beam specification and integration
sqrt_s = 14 TeV
$pdf_built_in_set = "cteq6l1"
beams = p, p => pdf_built_in

integrate (wppj) { iterations = 20:500000, 5:500000}

# Allocate plots
histogram m_lepton (0 GeV, 2000 GeV, 20 GeV)

histogram pt_lepton (100 GeV, 2000 GeV, 100 GeV)

analysis = record m_lepton (eval M [combine [E1,E2] ] );
```

```
record pt_lepton (eval Pt [E1])

# Set the desired numbers of events...
n_events = 400000
sample_format = lhef

# ... and simulate, requesting status information every 5000 events
?unweighted = true
simulate (wppjj) {checkpoint = 5000}

compile_analysis { $out_file = "WpWpjj.dat" }
```

# Bibliography

- [1] **ATLAS** Collaboration, ATLAS collaboration, *Observation of a new particle in the search for the Standard Model Higgs boson with the ATLAS detector at the {LHC}*. Physics Letters B **716** (2012) no. 1, 1 – 29.
- [2] **CMS** Collaboration, CMS collaboration, *Observation of a new boson at a mass of 125 GeV with the CMS experiment at the LHC*. Physics Letters B **716** (2012) no. 1, 30 – 61.
- [3] **ATLAS** Collaboration, G. Aad *et al.*, *Evidence for Electroweak Production of  $W^\pm W^\pm jj$  in  $pp$  Collisions at  $\sqrt{s} = 8$  TeV with the ATLAS Detector*. Phys.Rev.Lett. **113** (2014) 141803, [arXiv:1405.6241 \[hep-ex\]](#).
- [4] J. Ellis, *Theory Summary and Prospects*. [arXiv:1408.5866 \[hep-ph\]](#).
- [5] W. Kilian, T. Ohl, J. Reuter, and M. Sekulla, *High-Energy Vector Boson Scattering after the Higgs Discovery*. [arXiv:1408.6207 \[hep-ph\]](#).
- [6] A. Alboteanu, W. Kilian, and J. Reuter, *Resonances and Unitarity in Weak Boson Scattering at the LHC*. JHEP **0811** (2008) 010, [arXiv:0806.4145 \[hep-ph\]](#).
- [7] A. Ballestrero, D. B. Franzosi, L. Oggero, and E. Maina, *Vector Boson scattering at the LHC: counting experiments for unitarized models in a full six fermion approach*. JHEP **1203** (2012) 031, [arXiv:1112.1171 \[hep-ph\]](#).
- [8] J. Baglio, J. Bellm, F. Campanario, B. Feigl, J. Frank, *et al.*, *Release Note - VBFNLO 2.7.0*. [arXiv:1404.3940 \[hep-ph\]](#).
- [9] W. Kilian, T. Ohl, and J. Reuter, *WHIZARD: Simulating Multi-Particle Processes at LHC and ILC*. Eur.Phys.J. **C71** (2011) 1742, [arXiv:0708.4233 \[hep-ph\]](#).
- [10] M. E. Peskin and B. V. Schroeder, *An Introduction to Quantum Field Theory*. Westview Press, 1995.
- [11] I. Aitchison and A. Hey, *Gauge Theories in Particle Physics: Volume I: From Relativistic Quantum Mechanics to QED, Third Edition*. Graduate Student Series in Physics. Taylor & Francis, 2002.
- [12] R. Feynman, F. Morinigo, W. Wagner, and B. Hatfield, *Feynman Lectures on Gravitation*. Advanced Book Program. Westview Press, 2002.
- [13] W. Buchmueller and D. Wyler, *Effective lagrangian analysis of new interactions and flavour conservation*. Nuclear Physics B **268** (1986) no. 3-4, 621 – 653.
- [14] C. Lee, *The Evolution of Soft Collinear Effective Theory*. [arXiv:1410.4216 \[hep-ph\]](#).
- [15] C. Degrande, N. Greiner, W. Kilian, O. Mattelaer, H. Mebane, *et al.*, *Effective Field Theory: A Modern Approach to Anomalous Couplings*. Annals Phys. **335** (2013) 21–32, [arXiv:1205.4231 \[hep-ph\]](#).
- [16] C. Degrande, O. Eboli, B. Feigl, B. Jaeger, W. Kilian, *et al.*, *Monte Carlo tools for studies of non-standard electroweak gauge boson interactions in multi-boson processes: A Snowmass White Paper*. [arXiv:1309.7890 \[hep-ph\]](#).

- [17] K. Hagiwara, R. Peccei, D. Zeppenfeld, and K. Hikasa, *Probing the weak boson sector in  $e^+e^- \rightarrow W^+W^-$* . Nuclear Physics B **282** (1987) no. 0, 253 – 307.
- [18] H. Aihara, T. Barklow, U. Baur, J. Busenitz, S. Errede, *et al.*, *Anomalous gauge boson interactions*. arXiv:hep-ph/9503425 [hep-ph].
- [19] O. Eboli, M. Gonzalez-Garcia, and J. Mizukoshi,  *$pp \rightarrow jje^{+-}\mu^{+-}\nu\nu$  and  $jje^{+-}\mu^{+-}\nu\nu$  at  $O(\alpha_{em}^6)$  and  $O(\alpha_{em}^4\alpha_s^2)$  for the study of the quartic electroweak gauge boson vertex at CERN LHC*. Phys.Rev. **D74** (2006) 073005, arXiv:hep-ph/0606118 [hep-ph].
- [20] **Particle Data Group** Collaboration, J. Beringer *et al.*, *Review of Particle Physics (RPP)*. Phys.Rev. **D86** (2012) 010001.
- [21] B. Feigl, *Anomale Vier-Vektorboson-Kopplungen bei der Produktion von drei Vektorbosonen am LHC*. Diploma Thesis, Institut für theoretische Physik, KIT, Karlsruhe, Germany, 2009.
- [22] O. Schlimpert, *Anomale Kopplungen bei der Streuung schwacher Eichbosonen*. Diploma Thesis, Institut für theoretische Physik, KIT, Karlsruhe, Germany, 2013.
- [23] S. U. Chung, J. Brose, R. Hackmann, E. Klempt, S. Spanier, and C. Strassburger, *Partial wave analysis in K-matrix formalism*, 1995.
- [24] M. Jacob and G. Wick, *On the general theory of collisions for particles with spin*. Annals Phys. **7** (1959) 404–428.
- [25] D. G. Truhlar, C. A. Mead, and M. A. Brandt, *Time-Reversal Invariance, Representations for Scattering Wavefunctions, Symmetry of the Scattering Matrix, and Differential Cross-Sections*, pp. 295–344. John Wiley & Sons, Inc., 2007.
- [26] B. W. Lee, C. Quigg, and H. Thacker, *Weak Interactions at Very High-Energies: The Role of the Higgs Boson Mass*. Phys.Rev. **D16** (1977) 1519.
- [27] A. Alloul, N. D. Christensen, C. Degrande, C. Duhr, and B. Fuks, *FeynRules 2.0 - A complete toolbox for tree-level phenomenology*. Comput.Phys.Commun. **185** (2014) 2250–2300, arXiv:1310.1921 [hep-ph].
- [28] T. Hahn, *Feynman Diagram Calculations with FeynArts, FormCalc, and LoopTools*. PoS **ACAT2010** (2010) 078, arXiv:1006.2231 [hep-ph].
- [29] O. Eboli and M. Gonzalez-Garcia.  
<http://feynrules.irmp.ucl.ac.be/wiki/AnomalousGaugeCoupling>.
- [30] K. Arnold, M. Bahr, G. Bozzi, F. Campanario, C. Englert, *et al.*, *VBFNLO: A Parton level Monte Carlo for processes with electroweak bosons*. Comput.Phys.Commun. **180** (2009) 1661–1670, arXiv:0811.4559 [hep-ph].
- [31] D. Zeppenfeld, *Collider physics*. arXiv:hep-ph/9902307 [hep-ph].
- [32] G. P. Lepage, *VEGAS: An adaptive multidimensional integration program*.
- [33] M. Moretti, T. Ohl, and J. Reuter, *O’Mega: An Optimizing matrix element generator*. arXiv:hep-ph/0102195 [hep-ph].
- [34] J. Pumplin, D. Stump, J. Huston, H. Lai, P. M. Nadolsky, *et al.*, *New generation of parton distributions with uncertainties from global QCD analysis*. JHEP **0207** (2002) 012, arXiv:hep-ph/0201195 [hep-ph].
- [35] M. Rauch, F. Campanario, B. Feigl, and O. Schlimpert, *Multi-boson Production in Weak Boson Fusion*. arXiv:1407.3719 [hep-ph].

- 
- [36] J. Alwall, A. Ballestrero, P. Bartalini, S. Belov, E. Boos, *et al.*, *A Standard format for Les Houches event files*. *Comput.Phys.Commun.* **176** (2007) 300–304, [arXiv:hep-ph/0609017](https://arxiv.org/abs/hep-ph/0609017) [hep-ph].
- [37] H. Murayama, I. Watanabe, and K. Hagiwara, *HELAS: HELicity amplitude subroutines for Feynman diagram evaluations*. <http://inspirehep.net/record/336604/>.



# Acknowledgement

I would like to thank

*Prof. Zeppenfeld,*

for giving me the opportunity to write this thesis at the ITP, the suggestion of this interesting topic, many fruitful discussions and helpful suggestions,

*Prof. Mühlleitner,*

for taking the job of being the second reviewer,

*the admins Johannes Bellm and Robin Roth,*

for keeping the PCs running and solving every computer-related problem encountered in the last year,

*Michael Rauch and Robin Roth*

for many helpful discussions, giving me deep insights into the VBFNLO code, checking my work and proofreading,

*my office colleagues Robin Lorenz, Daniel Rauch and Alexander Wlotzka*

for not throwing me out of the office despite intense use of groaners, helpful discussions and proofreading,

*my family, my friends and my flatmates*

for being there and helping out whenever needed.